FREQUENCY-DOMAIN EQUALIZATION FOR SPACE-TIME BLOCK-CODED TRANSMISSIONS OVER FREQUENCY-SELECTIVE FADING CHANNELS

YANG YANG

NATIONAL UNIVERSITY OF SINGAPORE

2003

FREQUENCY-DOMAIN EQUALIZATION FOR SPACE-TIME BLOCK-CODED TRANSMISSIONS OVER FREQUENCY-SELECTIVE FADING CHANNELS

YANG YANG

(*B. Eng., Xi'an Jiaotong Univ., P. R. China*)

A THESIS SUBMITTED

FOR THE DEGREE OF MASTER OF ENGINEERING

DEPARTMENT OF ELECTRICAL AND COMPUTER ENGINEERING

NATIONAL UNIVERSITY OF SINGAPORE

2003

Acknowledgements

My thesis writing has often brought me back to two years ago when I first stepped foot on Singapore, full of curiosity and passion. Coming to Singapore has been a really great event in my life, which represents a turning point in my personal and academic development. During my two-year immersion here, I have been so fortunate to have had a lot of kind people around me who have taken the time and effort in helping smooth my way. Taking this opportunity, I would like to express my sincerest thanks to all of them, and especially to those mentioned in the following.

First and foremost, my ineffable gratitude goes to my two supervisors — Professor Tjhung Tjeng Thiang and Dr. Chew Yong Huat. I was so lucky to meet them in the early of 2002 when I was experiencing some changes during my stay here. Their aid made it possible for me to continue my research and study here, and to finally come out with this thesis. They have provided me great help in both my research and study. The guidance and encouragement they gave me during the period I worked on this thesis especially means a great deal to me. What I have learned from them, is not only the method and attitude to research, but the kindness and generosity to others.

I am deeply indebted to my parents for their constant caring and support throughout my life, especially for their considerateness and understanding over these years when I am pursuing my higher degree overseas. Whereas, being the only child in the family, I feel very guilty about not looking after them during these years. Taking this opportunity, I would like to say *sorry* to them.

I would like to express my hearty thanks to Miss Liao Wen Hui, Mr. Yang Yong and Mr. Tan Siew Chong for their understanding and encouragement. My sincere thanks also go to Dr. Zhang Zhihua, Mr. Shang Zhenhua, Ms. Zeng Ying and Mr. Wang Zhongfang for their help and support. Over these years, my friends have given me much more than I could ever expect; their friendships are priceless treasures to me.

I would also like to thank Ms. Zhang Jinbin for her kind help during my early stay at NUS, Mr. Shi Jianlin and Mr. Li Jiangtao for providing me temporary accommodations when I just arrived here, Dr. Qiang Hongfu for the happy leisure time that we had together. And my special thanks go to Miss Li Jin for our correspondence over years ever since we got to know each other.

Last but not least, my thanks go to the Department of Electrical and Computer Engineering in National University of Singapore and the Institute for Infocomm Research for giving me the opportunity to study here.

Contents

Summary

Growth in the demand for wideband services such as high-speed internet connection and high quality video transmission has sparked the need for reliable transmission at high data rates over wireless channels. To increase the data rate or improve the link quality, single-carrier frequency-domain equalization (FDE) and space-time block coding (STBC) have been gaining more and more interests recently. The objective of this thesis is to exploit the benefits of these two techniques by means of combining them together. Or more specifically, we investigate FDE schemes for STBC block transmissions over frequency-selective fading channels. These FDE schemes can be divided into two categories: the channel estimation based FDE and adaptive FDE.

For the first category, we present efficient linear and decision-feedback block equalization schemes according to zero-forcing (ZF) and minimum mean-square error (MMSE) criteria for STBC systems. Closed form expressions for tap coefficients of these FDE schemes are derived. We also show that our work in FDE can be readily extended to perform channel estimation. And a training based frequency-domain channel estimation scheme is proposed, in which training blocks

can be encoded by the same space-time coder as the data blocks. We examine the performance of these channel equalization and estimation schemes by applying them to the EDGE system. Simulation results indicate significant performance improvement achieved by STBC-FDE schemes as compared to the single transmitter case with FDE. Simulation results also demonstrate effectiveness of the frequency-domain channel estimation scheme.

As for the adaptive version, we present a systematic method of developing adaptive FDE for STBC transmissions using block adaptive algorithms. This adaptive scheme eliminates the need to perform separate channel estimation, i.e., channel estimation and equalization are performed jointly. Simulations results indicate that adaptive FDE scheme (based on block recursive least square (BRLS) algorithm) is effective in combating the ISI caused by multipath fading with relatively lower complexity. We also propose a diversity combining method. This scheme is implemented in the frequency domain in junction with the adaptive FDE, and can effectively mitigate the effects induced by channel variations.

In the end, we present our recommendations with regard to the applications of the above two STBC-FDE categories to practical systems, such as the EDGE system and broadband wireless access (BWA) systems.

List of Tables

List of Figures

Abbreviations

AWGN: Additive White Gaussian Noise
BER: Bit Error Rate
BLMS: Block Least Mean Square
BRLS: Block Recursive Least Square
BWA: Broadband Wireless Access
CDMA: Code Division Multiple Access
CIR: Channel Impulse Response
CP: Cyclic Prefix
CSI: Channel State Information
DFE: Decision-Feedback Equalization
DFT Discrete Fourier Transform
EDGE: Enhanced Data rates for GSM Evolution
FBLMS: Fast Block Least Mean Square
FDE: Frequency-Domain Equalization
FFT: Fast Fourier Transform
FIR: Finite Impulse Response
FSU-RLS: Fast Subsampled-Updating RLS
GMSK: Gaussian Minimum Shift Keying
GSM: Global System for Mobile communication
IBI: InterBlock Interference
IDFT: Inverse Discrete Fourier Transform
IFFT: Inverse Fast Fourier Transform
ISI: Intersymbol Interference
LE: Linear Equalization
LMS: Least Mean Square
LOS: Line Of Sight

MLSE:	Maximum Likelihood Sequence Estimation
MMSE:	Minimum Mean Square Error
MRRC:	Maximal-Ratio Receive Combining
NLOS:	Non-LOS
OFDM:	Orthogonal Frequency Division Multiplexing
PAR:	Peak-to-Average Ratio
QAM:	Quadrature Amplitude Modulation
RLS:	Recursive Least Square
RX:	Receiver
SC:	Single Carrier
SNR:	Signal to Noise Ratio
STBC:	Space-Time Block-Coding / Space-Time Block-Coded
STBCs:	Space-Time Block Codes
SU-RLS:	Subsampled-Updating RLS
TR-STBC:	Time-Reversal Space-Time Block Coding
TX:	Transmitter
ZF:	Zero Forcing
ZP:	Zero Padding

Notations

Scalar variables in this thesis are expressed as plain lower-case letters, vectors as bold face low-case letters and matrices as bold-face upper-case letters. Other notations used in the thesis include the following:

$\mathbf{A}^*$:	Conjugate of the matrix $\mathbf{A}$
$\mathbf{A}^T$:	Transpose of the matrix $\mathbf{A}$
$\mathbf{A}^H$:	Hermitian of the matrix $\mathbf{A}$
$\mathbf{A}^+$:	Pseudo inverse of the matrix $\mathbf{A}$
$Tr\{\mathbf{A}\}$:	The trace of the matrix $\mathbf{A}$
$E\{\mathbf{A}\}$:	Statistical expectation of the matrix $\mathbf{A}$
$\text{diag}(\mathbf{a})$:	A diagonal matrix with its diagonal vector given by $\mathbf{a}$
$\mathbf{A} \otimes \mathbf{B}$:	The Kronecker Product
$\mathbf{I}_N$:	The identity matrix of size $N \times N$
$\mathbf{0}_{M \times N}$:	The all-zero matrix of size $M \times N$
$\|\mathbf{a}\|$:	The Euclidean norm of vector $\mathbf{a}$

Chapter 1

Introduction

1.1 Literature Review

Wireless communications have experienced tremendous growth over the latest two decades, such that the goal for people to access the capabilities of the global network at any time without regard to location and mobility becomes increasingly achievable [1]. Meanwhile, the growing demand for wideband services such as high-speed internet connection and high quality video transmission, has further sparked the need for reliable transmission at high data rates over wireless channels. Unfortunately, as opposed to wireline, the wireless environment is quite harsh, and signals can undergo rapid fluctuations caused by multipath propagation when passing through wireless channels [2, 3]. Besides, the limited radio spectrum is another crucial obstacle to wireless communications. Therefore, techniques that can improve the quality and spectral efficiency of wireless communication links become both increasingly desirable and challenging, and undoubtedly, are of great com-

mercial interest.

Driven by such growth in demand for wideband services and together with the up-to-date advancement of semiconductor technology, a variety of efficient communication techniques along with sophisticated digital signal processing algorithms have been developed and are still under intensive studies in recent years. Some of them are equalization, coding, spread spectrum, diversity, multicarrier modulation, etc. Among these techniques, we are most interested in the two techniques, namely frequency-domain equalization (FDE)[1] and space-time block coding (STBC). In the remaining part of this section, we will present a brief review of these two techniques. More detailed explanation can be found in Chapter 3 and Chapter 4, respectively.

Frequency-Domain Equalization

As mobile radio channels are affected by multipath fading, some form of channel equalization is needed to compensate for the intersymbol interference (ISI). The traditional approach to compensate for the signal distortion is time-domain equalization, which usually takes the form of an adaptive linear equalizer or a decision-feedback equalizer (DFE) [4, 7]. The equalizer usually requires a specific algorithm to compute the tap coefficients to optimize a specified performance metric, and to adaptively update them according to the time variations in the channel conditions. However, for the wideband channel characterized by large delay spreads or long impulse response memory, resulting in ISI spanning over many symbol intervals, such

[1] In this thesis we consider single-carrier systems only, and the term FDE hereafter used throughout this thesis is assumed for single-carrier systems, unless otherwise stated.

time-domain equalization approach becomes unattractive because its complexity grows exponentially with channel memory or it requires very long FIR (finite impulse response) filters to achieve acceptable performance. An alternative approach is the FDE, which enjoys the primary advantage of a large reduction in the computational complexity due to the use of the computationally-efficient fast Fourier transform (FFT) [8, 9].

In fact, FDE is not a novel concept, as it has been proposed as early as two decades ago [10], but has so far been overlooked. Until recently, when analyzing the operation of OFDM (orthogonal frequency division multiplexing), which is a recognized multicarrier solution to combat delay spread by transmitting information over a group of low-bit-rate subcarriers, Sari et al., noticed a striking resemblance to FDE for traditional single-carrier systems [11, 12]. They further pointed that with FDE, single-carrier (SC) transmission can handle the same type of channels with similar performance and lower complexity compared to OFDM signaling. Moreover, the use of single-carrier FDE (SC-FDE) by taking the FFT of the received signal has several attractive advantages over OFDM [11, 12, 18]:

- Single-carrier modulation has reduced peak-to-average ratio (PAR) requirement than OFDM, thereby allowing the use of less costly power amplifiers.

- SC-FDE has the advantage of low sensitivity to nonlinear signal distortion, and significantly alleviates the carrier synchronization problems of OFDM.

- Channel coding, while desirable, is not essential for SC-FDE to combat frequency-selectivity, but it is indispensable to non-adaptive OFDM.

Subsequent to the work of Sari et al. [11, 12], research has been carried out to further exploit the characteristics of SC-FDE (e.g., [13, 14, 15]) or to look into its possible application to practical communication systems(e.g., [16, 17, 18]). This has made the concept of frequency-domain equalization experience a revival in wireless communications research. Details regarding the implementation of FDE are available in Section 3.3.

Space-Time Block Coding

Space-time block coding (STBC) is an open-loop transmit diversity technique that was first proposed by Alamouti [20] for two transmit antennas and was later generalized to an arbitary number of transmit antennas by Tarokh et al. [21]. According to the Alamouti's STBC scheme, symbols transmitted from the transmit antennas are encoded in space and time in a simple manner to ensure that transmissions from both antennas are orthogonal to each other. Alamouti's STBC scheme has been adopted in several third-generation cellular standards (e.g. CDMA2000 [23] and wideband CDMA [24]) and has been proposed for many wireless applications (e.g., [25, 26]) because of its many attractive features including the following [20, 30] :

- It can achieve full diversity at full transmission rate for any (real or complex) signal constellation.
- It does not require any feedback from the receiver to the transmitter, i.e., the channel state information (CSI).
- Its computation complexity is similar to maximal-ratio receiver combining

(MRRC). And maximum likelihood decoding involves only linear processing at the receiver (due to the orthogonal code structure).

Although the Alamouti-type STBC scheme enjoys the aforementioned advantages, it has also some limitations, for example, its simple decoding rule is valid only for the assumption of a flat-fading channel. However, when the delay spreads are significant and the channel becomes frequency selective [2, 3], this assumption will no longer be justified. Recently, intensive research efforts have been devoted to the design of space-time block codes (STBCs) for single-carrier transmissions over frequency-selective fading channels by implementing the Alamouti's orthogonal signaling scheme at block level instead of symbol level [27, 28, 29, 31]. Description of these designs will be given in detail in Section 4.3.

1.2 Thesis Outline

This thesis addresses the topic of FDE for space-time block-coded (STBC)[2] transmissions over frequency-selective fading channels. The objective of our research is to combine the above-mentioned two attractive techniques together to realize broadband equalization by exploiting the benefits of both techniques. This thesis is organized as follows.

Chapter 2 starts with a brief discussion of some properties that characterize the wireless channels, such as multipath, fading, Doppler, etc. The channel model

[2]In this thesis we will use the acronym STBC for both space-time block-coding and space-time block-coded, hopefully without introducing any ambiguity for understanding.

adopted for our research is also manifested in this chapter, which provides the necessary background knowledge for the remaining chapters.

Chapter 3 introduces the channel equalization techniques that are commonly used in practice to combat the multipath induced ISI. Several types of existing equalization techniques are examined in this chapter. Among them, our emphasis is placed on the FDE. We elucidate two ever existing FDE methods, with their respective characteristics elaborated. Moreover, similarities together with the differences between these methods are provided in this chapter, too.

Chapter 4 discusses the STBC technique. It begins with a brief review of the diversity techniques. After that, the Alamouti's STBC scheme, which is mainly designed for transmission over frequency-flat fading channels, is introduced. Next, we present a brief literature review on some existing studies on designing STBC schemes for single-carrier block transmissions over frequency-selective fading channels. In the end, the transmission format adopted in our research is described in detail, which lays the basis for our work in the ensuing chapters.

we acknowledge that there exist two general approaches for designing equalizers to compensate for channel distortions [32, 33]. One is to first estimate the channel impulse response and then design an equalizer based on the estimated channel; another approach is to do joint channel estimation and equalization given the received signal. In this thesis, we adopt both approaches to design the frequency-domain equalizers for STBC transmissions over frequency-selective fading channels, as detailed below.

Chapter 5 deals with the channel estimation based FDE for STBC transmis-

sions over multipath fading channels by employing FIR filterbanks, i.e., it follows the first design approach. At the beginning of this chapter, closed-form solutions for tap coefficients of the ZF (zero forcing) and MMSE frequency-domain linear and decision-feedback (DF) FIR filterbank equalizers are derived. After that, a training-based frequency-domain channel estimation method is proposed for space-time block multiple-antenna transmissions over frequency-selective fading channels. Performance of these proposed schemes is then studied via extensive simulations by applying them to one typical communication system, namely EDGE (enhanced data rates for global system for GSM evolution) [34]. Discussions and a summary are presented in this chapter as well.

Adopting the second design approach, Chapter 6 focuses on the adaptive FDE to realize joint channel estimation and equalization for STBC transmissions over frequency-selective fading channels. This chapter starts with a detailed treatment of adaptive FDE for the received distorted data blocks, along with various block recursive algorithms for updating the equalizer coefficients. After that, a diversity combining method is proposed for mitigating the detrimental effect introduced by frequency dispersion of fading channels. As in Chapter 5, performance study of the proposed schemes is carried out via simulations by applying these schemes to typical communication systems. We also present our recommendations with regard to the applications of the above two FDE categories to practical systems. This chapter ends with a discussion and summary.

Chapter 7 concludes this thesis with a thesis summary, and suggests the possible directions for future research.

1.3 Contributions

The overall contribution of this thesis is a systematic development of several practical state-of-art FDE schemes for STBC transmissions over frequency-selective fading channels. Simulation results demonstrating the performance of these schemes when applying to some typical wireless systems in multipath fading environment are presented. The pros and cons of these schemes are articulated, and recommendations of jointly applying both STBC and FDE to practical systems are also provided. Some specific contributions of this thesis are summarized as follows.

We categorize the existing FDE techniques into two major classes as well as point out their similarities and differences in Chapter 3. This work is achieved by a thorough literature survey, and it proves to be useful as it helps to give the readers a better comprehension of the existing FDE techniques. And to the best of the author's knowledge, similar study does not seem to exist in the literature even at the time of writing this thesis.

We derive closed-form expressions for tap coefficients of the frequency-domain ZF and MMSE FIR filterbank linear and nonlinear (DFE) equalizers in Chapter 5 for space-time block multiple-antenna transmissions over frequency-selective fading channels. We show that these schemes, with comparable complexity, achieve significant performance improvement over the single transmitter case with FDE.

We propose a training-based channel estimation method in Chapter 5 for space-time block multiple-antenna transmissions over frequency-selective fading channels. In this scheme, the training blocks can be encoded by the same space-

time coder as the data blocks at the transmitter. By exploiting the rich structure of STBC, this training scheme can be implemented in the frequency domain with a comparable low complexity.

We present adaptive FDE scheme for STBC transmissions over multipath channels in Chapter 6, where two unique block adaptive algorithms, namely, BLMS and BRLS, are employed for adjustment of the equalizer coefficients. This adaptive FDE scheme, as shown by simulations, obviates the need for separate channel estimation, and can realize joint channel estimation and equalization with relatively lower complexity.

We propose a diversity combining scheme in Chapter 6, where the diversity branches are combined in the frequency domain in conjunction with the adaptive FDE. It is shown by simulations that this diversity arrangement can assist the equalization and efficiently improve the BER performance when the Doppler spread increases.

Chapter 2

Wireless Channel Characteristics

Communications over the mobile radio channel face many challenging obstacles which must be overcome. In this chapter, we will describe a few basic concepts that concern the wireless propagation channel, where this knowledge is fundamental to the remainder of this thesis. For a more in-depth discussion about the wireless environment, readers can refer to [2] or [3].

In a mobile radio environment, the transmitted signal propagates to the receiver antenna along a number of different paths which arise from reflection, diffraction and scattering of the radiated energy; this phenomenon is referred to as *multipath propagation*. In general, there exist two types of fading effects that can be used to characterize the multipath propagation channels, namely *large-scale fading* and *small-scale fading*. Large-scale fading represents the average signal power attenuation or path loss due to mobile movement over large distances (several hundreds or thousands of meters), while small-scale fading refers to the rapid fluctuations in signal amplitude and phase that can be experienced as a result of small changes

(as small as a half-wavelength) in the spatial separation between a transmitter and receiver.

Since this thesis is mainly focused on mitigating the effects of small-scale fading by using some sophisticated signal processing techniques, these effects, including signal fading, delay spread and Doppler spread, will be thereby discussed in this chapter.

2.1 Signal Fading

Signal fading refers to the rapid variation in received signal strength over very short travel distances (a few wavelengths) or short time durations (on the order of seconds). This occurs because in a multipath propagation environment, the signal received by the mobile at any point in space may consist of a large number of horizontally travelling plane waves with random amplitudes, phases, delays and angle of arrivals. These multipath components combine vectorially at the receive antenna, and can cause the signal received by the mobile to distort or fade.

To characterize the small-scale spatial distribution of the received multipath signal amplitude, researchers have made enormous field measurements and physical modelling of the propagation channel. It has been found that in many situations, the Rayleigh distribution provides a good fit to the signal amplitude measurement where there is no line-of-sight or dominant path [2, 3]. Here let us denote the received signal as $s(t)$, which is a composite of all arriving waves. $s(t)$ can be

expressed as

$$\begin{aligned} s(t) &= x(t)\cos(\omega_c t) - y(t)\sin(\omega_c t) \\ &= \mathrm{Re}\left[(x(t) + jy(t))\ \exp(j\omega_c t)\right] \\ &= \mathrm{Re}[r(t)\exp(j(\omega_c t + \phi))] \end{aligned}$$

where $x(t)$ and $y(t)$ are the in-phase and quadrature components. $r(t)$ denotes the envelope of the complex signal $s(t)$, and it is related with $x(t)$ and $y(t)$ by

$$r(t) = \sqrt{x^2(t) + y^2(t)}.$$

If there are a sufficient large number of waves arriving at the receiver, by the central limit theorem, the in-phase and quadrature components $x(t)$ and $y(t)$ are independent Gaussian processes with zero means and equal variance σ^2. Thus the probability density function (pdf) of $x(t)$ and $y(t)$ can be written as

$$\begin{aligned} f(x) &= \frac{1}{\sqrt{2\pi\sigma^2}}\exp\left[-\frac{x^2}{2\sigma^2}\right] \qquad (-\infty < x < \infty) \\ f(y) &= \frac{1}{\sqrt{2\pi\sigma^2}}\exp\left[-\frac{y^2}{2\sigma^2}\right] \qquad (-\infty < y < \infty) \end{aligned}$$

Then the pdf of the envelope $r(t)$, is given by [35]

$$f(r) = \begin{cases} \dfrac{r}{\sigma^2}\exp\left[-\dfrac{r^2}{2\sigma^2}\right] & (r \geq 0) \\ 0 & (r < 0) \end{cases} \tag{2.1}$$

in which $2\sigma^2$ is the mean power of the multipath signal before envelope detection. Equation (2.1) is the Rayleigh density function.

On the other hand, when the line-of-sight paths exist in a multipath environment, or when there is a dominant reflected path, the Ricean distribution is a

statistical characterization of the signal amplitude distribution. The pdf of the the Ricean distribution is given by

$$f(r) = \begin{cases} \frac{r}{\sigma^2} \exp\left[-\frac{(r^2 + A^2)}{2\sigma^2}\right] I_0\left(\frac{Ar}{\sigma^2}\right) & (r \geq 0, A \geq 0) \\ 0 & (r < 0) \end{cases}$$

The Ricean distribution is related to the non-zero mean Gaussian distribution in a manner similar to the relationship between the Rayleigh and zero mean Gaussian distributions, the details will not be given here. But it is noteworthy that the Rayleigh distribution, as compared with the Ricean distribution, usually represents the pdf associated with the worst case of small-scale fading, since it results from the absence of LOS (line-of-sight) or dominant component of the received signal [36]. In this thesis, it is assumed that all small-scale fading follows the Rayleigh model as described above.

2.2 Delay Spread

When a narrow pulse propagates through a multipath channel, distorted replicas of the transmitted pulse will arrive at the receiver at various different times, making the received signal wider in the time domain than the originally transmitted signal pulse. This phenomenon is referred to as *delay spread*. The significance of delay spread depends on the duration of the signal relative to the coherence time of the channel, hence a quantitative characterization of the severity of channel delay spread is necessary.

One prevalent measure for characterizing channel delay spread is the *power*

delay profile $P(\tau)$. The power delay profile of an environment is obtained through field measurement by transmitting a short pulse and measuring the received power as a function of delay τ, at various locations in a small area. These measurements are then averaged over spatial locations to generate a profile of average received signal power with respect to the delay. And the span of delay spread is often manifested as the maximum excess delay, T_m, which is defined as the time difference between the first path and the last path. T_m is useful when there are only a few paths. However, with a large number of paths, root-mean-square (rms) delay spread is more representative of the effect of delay spread on the performance of radio receivers, and can be used as one qualitative measure of the severity of multipath propagation. The rms delay spread of a profile, σ_τ, is described as [3]

$$\sigma_\tau = \sqrt{\frac{\int (\tau - \bar{\tau})^2 P(\tau)\,\mathrm{d}\tau}{\int P(\tau)\,\mathrm{d}\tau}}, \tag{2.2}$$

where $\bar{\tau}$ is the mean excess delay of $P(\tau)$ and can be computed by

$$\bar{\tau} = \frac{\int \tau P(\tau)\,\mathrm{d}\tau}{\int P(\tau)\,\mathrm{d}\tau}. \tag{2.3}$$

Usually σ_τ can range from 1 to 20 μs in urban environments and from ten to a few hundred ns in indoor environments.

The rms delay spread σ_τ is closely related to another measure of delay spread in the frequency domain, which is referred to as the *coherence bandwidth*. Coherent bandwidth, B_c, represents a frequency range over which frequency components have a strong potential for amplitude correlation. That is, a signal's spectral components in that range are affected by the channel in a similar manner as, e.g., exhibiting strong fading or no fading. There is no exact relationship between B_c

and σ_τ, but in general the relation can be approximately expressed as

$$B_c \sim \frac{1}{c\,\sigma_\tau} \tag{2.4}$$

The constant c varies from to 5 to 50 depending on how strict the coherence bandwidth is to be defined, for example, if the frequency correlation is defined above 0.9, c takes the value of 50.

In general, the impact of the delay spread on the performance of digital radio receivers depends on the relationship between the rms delay spread of the channel and the symbol period of the digital modulation. More specifically, if the rms delay spread is much less than the symbol period, the delay spread has little impact on the performance of the communication system. This condition is often termed *flat fading*. In this case, all of the received multipath components of a symbol arrive within a small fraction of the symbol time duration; hence, the components are not resolvable. And there is no channel-induced ISI distortion, since the signal time spreading does not result in significant overlap among neighboring received symbols.

However, if the rms delay spread is a significant fraction of, or greater than, the symbol period, the channel delay spread significantly impairs the performance of the communication system. This condition is often referred to as *frequency-selective fading*. It occurs whenever the received multipath components of a symbol extend beyond the symbol's time duration, thus causing channel-induced ISI. Therefore, under such circumstance, some form of equalization is necessary to overcome the channel distortion. In this thesis, we assume the channel creates frequency-selective

fading on the received signal.

2.3 Doppler Spread

The relative motion between the transmitter and receiver results in an apparent shift in the frequency of the received signal. This apparent frequency shift is called *Doppler shift*. To analyze this effect, consider the simple one-path scenario illustrated in Figure 2.1, where the transmitter is assumed to be far away so that plane wave approximations hold at the receiver location. Assume a mobile moving

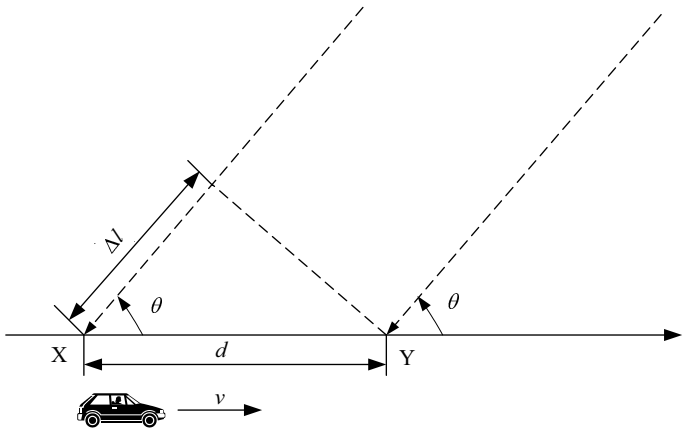

Figure 2.1: Illustration of Doppler shift

at a constant velocity v, along a path segment having length d between points X and Y, while the incident wave arrives at an angle of θ with regard to the motion of the mobile. Then, the difference in path lengths travelled by the wave from the transmitter to the mobile receiver at points X and Y is given by

$$\Delta l = d\cos\theta = v\Delta t\cos\theta \tag{2.5}$$

where Δt is the time required for the mobile to travel from X to Y. The phase change in the received signal due to the difference in path lengths is

$$\Delta\phi = \frac{2\pi\Delta l}{\lambda} = \frac{2\pi v\Delta t}{\lambda}\cos\theta \tag{2.6}$$

where λ is the wavelength of the received signal. Hence, the apparent change in received signal frequency, or Doppler shift, is given by

$$f_d = \frac{1}{2\pi}\frac{\Delta\phi}{\Delta t} = \frac{v}{\lambda}\cos\theta \tag{2.7}$$

The maximum Doppler shift will occur when $|\cos\theta| = 1$. Define the maximum positive Doppler shift to be f_m, so

$$f_m = \frac{vf_c}{c} \tag{2.8}$$

where f_c is the carrier frequency, c is the speed of light, and the relationship of $c = f_c\,\lambda$ is used.

It is straightforward from Equation (2.7) that the apparent received frequency will always be in the range of $f_c \pm f_m$, or the frequency spectrum of the received signal will be wider than that of the transmitted signal. This phenomenon of carrier frequency spreading is called *Doppler spread*. Doppler spread can be quantitatively characterized by the Doppler spectrum which is the power spectral density of the received signal. Using the Clarke and Gans model [2], and assuming the signal power received by a $\lambda/4$ antenna arrives uniformly from all incident angles in the range of $[0, 2\pi)$, the Doppler spectrum at the receiver is given by

$$S(f) = \frac{1.5}{\pi f_m\sqrt{1-\left(\frac{f-f_c}{f_m}\right)^2}} \qquad |f - f_c| \le f_m \tag{2.9}$$

This spectrum is plotted in Figure 2.2. It should be noted that the Doppler spectrum in Equation (2.9) only represents the time variation of a single Rayleigh distribution path. When delay spread is also involved, each path varies differently and the resulting channel variations can be complicated.

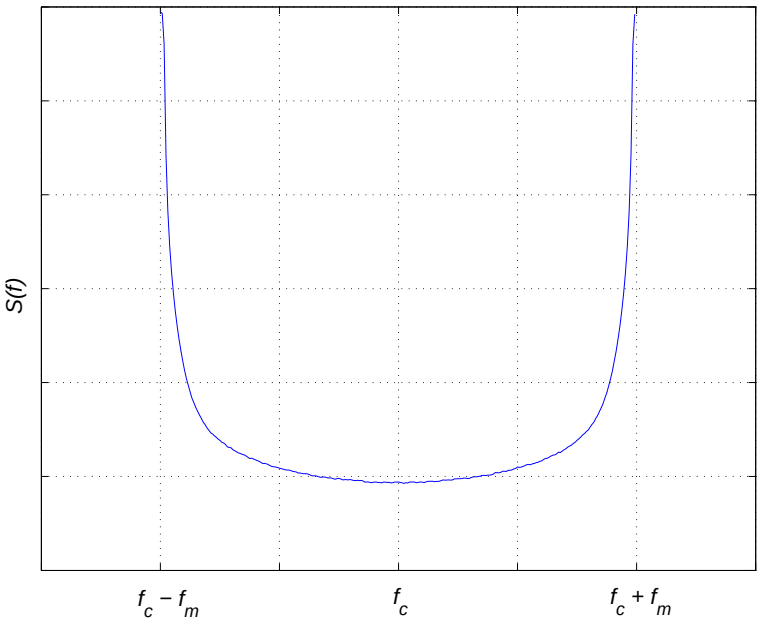

Figure 2.2: Doppler spectrum corresponding to uniform angle of arrival

Another useful statistical measure for describing the time varying nature of the channel is the *coherent time*, T_c , which is defined as the time duration over which the channel impulse response is essentially invariant. The coherent time T_c is inversely proportional to the maximum Doppler shift f_m. And as a rule of thumb for modern digital communications, it is approximately given by [2]

$$T_c = \frac{0.423}{f_m} \tag{2.10}$$

The bandwidth of the Doppler spectrum, or equivalently the maximum Doppler

shift f_m, is a statistical measure of the rate of channel variations. When the Doppler bandwidth is comparable to or greater than the bandwidth of the signal, the channel variations are as fast or faster than the signal variations. This is referred to as *fast fading*. Fast fading describes a condition where the time duration in which the channel behaves in a correlated manner is shorter compared to the time duration of a symbol. Therefore, it can be expected that the fading characteristics of the channel will change significantly while a symbol is sent over the channel, which leads to distortion of the baseband pulse shape and hence a consequent loss of signal-to-noise ratio (SNR) that often yields an irreducible error rate.

On the other hand, when the Doppler bandwidth is small compared to the bandwidth of the signal, the channel variations are slow relative to the signal variations. This is often termed *slow fading*. Here the time duration that the channel behaves in a correlated manner is longer as compared to the time duration of a transmission symbol. Thus, one can expect the channel state remains as if it is unchanged during the time in which a symbol is transmitted, and the transmitted symbols will likely not suffer from the pulse distortion described above. In this thesis, it will be assumed that the channel is a slow fading channel.

2.4 Summary

In this chapter we presented some typical features that characterize the wireless channel, including fading, delay spread and doppler spread. We also made clear the wireless propagation environment that we will consider in this thesis. The

transmitted signals will experience slow frequency-selective fading; the envelope of each of the multipath components conforms to the Rayleigh distribution.

Chapter 3

Channel Equalization Techniques

Time-varying multipath fading causes performance degradation and makes reliable wireless transmissions a challenge when compared to fiber, coaxial cable, line-of-sight microwave or even satellite transmissions. As an example, Figure 3.1 highlights three major performance categories in terms of bit error rate (BER) versus E_b/N_0 when 16-QAM transmissions propagating through additive white Gaussian noise (AWGN) channels, flat Rayleigh fading channels and frequency-selective fading channels[1]. It is clear that the performance degradation due to fading is too significant to be overlooked.

However, increasing the quality or reducing the effective error rate in a multipath fading channel is extremely difficult. Especially when the channel introduces signal distortion as a result of multipath fading, the system performance can exhibit an irreducible error rate, and regardless of how high E_b/N_0 is set to, the desired

[1]Here we use a simple two-ray model with the rms delay spread δ_τ given by $0.8T$, where T denotes symbol period.

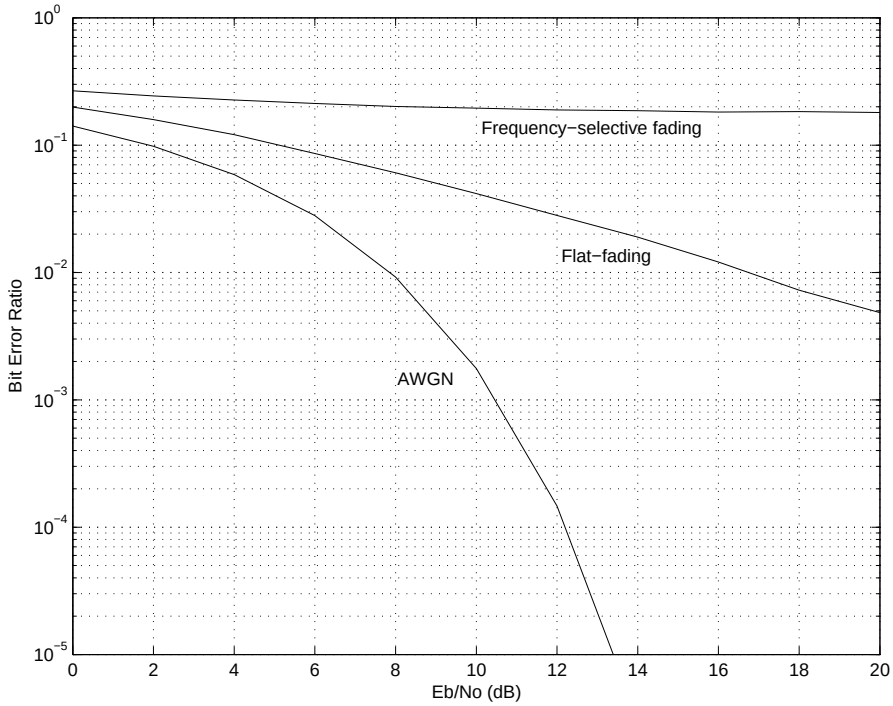

Figure 3.1: Performance comparison of 16-QAM in AWGN and fading channels

level of performance can never be achieved. In such cases, the general approach for improving performance is to use some form of mitigation to remove or reduce the distortion. Next, one can further ameliorate the effects of fading and strive to approach AWGN performance by using some form of diversity or coding [37]. In this chapter, we focus on the use of equalization techniques for combating the effects of signal distortion.

3.1 Linear and Decision-Feedback Equalization

Equalization can be used to compensate for ISI resulting from time-dispersive channels. According to how the output from an equalizer is used for subsequent control

(feedback), equalization techniques may be subdivided into two general types—linear and nonlinear equalization [5]. Linear equalizers usually find its use in applications where the channel distortion is not too harsh. In particular, the linear equalizer does not perform well on channels which have deep spectral nulls in their frequency-response characteristics. In an attempt to compensate for the channel distortion, the linear equalizer places a large gain in the vicinity of the spectral null, thereby significantly enhancing the additive noise present in the received signal. This is the case in multipath fading channels, and as a consequence, linear equalizers are generally avoided. Instead, nonlinear equalizers are normally adopted for such hostile environments, and are commonly used in practical wireless systems.

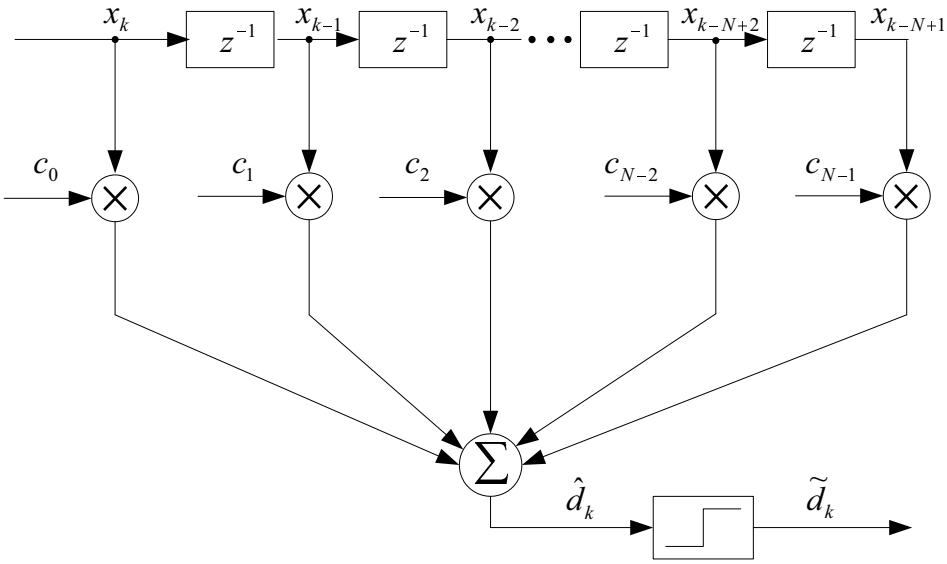

Figure 3.2: Linear transversal equalizer

Associated with each type of equalizer is one or more structures for implementing the equalizer [5]. Among these structures the simplest is the transversal (tapped-delay-line or nonrecursive) equalizer [7]. A linear equalizer can be imple-

mented in such manner as an FIR filter, which is illustrated in Figure 3.2. In this linear equalizer, the current and past values of the received signal are linearly weighted by the equalizer coefficients (or tap gains) c_n and summed to produce the output. If the delays and the tap gains are analog, the continuous output of the equalizer is sampled at the symbol rate and the samples are rendered to the decision device. This implementation, however, is commonly implemented in the digital domain where samples of the received digital signal at the symbol rate are stored in a digital shift register (memory). The output of the transversal filter before a decision is made can be expressed as

$$\hat{d}_k = \sum_{n=0}^{N-1} c_n x_{k-n} \tag{3.1}$$

where x_k is the input received signal, and c_n represents the complex filter coefficients or tap weights and $\hat{d}_k$ is the output of the equalizer at time index k. The estimate $\hat{d}_k$ is quantized to the nearest (in distance) information symbol to form the decision symbol $\tilde{d}_k$. If $\tilde{d}_k$ is not identical to the transmitted symbol d_k, an error has been made.

As for nonlinear equalization, several very effective methods have been developed over these years, including decision feedback equalization (DFE), maximum likelihood symbol detection and maximum likelihood sequence estimation (MLSE) [5]. Here we only focus our attention on the DFE method, which is particularly useful for channels with severe amplitude distortion. The basic idea behind DFE is that if the values of the symbols already detected are known (past decisions are assumed to be correct), then the ISI induced by these symbols can be cancelled

exactly, by subtracting past symbol values with appropriate weighting from the equalizer output [7]. Similar to linear equalization, the DFE can also be realized in the direct transversal form, as shown in Figure 3.3. This type of DFE consists

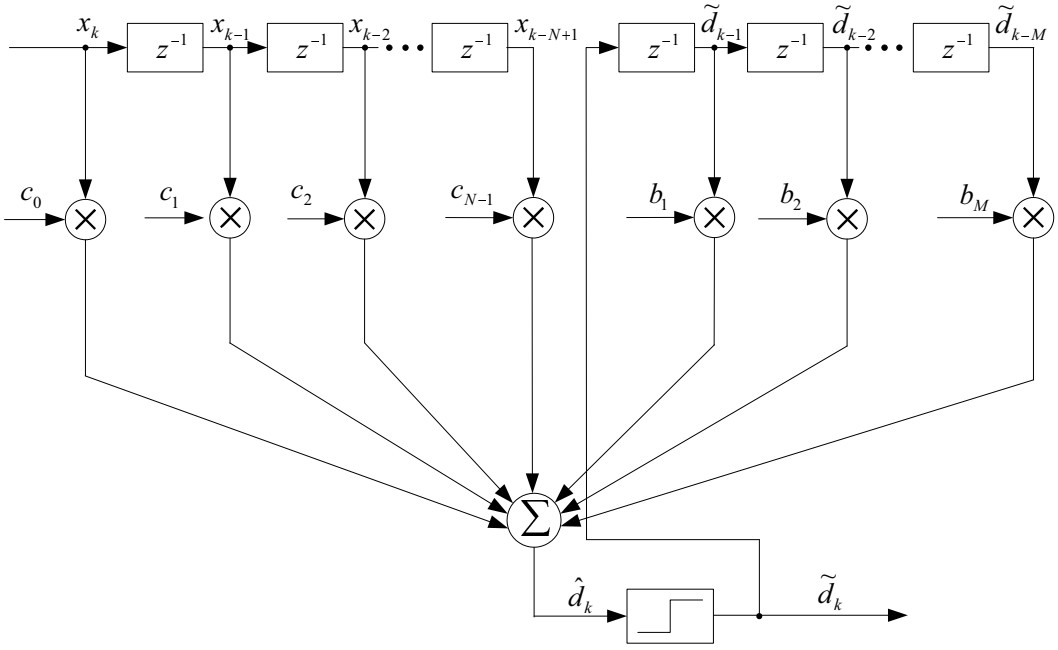

Figure 3.3: Decision feedback equalizer

of a feedforward filter and a feedback filter. The forward part is just like the linear transversal equalizer discussed previously. The feedback filter is driven by decisions on the output of the detector, and its coefficients can be adjusted to cancel the ISI on the current symbol from past detected symbols. The equalizer has N taps in the feedforward filter and M taps in the feedback filter. Its output can be expressed as:

$$\hat{d}_k = \sum_{n=0}^{N-1} c_n x_{k-n} + \sum_{m=1}^{M} b_m \tilde{d}_{k-m} \tag{3.2}$$

where c_n and x_k are the tap gains and the inputs, respectively, to the forward filter, b_m are the tap gains for the feedback filter, and $\tilde{d}_i (i < k)$ is the previous decision

made on the detected signal. That is, once $\hat{d}_k$ is obtained by using Equation (3.2), $\tilde{d}_k$ is decided from it. Then $\tilde{d}_k$ along with previous decisions $\tilde{d}_{k-1}$, $\tilde{d}_{k-2}$, ... are fed back into the equalizer, and $\hat{d}_{k+1}$ is obtained using Equation (3.2).

In this thesis, we consider both linear equalization and DFE for the received signal and both types of equalization are realized in the transversal form as described above. Since the signal is collected as a block of symbols other than individual symbol upon being received, these linear and decision-feedback equalizers will be implemented in *filterbanks* at the receiver. Details about this implementation will be delineated in Chapter 5.

3.2 Adaptive Equalization

In most communication systems that employ equalizers, the channel characteristics are unknown a priori, and the channel response is generally random and time-varying. In such a case, the tap coefficients of the equalizer must be designed to be adaptively adjustable to the time-varying channel response [4]. Such equalizers are usually referred to as adaptive equalizers. There are a class of algorithms that may be used to adaptively adjust the equalizer coefficients according to some specified performance criterion such as zero-forcing (ZF) or minimum mean square error (MMSE). These criteria and associated adaptive algorithms will be briefly reviewed in the following.

According to the ZF criterion, the equalizer coefficients c_n, $n = 0, 1, \cdots, N-1$ are chosen to force the samples of the combined channel and equalizer impulse

response to zero at all except one of the T-spaced sample points in the span of the equalizer. Such an equalizer is commonly called a ZF equalizer. If we let the number of coefficients of a ZF equalizer increase without bound, an infinite length equalizer with zero ISI at the output can be obtained. The frequency response $C(f)$ of such an equalizer is periodic with a period equal to the symbol rate $1/T$ provided that the tap spacing is equal to the symbol duration T. The combined response of the channel in tandem with the equalizer must satisfy Nyquist's first criterion

$$C(f)H'(f) = 1, \qquad |f| \leq 1/2T \tag{3.3}$$

where $H'(f)$ is the folded frequency response of the channel. Equation (3.3) indicates that an infinite length zero-ISI equalizer is simply an inverse filter which inverts the folded frequency response of the channel. This infinite length equalizer is usually implemented by a truncated-length version. However, such an inverse filter may excessively enhance noise at frequencies where the folded channel spectrum has high attenuation, and hence is not often used for wireless links [7].

In practice, the criterion most commonly used in optimizing the equalizer coefficients is the minimization of the mean square error (MSE) between the desired equalizer output and the actual equalizer output [5], i.e.,

$$\mathbf{J} = E\{[d_k - \mathbf{c}_k^T \mathbf{x}_k]^2\}, \tag{3.4}$$

where $\mathbf{c}_k$ represents the vector of the equalizer coefficients at time index k, $\mathbf{x}_k$ is the signal vector for the signal samples stored in the FIR equalizer at time index k. The minimization of the MSE results in the optimum Wiener filter solution for

the coefficient vector, which may be expressed as [4]

$$\mathbf{c}_{\text{opt}} = \mathbf{R}^{-1}\mathbf{p} \tag{3.5}$$

where $\mathbf{R}$ is the autocorrelation matrix of the vector of signal samples in the equalizer at time instant k, i.e., $\mathbf{R} = E\{\mathbf{x}_k^*\mathbf{x}_k^T\}$; $\mathbf{p}$ is the vector of cross correlations between the desired data symbol and the signal samples in the equalizer at time index k, i.e., $\mathbf{p} = E\{d_k\mathbf{x}_k^*\}$.

Alternatively, the minimization of the MSE can be carried out recursively by use of the stochastic gradient algorithm introduced by Widrow [38]. This algorithm is more commonly referred to as the least mean square (LMS) algorithm, and may be computed iteratively by the following equations:

1. *Equalizer output*:

$$\hat{d}_k = \mathbf{c}_k^T\,\mathbf{x}_k \tag{3.6}$$

2. *Error signal*:

$$e_k = d_k - \hat{d}_k \tag{3.7}$$

3. *Coefficients adaptation*:

$$\mathbf{c}_{k+1} = \mathbf{c}_k + \mu\, e_k\, \mathbf{x}_k^* \tag{3.8}$$

where e_k is the error signal defined as the difference between the kth transmitted symbol d_k and its corresponding estimate $\hat{d}_k$ at the output of the equalizer, and μ is the step size parameter. It is well known that the step size parameter μ controls the rate of adaption of the equalizer as well as the stability of the LMS algorithm.

For stability, the value of μ is chosen from [4]

$$0 < \mu < \frac{2}{\lambda_{\max}} \tag{3.9}$$

where $\lambda_{\max}$ is the largest eigenvalue of the signal correlation matrix. A choice of μ just below the upper limit in Equation (3.9) provides rapid convergence, but meanwhile it also introduces large fluctuations in the equalizer coefficients during steady-state operation. These fluctuations constitute a form of self-noise whose variance increases with an increase in μ. As a consequence, the choice of μ is a trade-off between rapid convergence and the desirability to keep the variance of self-noise small.

The convergence rate of the LMS is slow due to the fact that there is only one single parameter, namely μ to control the rate of adaptation. To achieve faster convergence, complex algorithms which involve additional parameters are used. A faster converging algorithm can be obtained if a recursive least squares (RLS) algorithm is employed for adjustment of the equalizer coefficients. For the linear FIR equalizer, the RLS algorithm that is obtained for the minimization of the sum of exponentially weighted squared errors, i.e.,

$$\mathbf{J} = \sum_{n=0}^{k} \lambda^{k-n} \left| d_n - \mathbf{c}_k^T \mathbf{x}_n \right|^2 \tag{3.10}$$

may be expressed as [4]

1. *Compute equalizer output*:

$$\hat{d}_k = \mathbf{c}_{k-1}^T \mathbf{x}_k \tag{3.11}$$

2. *Compute error signal*:

$$e_k = d_k - \hat{d}_k \tag{3.12}$$

3. *Compute Kalman gain vector*:

$$\mathbf{k}_k = \frac{\mathbf{P}_{k-1}\mathbf{x}_k^*}{\lambda + \mathbf{x}_k^T \mathbf{P}_{k-1}\mathbf{x}_k^*} \tag{3.13}$$

4. *Update inverse of the correlation matrix*:

$$\mathbf{P}_k = \frac{1}{\lambda}\left[\mathbf{P}_{k-1} - \mathbf{k}_k \mathbf{x}_k^T \mathbf{P}_{k-1}\right] \tag{3.14}$$

5. *Update equalizer coefficients*:

$$\mathbf{c}_k = \mathbf{c}_{k-1} + \mathbf{k}_k\, e_k \tag{3.15}$$

$$= \mathbf{c}_{k-1} + \mathbf{P}_k\, \mathbf{x}_k^*\, e_k \tag{3.16}$$

Here the exponential weighting factor or forgetting factor, λ, is selected to be in the range of $0 < \lambda < 1$, and provides a fading memory in the estimation of the optimum equalizer coefficients. $\mathbf{P}_k$ is an $(N \times N)$ square matrix which is the inverse of the data autocorrelation matrix:

$$\mathbf{R}_k = \sum_{n=0}^{k} \lambda^{k-n}\, \mathbf{x}_n^*\, \mathbf{x}_n^T \tag{3.17}$$

Initially $\mathbf{P}_0$ may be selected to be proportional to the identity matrix.

The above-described LMS and RLS algorithms are both employed in our ensuing work to adaptively update the equalizer coefficients. However, as the received symbols are collected in blocks at the receiver, these adaptive algorithms, will be accordingly implemented in a block level and are hereby called block LMS (BLMS) and block RLS (BRLS) algorithms. Details about the BLMS and BRLS algorithms together with their applications in adaptive equalization will be given in Chapter 6.

3.3 Frequency-Domain Equalization

At the very beginning of this thesis, we have introduced the technique of frequency-domain equalization (FDE) which offers a large reduction in the computational complexity. So far there exists a number of literature devoted to the topic of FDE or its related applications [8]-[19], and the FDE in these various published literature shares the similarities of using the computationally-efficient FFT operations. However, after a thorough literature survey, we found that the rationales behind the available FDE techniques are not exactly the same, and they can be divided into two unique types. The first type of FDE, in its nature, is a fast (numerically efficient) implementation of the block-adaptive filter by using well-known frequency domain overlap-save or overlap-add processing methods [44]. Examples of this type can be found in [8], [10], [39], [40], etc. The other type is largely based on the important eigen-decomposition property of circulant matrices [43], and examples are available in [11], [14], [17], [18], etc. In the following, we will present a description and comparison of the above-mentioned two FDE methods.

3.3.1 FDE Based on Block-adaptive Filter

The conventional LMS algorithm that was previously introduced in Section 3.2 with application in adaptive equalization usually updates the filter coefficients on a sample-by-sample basis. As a consequence, this algorithm may seem inadequate for a block-adaptive filter in which the tap weights are updated after the collection of each block of data samples, so that adaption of the filter should proceed on a

block-by-block basis instead. Figure 3.4 depicts the block diagram of such a block-adaptive filter. As can be seen from this diagram, the incoming data sequence $u(n)$

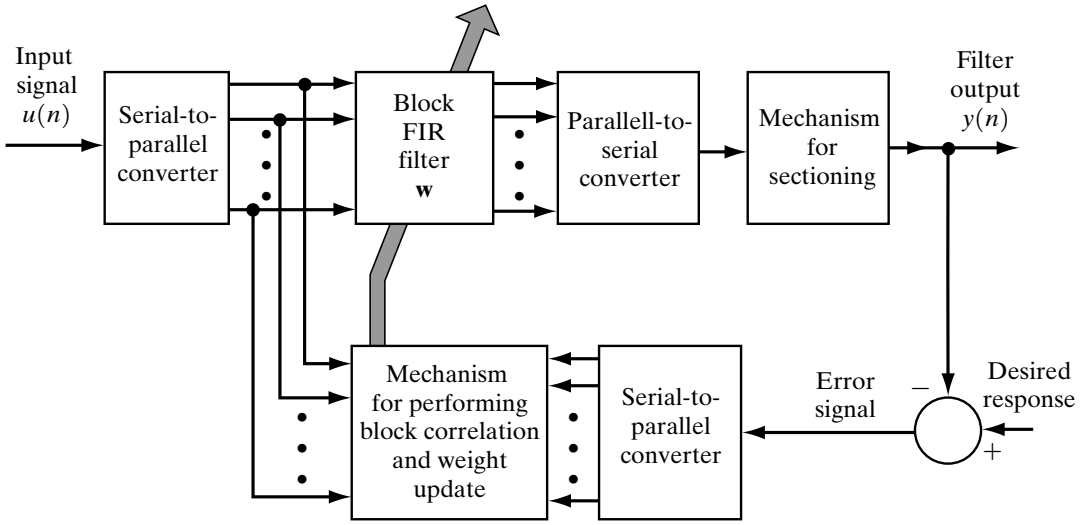

Figure 3.4: Block-adaptive filter (Taken from [42])

is sectioned into L-point blocks by means of a serial-to-parallel converter, and the blocks of input data so produced are applied to an FIR filter of length M, one block at at a time.

One generalized form of the LMS algorithm, i.e., block LMS (BLMS) algorithm can be used to adapt the block-adaptive filter [42]. Using k to denote the block index, this BLMS recursion is given by

$$\mathbf{w}(k+1) = \mathbf{w}(k) + \mu \sum_{i=0}^{L-1} \mathbf{u}^*(kL+i)e(kL+i). \tag{3.18}$$

where μ is the algorithm step-size parameter and $\mathbf{u}(kL+i)$ is the column vector of the input signal. The output produced by the filter in response to the signal vector $\mathbf{u}(kL+i)$ is given by

$$y(kL+i) = \mathbf{w}^T(k)\mathbf{u}(kL+i) \qquad i = 0, 1, \ldots, L-1, \tag{3.19}$$

where the filter tap-weight vector, $\mathbf{w}(k)$ is held constant for the duration of the data block. And the error signal

$$e(kL+i) = d(kL+i) - y(kL+i) \qquad i = 0, 1, \ldots, L-1, \tag{3.20}$$

is obtained by comparing the filter output against the desired response. For the sake of convenience we rewrite the Equation (3.18) as

$$\mathbf{w}(k+1) = \mathbf{w}(k) + \mu\boldsymbol{\phi}(k). \tag{3.21}$$

The M-by-1 vector $\boldsymbol{\phi}(k)$ is a cross-correlation vector given by

$$\begin{aligned} \boldsymbol{\phi}(k) &= \sum_{i=0}^{L-1} \mathbf{u}^*(kL+i)e(kL+i) \\ &= \mathbf{A}^H(k)\mathbf{e}(k) \end{aligned} \tag{3.22}$$

where the H on $\mathbf{A}^H(k)$ signifies the Hermitian transposition (i.e., combined complex conjugation and transposition) of $\mathbf{A}(k)$, the $L \times M$ data matrix $\mathbf{A}(k)$ is defined by

$$\mathbf{A}(k) = [\mathbf{u}(kL), \mathbf{u}(kL+1), \ldots, \mathbf{u}(kL+L-1)]^T, \tag{3.23}$$

and the $L \times 1$ error signal vector $\mathbf{e}(k)$ is given by

$$\mathbf{e}(k) = [e(kL), e(kL+1), \ldots, e(kL+L-1)]^T. \tag{3.24}$$

The computation of the filter output in Equation (3.19) and the estimation of the gradient in Equation (3.22) are the operations of linear convolution and linear correlation, respectively, and they also constitute the areas where the computational burden of the BLMS algorithm lies. Since the FFT algorithm provides a powerful tool for performing fast convolution and fast correlation [44], we see that

it is feasible to employ the frequency-domain method for efficient implementation of the BLMS algorithm. Specifically, rather than performing the adaptation in the time domain as is done in the conventional LMS algorithm, the filter parameters are adapted in the frequency domain by using the FFT algorithm. The BLMS algorithm so implemented is referred to as the fast BLMS (FBLMS) algorithm. This type of adaptive filter is termed frequency-domain adaptive filter (FDAF), and its application to channel equalization can be referred to as FDE, which is the case in [39], [40], etc.

According to digital signal processing theory, there exist two well-known techniques for performing a linear convolution using FFT algorithms, and they are referred to as the overlap-save and overlap-add sectioning methods [44]. However, the overlap-add method has been found to be computationally less efficient than the overlap-save method when applied to the implementation of the BLMS algorithm [41]. Also, it is noteworthy that although the filter can be implemented with any amount of overlap, the use of 50% percent overlap (i.e., block size equal to the number of weights) is the most efficient. Henceforth, implementation of the FBLMS algorithm is commonly based on the overlap-save method with 50% overlap. Figure 3.5 shows a signal-flow graph representation of the FBLMS algorithm [9], and it can be seen that this algorithm represents a precise frequency-domain implementation of the BLMS algorithm. Due to the limited space, details about the implementation of the FBLMS algorithm as well as the overlap-save method are not covered here; readers can refer to [8] and [9] for more details.

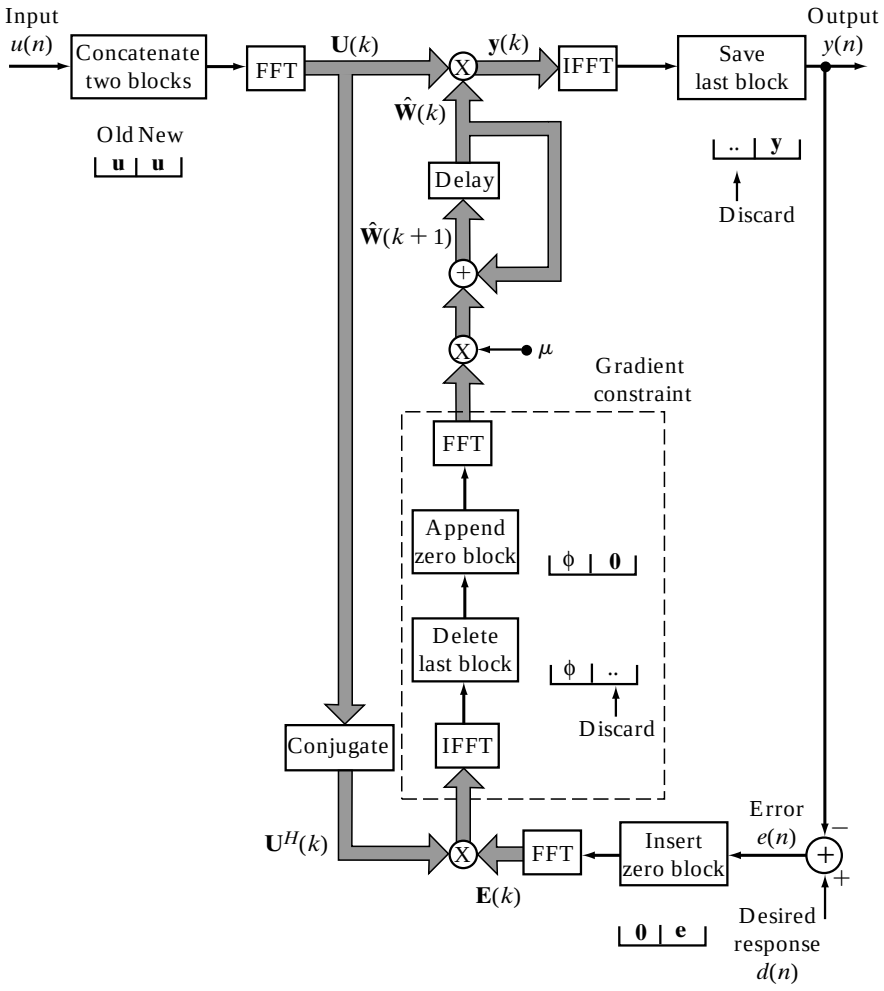

Figure 3.5: Implementation of the FBLMS algorithm (Taken from [42])

3.3.2 FDE Based on Circulant Matrices

Channel induced ISI is a major performance limiting factor for transmissions over wireless dispersive media. To mitigate such a a time-domain dispersive effect that gives rise to frequency selectivity, it proves useful to transmit the data symbols in blocks [45]. Here we consider single-carrier block transmission over an additive-noise frequency-selective channel with memory (or channel order) v, and its equalization, as shown later, can be implemented in the frequency domain.

We assume the channel impulse response (CIR) is constant over a block of length $(N + v)$, and may be varied from block to block. We also assume that each

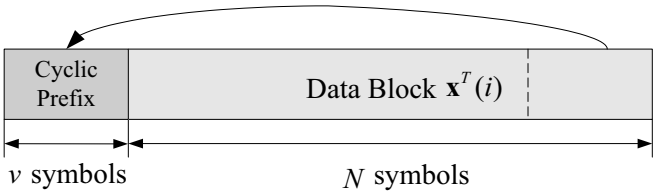

Figure 3.6: CP-based block transmissions

data block of length $N \gg v$ is preceded by a length-v cyclic prefix (CP) as depicted in Figure 3.6. The interblock interference (IBI) can be eliminated at the receiver by discarding the received symbols corresponding to the CP. Hence, out of every $(N + v)$ received symbols, only N symbols are processed.

Let us define the ith transmitted block to be

$$\mathbf{x}(i) = [x(iN), x(iN + 1), \ldots, x(iN + N - 1)]^T, \tag{3.25}$$

and the ith received block as

$$\mathbf{y}(i) = [y(iN), y(iN + 1), \ldots, y(iN + N - 1)]^T. \tag{3.26}$$

With symbol rate sampling, let $\mathbf{h} = [h(0), h(1), \ldots, h(v)]^T$ be the equivalent discrete-time CIR (that includes transmit-receive filters as well as multipath effects). Thus, the CP insertion at the transmitter together with CP removal at the reciever yields the following channel input-output relationship in matrix-vector form:

$$\mathbf{y}(i) = \mathbf{H}\mathbf{x}(i) + \mathbf{n}(i) \tag{3.27}$$

where $\mathbf{n}(i)$ is the corresponding noise vector with a size of $N \times 1$. The input symbols and noise are assumed to be complex, zero-mean, and uncorrelated with variance

σ_x^2 and σ_n^2, respectively. The $N \times N$ channel matrix $\mathbf{H}$ is circulant with its (k,l)th entry given by $h(\,(k-l)\ mod\ N)$; or looks like

$$\mathbf{H} = \begin{bmatrix} h(0) & 0 & \cdots & h(v) & \cdots & h(1) \\ h(1) & h(0) & \ddots & 0 & \ddots & \vdots \\ \vdots & h(1) & \ddots & \vdots & \ddots & h(v) \\ h(v) & \vdots & \ddots & h(0) & \ddots & 0 \\ \vdots & h(v) & \ddots & \vdots & \ddots & \vdots \\ 0 & \cdots & \cdots & h(v-1) & \cdots & h(0) \end{bmatrix} \tag{3.28}$$

Since $\mathbf{H}$ is a circulant matrix, it can be expressed in terms of its eigenvalues and associated eigenvectors, i.e., eigendecomposition, as follows [43]

$$\mathbf{H} = \mathbf{F}_N^H \mathbf{\Lambda} \mathbf{F}_N \tag{3.29}$$

where $\mathbf{F}_N$ is the orthonormal discrete Fourier transform (DFT) matrix whose (k,l)th entry is given by $\mathbf{F}_{k,l} = N^{-1/2}\exp(-j2\pi k\, l/N)$, where $0 \leq k,l \leq N-1$; and $\mathbf{\Lambda}$ is a diagonal matrix with its (k,k) element equal to the kth DFT coefficient of the CIR , i.e., $\mathbf{\Lambda}_{k,k} = \sum_{n=0}^{N-1} h(n)\, exp(-j2\pi n\, k/N)$. It is also noteworthy that the $N \times N$ matrix $\mathbf{F}_N$ is unitary, i.e., $\mathbf{F}_N^{-1} = \mathbf{F}_N^H$. The diagonal of $\mathbf{\Lambda}$ contains uniformly sampled samples of channel frequency response. This implies that when nulls of the channel frequency response are not sampled, $\mathbf{H}$ is full rank and invertible, and thus the symbol detectability can be guaranteed [45].

After discarding CP at the receiver, the received time-domain block $\mathbf{y}(i)$ is transformed to the frequency domain by means of N-point DFT operations, as shown in Figure 3.7. Then, based on the eigen-decomposition property of circulant

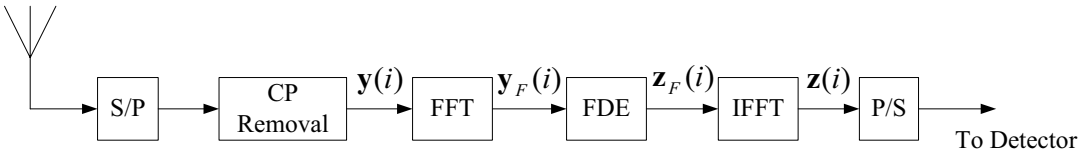

Figure 3.7: FDE receiver block diagram

matrix $\mathbf{H}$, the input-output relationship can be described as

$$\begin{aligned} \mathbf{y}_{\mathcal{F}}(i) &= \mathbf{F}_N \mathbf{y}(i) = \mathbf{F}_N \mathbf{F}_N^H \mathbf{\Lambda} \mathbf{F}_N \mathbf{x}(i) + \mathbf{F}_N \mathbf{n}(i) \\ &= \mathbf{\Lambda} \mathbf{x}_{\mathcal{F}}(i) + \mathbf{n}_{\mathcal{F}}(i) \end{aligned} \tag{3.30}$$

where $\mathbf{x}_{\mathcal{F}}(i)$ and $\mathbf{n}_{\mathcal{F}}(i)$ are N-point DFT of $\mathbf{x}(i)$ and $\mathbf{n}(i)$, respectively. Since elements in Equation (3.30) are purely expressed in the frequency domain, it is desirable here to implement equalization in the frequency domain by sample-by-sample multiplication of the DFT of equalizer response with the DFT of received signal, rather than convolving the equalizer response with the received signal in time domain. The MMSE frequency-domain equalizer for this single-carrier transmission system is represented by the $N \times N$ diagonal matrix $\mathbf{W}_{MMSE}$:

$$\mathbf{W}_{MMSE} = \mathbf{\Lambda}^H \left(\mathbf{\Lambda} \mathbf{\Lambda}^H + \frac{1}{\text{SNR}} \mathbf{I}_N \right)^{-1} \tag{3.31}$$

where $\text{SNR} = \sigma_x^2 / \sigma_n^2$. The frequency-domain equalized output, denoted by $\mathbf{z}_{\mathcal{F}}(i) = \mathbf{W}_{MMSE}\, \mathbf{y}_{\mathcal{F}}(i)$, is transformed back to time domain by implementing the operations of inverse DFT (IDFT). The corresponding output is a $N \times 1$ vector $\mathbf{z}(i)$ given by

$$\begin{aligned} \mathbf{z}(i) &= \mathbf{F}_N^H \mathbf{z}_{\mathcal{F}}(i) \;=\; \mathbf{F}_N^H \mathbf{W}_{MMSE}\, \mathbf{y}_{\mathcal{F}}(i) \\ &= \mathbf{F}_N^H \mathbf{\Lambda}^H \left(\mathbf{\Lambda} \mathbf{\Lambda}^H + \frac{1}{\text{SNR}} \mathbf{I}_N \right)^{-1} \mathbf{\Lambda} \mathbf{F}_N \mathbf{x}(i) + \tilde{\mathbf{n}}(i) \end{aligned} \tag{3.32}$$

where $\tilde{\mathbf{n}}(i) = \mathbf{F}_N^H \mathbf{W}_{MMSE} \mathbf{F}_N \mathbf{n}(i)$. Define $\mathbf{G} = \mathbf{F}_N^H \mathbf{W}_{MMSE} \mathbf{F}_N$, then the $\mathbf{G}$, in nature, is the equivalent time-domain equalizer, i.e., it estimates $\mathbf{x}(i)$ from $\mathbf{y}(i)$. Finally $\mathbf{z}(i)$ is rendered to the detector, and hard decisions are made on $\mathbf{x}(i)$.

The above explication denotes another type of FDE which is available in [11], [16], [17], [18] and so on. This type of FDE (hereafter refereed to as Type II), shares a lot of similarities with the previously described FDE (hereafter refereed to as Type I) that is based on block-adaptive filter, which includes the following:

- Both types belong to the category of block equalization, i.e., equalization is carried out on a block-by-block basis, rather than sample-by-sample basis.

- Both types induce redundancy when converting linear convolution (or linear correlation) to circular convolution, which is essential for the implementation of FFT. In Type I, the redundancy takes the form of 50% percent overlap; while Type II relies on the CP which consists of redundant symbols replicated at the beginning of each transmitted block.

- Both types of FDE utilize FFT to achieve savings in the computational complexity. Although in above description of Type II we state only the use of orthonormal DFT, it is obvious that this orthonormal DFT can be readily computed by means of FFT.

- Equalization for either type is performed by element-by-element multiplication of the transformed input with the frequency-domain equalizer coefficients. Hard decisions are identically made in time domain, which is different

from another technique of OFDM where FFT or IFFT operations are also employed, but decisions are made in the frequency domain.

However, rationales for these two types are quite different. The Type I, as previously pointed out, is a fast implementation of the block-adaptive filter. This type of FDE does not require special processing at the transmitter as Type II does, e.g., block transmissions and appending CP. It works quite similarly with the ordinary adaptive equalizers, but in a comparatively more efficient way. Therefore, its emphasis is solely placed on the efficient implementation of block adaptive filters. The other type of FDE, on the contrary, deploys block transmissions at the transmitter, and relies on CP to facilitate the construction of a circulant channel matrix. Then the eigen-decomposition property of circulant matrices is utilized in conjunction with FFT operations, and as a consequence, frequency equalization can be applied to the transformed equalizer input. It is obvious that this type of FDE involves both transmitter design and receiver processing, which is different from Type I.

In this thesis, we only consider the FDE of Type II. And the FDE hereafter used in the remaining of this thesis denotes only the Type II.

3.4 Summary

In this chapter, we introduced several different types of equalization methods that will be covered in the remainder of the thesis, including linear and nonlinear equalization, adaptive equalization and FDE. Among these equalization methods, our

focus was placed on the FDE. We categorized the FDE techniques that ever appear in the literature into two types, and their similarities and differences were also examined in detail.

Chapter 4

STBC for Fading Channels

Besides implementing equalization to combat the ISI that results from frequency-selective fading channels, we can further ameliorate the effects of fading and strive to approach AWGN performance by using some form of diversity or channel coding, as suggested in [37]. In this chapter, we proceed to discuss space-time block coding (STBC), a marvellous technique that can provide both diversity and coding gains. Before our discussion of STBC as well as its application in fading channels, we first present a brief introduction on the diversity techniques.

4.1 Concept of Diversity

Diversity is a powerful communication technique that can be used to improve received signal quality or the link performance in hostile mobile radio environments. It exploits the random nature of radio propagation by providing the receiver with independent (or at least highly uncorrelated) renditions of the signal. Concept of

the diversity is rather simple. If one radio path experiences a deep fade, another independent path may have a strong signal. Therefore, if the receiver can be supplied with several replicas of the same information signal transmitted over independently fading channels, the probability that all the signal components will fade simultaneously is reduced considerably. There are several ways in which diversity can be implemented to provide the receiver with independently fading replicas of the same information-bearing signal. Some of them are time diversity, frequency diversity and space diversity.

Time and frequency diversity normally introduce redundancy in time and/or frequency domain, therefore, they may induce loss in bandwidth efficiency [46]. As for the space diversity, which is usually accomplished by deploying multiple antennas at the transmitter and/or the receiver, it can reduce the effect of multipath fading without necessarily sacrificing precious bandwidth resources, and hence is a practical, effective and widely applied technique for wireless systems. Depending on whether multiple antennas are used for transmission or reception, space diversity can be divided into two categories: receive-antenna diversity and transmit-antenna diversity.

In receive-antenna diversity schemes, multiple antennas separated by a few wavelengths are employed at the receiver to obtain independent replicas of the transmitted signal. These signal replicas are then combined according to certain criteria to combat the loss in SNR. The methods for receiver-antenna diversity can be classified into distinct categories, and some of them are: selection diversity, maximal ratio combining and equal gain combining. Details about these methods

can be found in [2].

In practice, receive-antenna diversity, including the above-mentioned three schemes, has been deployed in several wireless systems such as GSM and IS-136 to improve the up-link (from mobiles to base stations) transmissions [47]. However, due to the cost, size and power limitations of the remote units, diversity techniques have almost exclusively been applied to base stations to improve their reception quality [20]. Consequently, the down-link (from base stations to mobiles) becomes the capacity bottleneck in modern wireless systems This situation has motivated rapidly growing research efforts on transmit-antenna diversity.

Transmit-antenna diversity deploys multiple antennas at the transmitter and is suitable for down-link transmission because having even a large number of antennas at base stations can still be feasible and economical. But as opposed to the frequently used receive-antenna diversity, there have been only a few industrial applications exploiting transmit diversity [49]. This is partly due to the existence of two major obstacles to implement transmit diversity [46]: (i) unlike the receiver, the transmitter does not have instantaneous information about the fading channels; (ii) the transmitted signals from different antennas will interfere with each other in space domain before they arrive at the receiver. Hence, to exploit the diversity from multiple transmissions, transmit diversity schemes must rely on some additional processing on the signal to be transmitted. So far, a number of transmit diversity schemes have been proposed, and can be classified into three general categories: (i) schemes using feedback; (ii) schemes invoking feedforward or training information; (iii) blind schemes. Details of these schemes can be found in [22] or

[48].

Recently, Tarokh et al. proposed space-time trellis (STT) coding that can provide both the diversity advantage of multiple transmit antennas and coding gains by jointly considering the channel coding, modulation, transmit and receiver diversity in their designs[22, 48]. STT codes perform quite well at the cost of relatively high complexity. In addressing the issue of decoding complexity, Alamouti [20] introduced a remarkable transmit diversity scheme which improves the signal quality at the receiver by simple processing across two antennas at the transmitter. This scheme, together with its improved versions (for block transmissions over frequency-selective fading channels) will be given in detail in the following sections.

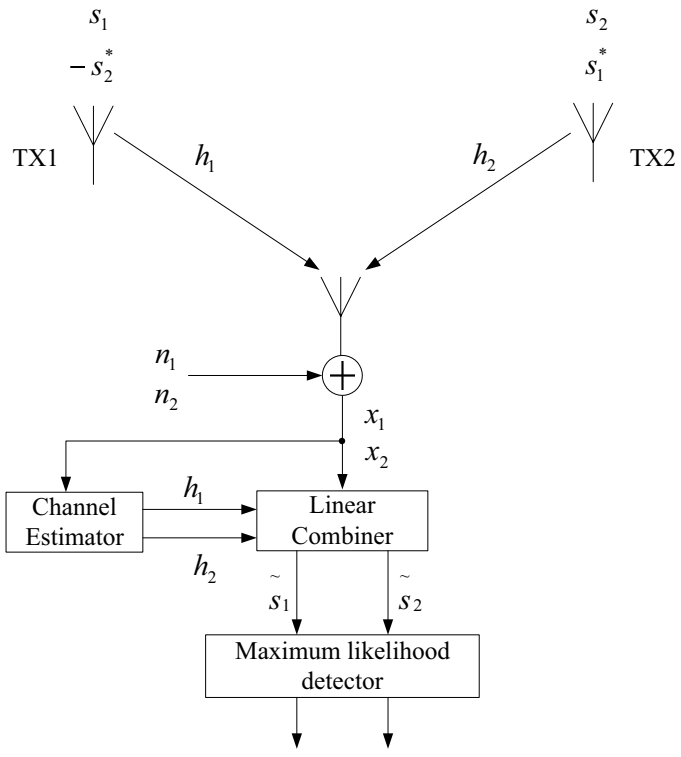

Figure 4.1: Illustration of the simple two-transmitter STBC scheme

4.2 STBC for Flat Fading Channels

This section presents the Alamouti's STBC scheme as defined in [20]. Let us consider the 2-TX 1-RX case. Figure 4.1 shows baseband representation of this scheme. The input symbols to the block encoder are divided into groups of two symbols each. At a given symbol period, two symbols are simultaneously transmitted from the antennas TX1 and TX2. The signal transmitted from antenna TX1 is s_1, and the signal transmitted from antenna TX2 is s_2. In the next symbol period, the signals $-s_2^*$ and s_1^* are simultaneously transmitted from antennas TX1 and TX2, respectively. This encoding and transmission process is also shown in Table 4.1.

Table 4.1: Encoding and transmission sequence for STBC

	time t	time $t+T$
TX1	s_1	$-s_2^*$
TX2	s_2	s_1^*

Let h_1 and h_2 denote the channels from the first and second transmit antennas to the receive antenna, respectively. Assuming the channel fading remains constant over the corresponding two consecutive symbols, we can write

$$h_1(t) = h_1(t+T) = h_1 = |h_1|e^{j\,\theta_1} \tag{4.1}$$

$$h_2(t) = h_2(t+T) = h_2 = |h_2|e^{j\,\theta_2} \tag{4.2}$$

where T is the symbol duration. Then the signals received over nondispersive or

narrow-band channels can be expressed as

$$x_1 = h_1 s_1 + h_2 s_2 + n_1 \tag{4.3}$$

$$x_2 = -h_1 s_2^* + h_2 s_1^* + n_2 \tag{4.4}$$

where x_1 and x_2 denote the first and second received signals, respectively; n_1 and n_2 represent the AWGN and are modelled as i.i.d. complex Gaussian random variables with zero mean and power spectral density $N_0/2$ per dimension. We define the received signal vector $\mathbf{x} = [x_1 \;\; x_2^*]^T$, the code symbol vector $\mathbf{s} = [s_1 \;\; s_2]^T$, and the noise vector $\mathbf{n} = [n_1 \;\; n_2^*]^T$. Then Equation (4.3) and (4.4) can be rewritten in a matrix form as

$$\mathbf{x} = \mathbf{H}\mathbf{s} + \mathbf{n} \tag{4.5}$$

where the channel matrix $\mathbf{H}$ is given by

$$\mathbf{H} = \begin{bmatrix} h_1 & h_2 \\ h_2^* & -h_1^* \end{bmatrix} \tag{4.6}$$

and the vector $\mathbf{n}$ is a complex Gaussian random vector with zero mean and covariance $N_0 \cdot \mathbf{I}$.

Since the channel matrix $\mathbf{H}$ is orthogonal, that is

$$\mathbf{H}^H \mathbf{H} = \rho \mathbf{I} \tag{4.7}$$

where $\rho = |h_1|^2 + |h_2|^2$, then the received signal can be decoupled by premultiplication the Hermitian of channel matrix, and we can obtain

$$\begin{aligned} \tilde{\mathbf{s}} &= \mathbf{H}^H \mathbf{x} \\ &= \mathbf{H}^H \mathbf{H}\mathbf{s} + \mathbf{H}^H \mathbf{n} \\ &= \rho \mathbf{s} + \tilde{\mathbf{n}}. \end{aligned} \tag{4.8}$$

Here $\tilde{\mathbf{s}}$ is defined as $\tilde{\mathbf{s}} = [\tilde{s}_1 \;\; \tilde{s}_2]^T$, where $\tilde{s}_1$ and $\tilde{s}_2$ are soft decisions for transmitted signals s_1 and s_2, respectively. The vector $\tilde{\mathbf{n}}$, defined as $\tilde{\mathbf{n}} = \mathbf{H}^H\mathbf{n}$, has a zero mean and covariance ρN_0, i.e., the elements of $\tilde{\mathbf{n}}$ are independent and identically distributed. Equation (4.8) can be expressed in element form as given by

$$\begin{aligned} \begin{bmatrix} \tilde{s}_1 \\ \tilde{s}_2 \end{bmatrix} &= \begin{bmatrix} h_1^* & h_2 \\ h_2^* & -h_1 \end{bmatrix} \begin{bmatrix} x_1 \\ x_2^* \end{bmatrix} \\ &= \begin{bmatrix} h_1^* x_1 + h_2 x_2^* \\ h_2^* x_1 - h_1 x_2^* \end{bmatrix}. \end{aligned} \tag{4.9}$$

Equation (4.9) specifically denotes the linear combination performed at the receiver, which consists of only simple signal processing to extract the signal s_1 and s_2 from the received signals x_1 and x_2, as well as to separate them. It is noteworthy that such implementation of decoupling the symbols transmitted requires knowledge of the channel at the receiver. The channel state information can be obtained by sending training or pilot symbols or sequences for the receiver to estimate the channel from each of the transmitter antennas to the receive antenna.

The combiner output, i.e., the soft decisions of $\tilde{s}_1$ and $\tilde{s}_2$, is then passed to the maximum likelihood detector of Figure. 4.1. Let us define $\mathcal{S}$ as the set of all possible transmitted symbol pairs $\hat{\mathbf{s}} = \{s_1, \; s_2\}$. Assuming that all symbol pairs are equiprobable, the maximum likelihood decision rule can be expressed as

$$\hat{\mathbf{s}} = \arg \min_{\hat{\mathbf{s}} \in \mathcal{S}} \parallel \tilde{\mathbf{s}} - \rho\, \hat{\mathbf{s}} \parallel . \tag{4.10}$$

In this case, the diversity order provided by this scheme is 2, which is equal to that of two-branch of maximal-ratio receive combining (MRRC) scheme [20].

Above is the example of the encoding and decoding process for Alamouti's STBC scheme using only one receiver. However, this example can be readily extended to an arbitrary number of receivers, as shown in [20]. It can be further generalized to an arbitrary number of transmit antennas. For discussion about the generalized STBC schemes, readers can refer to [21].

4.3 STBC for Frequency-Selective Fading Channels

4.3.1 Review of Papers in the Literature

In the last section, we have described the Alamouti's STBC scheme [20] that using two transmit and only one receive antenna achieves similar diversity gain at the subscriber as that can be achieved by using one transmit and two receive antennas. However, this scheme assumes that there is no ISI in the channel, which will not be the case if the channel experiences a nonnegligible delay spread, consequently giving rise to frequency selectivity. Such fact necessitates well designed STBCs for single-carrier transmissions over frequency-selective fading channels. On the other hand, since we intend to combine the techniques of STBC and FDE together to realize broadband equalization by exploiting their benefits, it is desirable if the STBC scheme could facilitate the implementation of equalization in the frequency domain. In the following, we present a brief review of some related published literature on the STBC design for frequency-selective fading channels together with their possible links to FDE.

Lindskog et al. [27] developed a time-reversal space-time block coding (TR-

STBC) method which is similar to the Alamouti's scheme in [20], but can handle channels with ISI by imposing the Alamouti orthogonal structure at a block and not at a symbol level. However, in [27], this TR-STBC scheme was not linked to FDE, as its equalization and decoding were mostly implemented in time domain rather in frequency domain.

In [28], Vook et al. proposed a simple time-domain transmission scheme which allows the space-time encoding and decoding to be carried out in the frequency domain for single carrier systems over high delay spread channels. Two frequency-domain equalized single-carrier systems were treated in their paper: one has OFDM-type CP and the other has prefixes consisting of all zero symbols. Their work, to the best of our knowledge, is the first to combine the SC-FDE with STBC, although the authors have not explicitly claimed it.

It was Al-Dhahir [29] who first explicitly proposed the idea of single-carrier frequency-domain equalized space-time block-coding (SC FDE-STBC), i.e., incorporating the STBC with SC-FDE to exploit their joint benefits. The algorithm employed in this FDE technique is based on the MMSE criterion that is the same as in [28]. The single-carrier system in [29] is cyclic prefixed, which is only one of the cases described in [28].

Recently, Zhou et al. [31] investigated the design of STBCs for single-carrier block transmissions in the presence of frequency-selective fading channels. They proposed novel transmission formats which subsume those in [27], [28], [29], as special cases. Their new schemes can be readily applied to single carrier modulation systems in conjunction with the frequency equalization, similar to those in [28] and

[29]. Their schemes are also claimed to be capable of achieving a maximum diversity of order $N_t N_r(L+1)$ in rich scattering environment, where N_t is the number of transmit antennas, N_r is the receive antennas, and $(L+1)$ is the number of taps corresponding to each FIR channel.

As counterparts of orthogonal STBCs [20, 21], but for frequency-selective fading channels, the schemes in [31] are of special interest due to their smooth linkage with FDE as well as their generality as compared with those in [27], [28] or [29]. Therefore in this thesis, we adopt the STBC technique in [31] for our transmitter design. And our ensuing equalization schemes, including the channel estimation based FDE and the adaptive FDE, are accordingly designed for such space-time block-coded single-carrier transmissions over frequency-selective fading channels.

4.3.2 STBC Block Transmissions

Now let us describe the transmission formats used in this thesis, together with some preliminary signal processing techniques at the receiver. The relevant and effective method of suppressing the ISI will be introduced in the later chapters. It is also necessary to note that although we adopt the schemes as described in [31], the transmission signals described here may be slightly different from those in [31] since we intend to apply them to some existing communication systems. Before beginning our work, we first introduce some common notations that will be employed in the context to facilitate our following explanation. We use bold upper case letters to denote matrices, while bold lower case letters signify column vectors. Superscript $\{\cdot\}^H$, $\{\cdot\}^*$ and $\{\cdot\}^T$ denote Hermitian, conjugate and transpose, respectively. $\mathbf{I}_K$

denotes the identity matrix of size $K \times K$, $\mathbf{0}_{M\times N}$ denotes an all-zero matrix with size $M \times N$, and $\mathbf{F}_N$ denotes an $N \times N$ orthonormal DFT matrix whose (p, q) th entry is given by $N^{-1/2}\exp(-j2\pi p\, q/N)$, where $0 \leq p,\, q \leq N-1$. diag$(\mathbf{x})$ stands for a diagonal matrix with $\mathbf{x}$ on its main diagonal. We use $[\mathbf{x}]_p$ to denote the p th entry of a vector $\mathbf{x}$, and $[\mathbf{A}]_{p,\,q}$ to denote the $(p,\, q)$ th entry of a matrix $\mathbf{A}$.

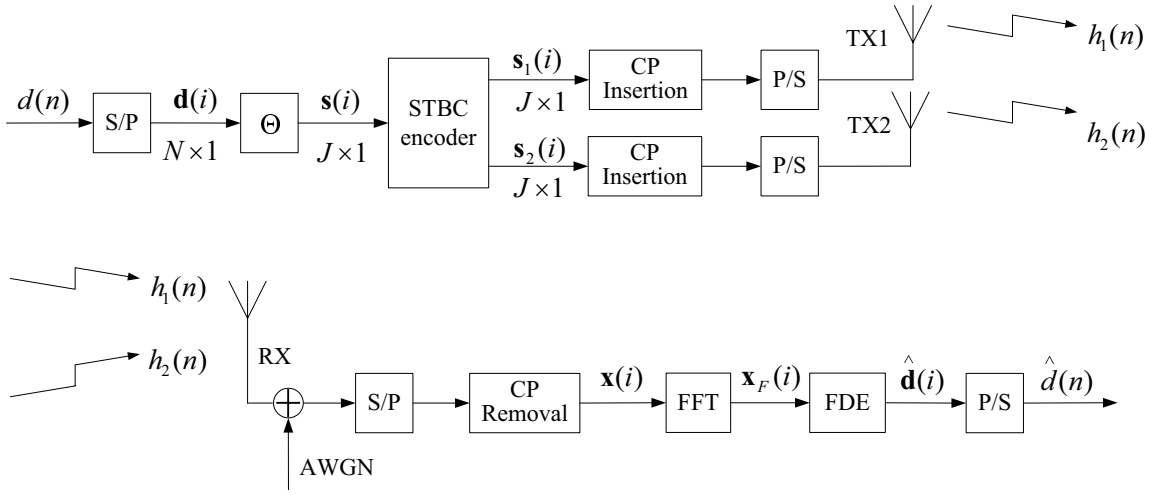

Figure 4.2: Single-carrier STBC baseband transceiver model

Figure. 4.2 depicts the baseband representation of the discrete-time equivalent model of a communication system with two transmit antennas and one receive antenna. Here we place the emphasis on the 2-TX 1-RX case only, and it in fact, can be generalized to more than two transmit antennas and multiple receive antennas; readers are referred to [31].

The information bearing data symbols $d(n)$ are first parsed into $N \times 1$ blocks $\mathbf{d}(i)$ given by

$$\mathbf{d}(i) = [d(iN),\ d(iN+1),\ \ldots,\ d(iN+N-1)]^T, \tag{4.11}$$

where the serial index n in $d(n)$ is related to the block index i in $\mathbf{d}(i)$ by

$$n = iN + j, \qquad j \in [0, N-1] \tag{4.12}$$

The blocks $\mathbf{d}(i)$ are then precoded by a $J \times N$ matrix Θ, whose entries can be in the complex field. Such precoding yields

$$\mathbf{s}(i) = \Theta\, \mathbf{d}(i), \tag{4.13}$$

where $\mathbf{s}(i)$ is a $J \times 1$ vector. It is noted here that the linear processing by Θ can be either redundant when $J > N$, or nonredundant when $J = N$. In this thesis, we consider both redundant and nonredundant cases, as will be described soon.

At the space-time encoder, two consecutive blocks $\mathbf{s}(2i)$ and $\mathbf{s}(2i+1)$ are taken as input, and output is a $2J \times 2$ STBC matrix, as shown in Table. 4.2. Here $\mathbf{P}$ is a

Table 4.2: STBC Encoding and block transmission sequence

	time slot $2i$	time slot $2i+1$
TX1	$\mathbf{s}_1(2i) = \mathbf{s}(2i)$	$\mathbf{s}_1(2i+1) = -\mathbf{P}\mathbf{s}^*(2i+1)$
TX2	$\mathbf{s}_2(2i) = \mathbf{s}(2i+1)$	$\mathbf{s}_2(2i+1) = \mathbf{P}\mathbf{s}^*(2i)$

permutation matrix which is drawn from a set of permutation matrices $\{\mathbf{P}_J^{(n)}\}_{n=0}^{J-1}$, with J denoting the dimensionality $J \times J$. Each $\mathbf{P}_J^{(n)}$ performs a reverse cyclic shift (which depends on the value of n) when applied to an arbitrary $J \times 1$ vector as given by

$$\mathbf{a} = [a(0),\ a(1),\ \ldots\ a(J-1)]^T, \tag{4.14}$$

and the pth element of $\mathbf{P}_J^{(n)}\mathbf{a}$ is expressed as

$$[\mathbf{P}_J^{(n)}\mathbf{a}]_p = a((J-p+n-1) \bmod J) \qquad p \in [0, J-1]. \tag{4.15}$$

We consider two important special cases of $\mathbf{P}_J^{(0)}$ $(n = 0)$ and $\mathbf{P}_J^{(1)}$ $(n = 1)$, respectively. The output of $\mathbf{P}_J^{(0)}\mathbf{a}$ is:

$$\mathbf{P}_J^{(0)}\mathbf{a} = [a(J-1),\ a(J-2),\ \ldots,\ a(0)]^T, \tag{4.16}$$

which performs the reverse of $\mathbf{a}$, while $\mathbf{P}_J^{(1)}\mathbf{a}$ is:

$$\begin{aligned} \mathbf{P}_J^{(1)}\mathbf{a} &= [a(0),\ a(J-1),\ a(J-2),\ \ldots,\ a(1)]^T && (4.17)\\ &= \mathbf{F}_J^H\mathbf{F}_J^H\mathbf{a} && (4.18) \end{aligned}$$

which corresponds to taking the J-point IFFT twice on the vector $\mathbf{a}$.[1] In the above notation, [27] uses only $\mathbf{P}_J^{(0)}$, [29] uses only $\mathbf{P}_J^{(1)}$, and [28] employs both $\mathbf{P}_J^{(0)}$ and $\mathbf{P}_J^{(1)}$. But the work in [31] allows the use of any $\mathbf{P}$ from the set of $\{\mathbf{P}_J^{(n)}\}_{n=0}^{J-1}$, which, in such sense, can be regarded as a generalized version of that in [27], [28] and [29].

As shown in Table 4.2, at each block transmit time interval i, the block $\mathbf{s}_1(i)$ and $\mathbf{s}_2(i)$ are forwarded to the first (TX1) and second (TX2) antenna, respectively. Then we have

$$\mathbf{s}_1(2i+1) = -\mathbf{P}\mathbf{s}_2^*(2i), \quad \mathbf{s}_2(2i+1) = \mathbf{P}\mathbf{s}_1^*(2i), \tag{4.19}$$

which indicates that each transmitted block from one antennas at time slot $2i+1$ is a conjugate and permuted version of the corresponding transmitted block from the other antenna at a time slot $2i$ (with a sign change for the first antenna). For flat fading channels, symbol blocking is unnecessary because there is no signal distortion, hence $J = N = 1$ and $\mathbf{P} = \mathbf{I}_1 = 1$, and the design in Table 4.2 reduces to the well known Alamouti's STBC scheme [20]. However, for frequency-selective

[1] Proof of this is provided in Appendix A, which is not available in [31].

multipath channels, the permutation matrix $\mathbf{P}$ is of great importance because it, together with the circulant channel matrix, makes possible the implementation of FFT as will be clarified later. Then the CP approach which inserts a CP for each block before transmission is adopted to avoid interblock interference (IBI) in the presence of frequency-selective multipath channels. The transmission sequences from both antennas are depicted in Fig. 4.3.

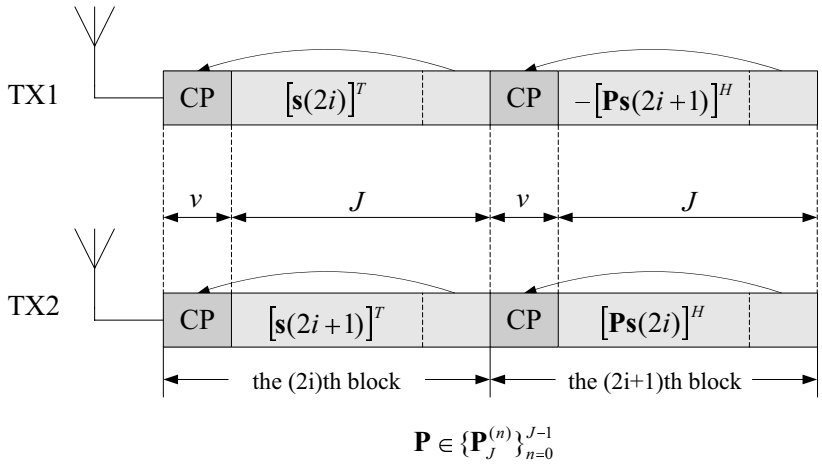

Figure 4.3: CP-based STBC block transmissions

Now let us consider the multipath channel. Before we elaborate further, it is necessary for us to make clear some assumptions regarding the channel. The channel here, is assumed to be frequency-selective, but its response remains time invariant over the transmission of a STBC burst (consisting of two consecutive data blocks), but can vary from burst to burst. That is, the channel is assumed to be quasi-static. With symbol rate sampling, we define $\mathbf{h}_\mu = [h_\mu(0),\ h_\mu(1),\ \ldots,\ h_\mu(v)]^T$ as the equivalent discrete-time channel impulse response between the transmit antennas and the single receive antenna, where v is

the channel order or channel memory. When the length of CP is chosen to be at least as long as the channel order, the IBI can be avoided at the receiver by simply discarding the received samples corresponding to the CP. Hence the CP insertion at the transmitter together with CP removal at the receiver yields the channel input-output relationship that could be expressed in matrix vector form as

$$\mathbf{x}(i) = \sum_{\mu=1}^{2} \mathbf{H}_\mu \mathbf{s}_\mu(i) + \mathbf{n}(i) \tag{4.20}$$

where the channel matrix $\mathbf{H}_\mu$ is circulant matrix with $[\mathbf{H}_\mu]_{p,\,q} = h_\mu((p-q)\, mod\, J)$, and the additive Gaussian noise $\mathbf{n}(i)$ is assumed to be white with each element having zero mean and variance of N_0.

In the following, two attractive properties of circulant matrices are presented. These properties are of special importance to this block-level space-time coding scheme, and will be exploited at the receiver for both space-time decoding and equalization.

1. As we have introduced earlier in Equation (3.29) of Section 3.3, circulant matrices can be diagonalized by FFT operations:

$$\mathbf{H}_\mu = \mathbf{F}_J^H \,\mathrm{diag}(\mathbf{h}_{\mu\mathcal{F}})\, \mathbf{F}_J \quad \text{and} \quad \mathbf{H}_\mu^H = \mathbf{F}_J^H \,\mathrm{diag}(\mathbf{h}_{\mu\mathcal{F}}^*)\, \mathbf{F}_J \tag{4.21}$$

where $\mathrm{diag}(\mathbf{h}_{\mu\mathcal{F}})$ is a $J \times J$ diagonal matrix with its diagonal given by

$$\mathbf{h}_{\mu\mathcal{F}} = [H_\mu(e^{j0}),\ \ldots,\ H_\mu(e^{j2\pi(J-1)/J})]^T. \tag{4.22}$$

That is, the pth entry of the vector $\mathbf{h}_{\mu\mathcal{F}}$ is the channel frequency response

$$H_\mu(z) = \sum_{l=0}^{v} h_\mu(l) z^{-l} \tag{4.23}$$

evaluated at the frequency of $z = e^{j2\pi p/J}$.

2. Pre- and postmultiplying the circulant channel matrix $\mathbf{H}_\mu$ by the permutation matrix $\mathbf{P}$ yields the transpose of $\mathbf{H}_\mu$:

$$\mathbf{P}\mathbf{H}_\mu\mathbf{P} = \mathbf{H}_\mu^T \quad \text{and} \quad \mathbf{P}\mathbf{H}_\mu^*\mathbf{P} = \mathbf{H}_\mu^H. \tag{4.24}$$

Proof of Equation (4.24) can be found in [31], therefore will not be repeated here.

In view of the space-time coded blocks satisfying Equation (4.19), now let us consider two consecutive received blocks, i.e., the $(2i)$ th and $(2i+1)$ th blocks as predefined in Equation (4.20):

$$\mathbf{x}(2i) = \mathbf{H}_1\mathbf{s}_1(2i) + \mathbf{H}_2\mathbf{s}_2(2i) + \mathbf{n}(2i) \tag{4.25}$$

$$\mathbf{x}(2i+1) = -\mathbf{H}_1\mathbf{P}\mathbf{s}_2^*(2i) + \mathbf{H}_2\mathbf{P}\mathbf{s}_1^*(2i) + \mathbf{n}(2i+1). \tag{4.26}$$

Then left-multiplying Equation (4.26) by $\mathbf{P}$, conjugating, and using the Property 2, we obtain

$$\mathbf{P}\mathbf{x}^*(2i+1) = -\mathbf{H}_1^H\mathbf{s}_2(2i) + \mathbf{H}_2^H\mathbf{s}_1(2i) + \mathbf{P}\mathbf{n}^*(2i+1). \tag{4.27}$$

Here it is noteworthy that without the permutation matrix $\mathbf{P}$ inserted at the transmitter, it would have been impossible to have the Hermitian form of the channel matrix appearing in Equation (4.27) which can facilitate the frequency-domain processing of the received blocks.

We make use of the Property 1 by multiplying the blocks $\mathbf{x}(i)$ with the FFT matrix $\mathbf{F}_J$ that implements the J-point FFT of the elements in $\mathbf{x}(i)$. Let us define

the following J-point FFT operations:

$$\mathbf{x}_{\mathcal{F}}(2i) = \mathbf{F}_J\mathbf{x}(2i), \quad \mathbf{x}^*_{\mathcal{F}}(2i+1) = \mathbf{F}_J\mathbf{P}\mathbf{x}^*(2i+1) \tag{4.28}$$

$$\mathbf{n}_{\mathcal{F}}(2i) = \mathbf{F}_J\mathbf{n}(2i), \quad \mathbf{n}^*_{\mathcal{F}}(2i+1) = \mathbf{F}_J\mathbf{P}\mathbf{n}^*(2i+1). \tag{4.29}$$

For notational convenience, we use $\mathbf{D}_1$ and $\mathbf{D}_2$ to denote the diagonal matrices $\text{diag}(\mathbf{h}_{1\mathcal{F}})$ and $\text{diag}(\mathbf{h}_{2\mathcal{F}})$, respectively. Then applying the Property 1 on both Equation (4.25) and Equation (4.27), we have the blocks in frequency-domain as given by:

$$\mathbf{x}_{\mathcal{F}}(2i) = \mathbf{D}_1\mathbf{F}_J\mathbf{s}_1(2i) + \mathbf{D}_2\mathbf{F}_J\mathbf{s}_2(2i) + \mathbf{n}_{\mathcal{F}}(2i) \tag{4.30}$$

$$\mathbf{x}^*_{\mathcal{F}}(2i+1) = -\mathbf{D}^*_1\mathbf{F}_J\mathbf{s}_2(2i) + \mathbf{D}^*_2\mathbf{F}_J\mathbf{s}_1(2i) + \mathbf{n}^*_{\mathcal{F}}(2i+1) \tag{4.31}$$

It should be noted here that the permutation, conjugation, and FFT operations on the received block $\mathbf{x}(i)$ do not introduce any information loss, and the additive noises in Equations (4.30) and (4.31) remain white [31]. This is important because it is the basis that our ensuing work of equalization relies on. We shall further point that the diagonal of $\mathbf{D}_1$ or $\mathbf{D}_2$ is of DFT, while the operations of $\mathbf{F}_J\mathbf{s}_1(i)$ etc., is actually the orthonormal FFT. Although both of them can be realized by FFT, they are actually different here.

By defining $\bar{\mathbf{x}}_{\mathcal{F}}(i) = [\mathbf{x}^T_{\mathcal{F}}(2i) \quad \mathbf{x}^H_{\mathcal{F}}(2i+1)]^T$, we can combine Equation (4.30) and Equation (4.31) together into a single block matrix-vector form, as shown below

$$\bar{\mathbf{x}}_{\mathcal{F}}(i) = \begin{bmatrix} \mathbf{D}_1 & \mathbf{D}_2 \\ \mathbf{D}^*_2 & -\mathbf{D}^*_1 \end{bmatrix} \begin{bmatrix} \mathbf{F}_J\mathbf{s}(2i) \\ \mathbf{F}_J\mathbf{s}(2i+1) \end{bmatrix} + \begin{bmatrix} \mathbf{n}_{\mathcal{F}}(2i) \\ \mathbf{n}^*_{\mathcal{F}}(2i+1) \end{bmatrix} \tag{4.32}$$

where the relationship of $\mathbf{s}_1(2i) = \mathbf{s}(2i)$ and $\mathbf{s}_2(2i) = \mathbf{s}(2i+1)$ have been used from the transmission design in Table 4.2.

In the following, we will consider two special schemes: the CP-only scheme and the ZP-only[2] scheme, which are specially important to our ensuing work.

CP-only

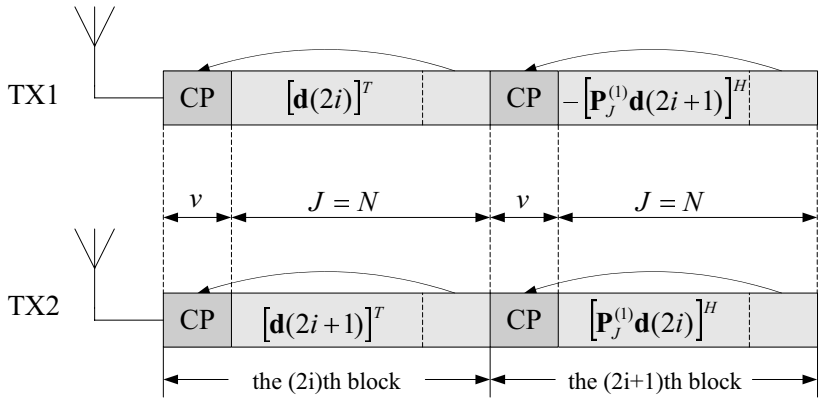

Figure 4.4: The CP-only scheme with $\Theta = \mathbf{I}_N$ and $\mathbf{P} = \mathbf{P}_J^{(1)}$

We use *CP-only* to denote the block transmissions without precoding, i.e., $\Theta = \mathbf{I}_N$, $J = N$, and $\mathbf{s}(i) = \mathbf{d}(i)$. Additionally we specifically use the permutation matrix $\mathbf{P}$ as $\mathbf{P}_J^{(1)}$. For this special case, we depict the transmission blocks from both antennas in Figure 4.4. Equation (4.26) can be rewritten as

$$\begin{aligned}
\mathbf{x}(2i+1) &= -\mathbf{H}_1\mathbf{P}_J^{(1)}\mathbf{s}_2^*(2i) + \mathbf{H}_2\mathbf{P}_J^{(1)}\mathbf{s}_1^*(2i) + \mathbf{n}(2i+1). \\
&= -\left[\mathbf{F}_J^H\mathbf{D}_1\mathbf{F}_J\right]\left[\mathbf{F}_J^H\mathbf{F}_J^H\mathbf{s}_2^*(2i)\right] + \left[\mathbf{F}_J^H\mathbf{D}_2\mathbf{F}_J\right]\left[\mathbf{F}_J^H\mathbf{F}_J^H\mathbf{s}_1^*(2i)\right] + \mathbf{n}(2i+1) \\
&= -\mathbf{F}_J^H\mathbf{D}_1\left[\mathbf{F}_J\mathbf{s}_2(2i)\right]^* + \mathbf{F}_J^H\mathbf{D}_2\left[\mathbf{F}_J\mathbf{s}_1(2i)\right]^* + \mathbf{n}(2i+1) \qquad (4.33)
\end{aligned}$$

where for the second equality, we rely on both the Property 1 and Equation (4.18), and for the third one, we note that $\mathbf{F}_J$ is a unitary symmetric matrix. To obtain

[2]Here ZP is the abbreviation of Zero Padding.

the FFT processed blocks similar as in Equation (4.31), it is obvious that we need only conjugation, and FFT operation on the received blocks $\mathbf{x}(2i+1)$, obviating the need for permutation operation. This benefit owes to Equation (4.18).

This CP-only scheme was also introduced in [28] and [29]. In this thesis, this scheme is mainly used for the training-based channel estimation as will be covered in the next chapter.

ZP-only

The CP-only scheme that we just discussed can be regarded to have linear nonre-

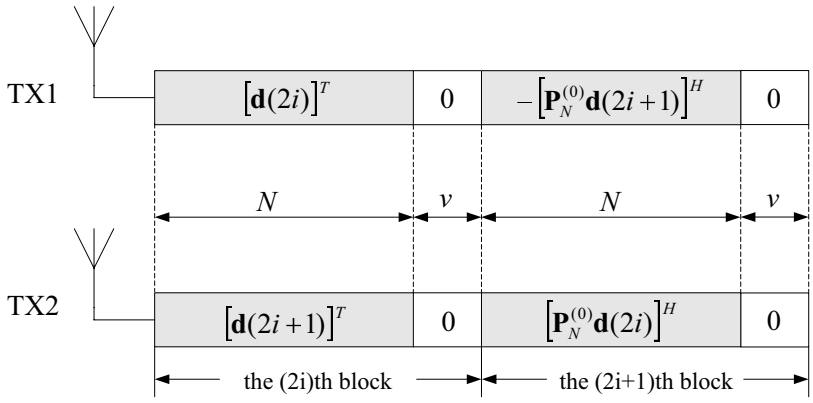

Figure 4.5: The ZP-only scheme with $\Theta = [\mathbf{I}_N^T \; \mathbf{0}_{v\times N}^T]^T$ and $\mathbf{P} = \mathbf{P}_J^{(N)}$

dundant precoding due to $J = N$. Now let us consider another case with redundant precoding where $J > N$. The precoder Θ is defined as

$$\Theta = [\mathbf{I}_N^T \quad \mathbf{0}_{v\times N}^T]^T, \tag{4.34}$$

where Θ is a $J \times N$ matrix, and $J = N + v$. Such precoding on data blocks $\mathbf{d}(i)$ yields $J \times 1$ symbol blocks $\mathbf{s}(i)$ as given by

$$\mathbf{s}(i) = \Theta\, \mathbf{d}(i) = \left[\mathbf{d}^T(i) \quad \mathbf{0}_{v\times 1}^T\right]^T. \tag{4.35}$$

This type of precoding corresponds to append each data block $\mathbf{d}(i)$ with v zeroes. As for the permutation matrix, we fix $\mathbf{P} = \mathbf{P}_J^{(N)}$. Then we have

$$\mathbf{P}_J^{(N)}\mathbf{s}(i) = \left[[\mathbf{P}_N^{(0)}\mathbf{d}(i)]^T \quad \mathbf{0}_{v\times 1}^T\right], \tag{4.36}$$

which implies that this permutation operation does not change the original position of the data block and zero block, and the data block is time reversed. The presence of these padding zero blocks in Equations (4.35) and (4.36) can avoid IBI as their length is equal to the channel order v. Therefore, the following CP-insertion operation at the transmitter can be removed; or from another point of view, we can regard the zero block from previous block as the CP for the current block. We term this special scheme as *ZP-only*, and the resulting transmission format is illustrated in Figure 4.5. In this thesis, this ZP-only scheme is adopted for data transmission format as will be detailed in the next chapter.

4.4 Summary

This chapter examined the technique of STBC. We started with a brief introduction of the diversity techniques, and it is followed by a description of Alamouti's STBC scheme, which is mainly designed for frequency flat fading channels. After that, we proceeded to the block STBC scheme that was proposed recently in the literature (a short literature review was also provided) for frequency-selective fading channels. This scheme is of interest as it can provide diversity gains as the Alamouti's original scheme does, and may facilitate the implementation of FDE, hence is adopted in our work for transmitter design. Additionally, we also introduced two specific block

STBC schemes: CP-only and ZP-only, which will be used in our ensuing work for data transmission and channel estimation, respectively.

Chapter 5

Channel Estimation Based FDE for STBC Transmissions

In the last chapter, we introduced the STBC block transmissions designed for multipath fading channels. Whereas, such transmitter design, if considered alone, cannot provide a satisfactory or AWGN-like performance since the ISI in the received signals have not yet been removed. As a result, some form of mitigation methods, such as equalization, remains necessary at the receiver to further improve the link quality, as we previously discussed in Chapter 3.

In this chapter, we proceed to the development of equalization schemes for STBC transmissions over multipath fading channels. Or specifically, we will look into some frequency-domain block equalization schemes implemented using FIR filterbanks. These schemes are developed to optimize the performance according to some specified criterion such as ZF or MMSE criterion. And knowledge of the channel is assumed to be fully known at the receiver. That is, these equalization

schemes need to perform channel estimation. Training based channel estimation is developed in this chapter.

5.1 Linear and Nonlinear ZF Equalization

Before our discussion on the FDE schemes, we introduce some preliminary processing blocks at the receiver, which can facilitate our development of equalization schemes. We reproduce here the result of Equation (4.32) from the last chapter:

$$\bar{\mathbf{x}}_{\mathcal{F}}(i) = \begin{bmatrix} \mathbf{D}_1 & \mathbf{D}_2 \\ \mathbf{D}_2^* & -\mathbf{D}_1^* \end{bmatrix} \begin{bmatrix} \mathbf{F}_J \mathbf{s}(2i) \\ \mathbf{F}_J \mathbf{s}(2i+1) \end{bmatrix} + \begin{bmatrix} \mathbf{n}_{\mathcal{F}}(2i) \\ \mathbf{n}_{\mathcal{F}}^*(2i+1) \end{bmatrix} \tag{5.1}$$

where $\mathbf{D}_1$ and $\mathbf{D}_2$ are both $J \times J$ diagonal matrices. Let us define

$$\mathbf{D} = \begin{bmatrix} \mathbf{D}_1 & \mathbf{D}_2 \\ \mathbf{D}_2^* & -\mathbf{D}_1^* \end{bmatrix} \tag{5.2}$$

and it is easy to verify that $\mathbf{D}$ is orthogonal, i.e.,

$$\mathbf{D}^H \mathbf{D} = \mathbf{I}_2 \otimes \mathbf{D}_{12}^2 \tag{5.3}$$

where $\otimes$ denotes Kronecker product, and $\mathbf{D}_{12}$ is a $J \times J$ diagonal matrix with its nonnegative diagonal entries given by

$$\mathbf{D}_{12} = [\mathbf{D}_1^H \mathbf{D}_1 + \mathbf{D}_2^H \mathbf{D}_2]^{1/2}. \tag{5.4}$$

To decouple the frequency-domain data block $\tilde{\mathbf{x}}_{\mathcal{F}}(i)$ as well as to keep the resulting noise remaining white, we can multiply $\tilde{\mathbf{x}}_{\mathcal{F}}(i)$ by a special unitary matrix $\mathcal{D}_U$ which is given by

$$\mathcal{D}_U = \mathbf{D}(\mathbf{I}_2 \otimes \mathbf{D}_{12}{}^{-1}). \tag{5.5}$$

Here we assume $\mathbf{h}_1$ and $\mathbf{h}_2$ do not share common zeros on the FFT grids, so that $\mathbf{D}_{12}$ is full rank and invertible. Then the unitary matrix $\mathcal{D}_U$ can be constructed as in Equation (5.5), we have

$$\mathcal{D}_U^H \mathcal{D}_U = \mathbf{I}_{2J} \text{ and } \mathcal{D}_U^H \mathbf{D} = \mathbf{I}_2 \otimes \mathbf{D}_{12}. \tag{5.6}$$

Multiplying Equation (5.1) by $\mathcal{D}_U^H$, we obtain

$$\begin{aligned} \bar{\mathbf{y}}_{\mathcal{F}}(i) &= \mathcal{D}_U^H \bar{\mathbf{x}}_{\mathcal{F}}(i) \\ &= \begin{bmatrix} \mathbf{D}_{12}\mathbf{F}_J\mathbf{s}(2i) \\ \mathbf{D}_{12}\mathbf{F}_J\mathbf{s}(2i+1) \end{bmatrix} + \mathcal{D}_U^H \begin{bmatrix} \mathbf{n}_{\mathcal{F}}(2i) \\ \mathbf{n}_{\mathcal{F}}^*(2i+1) \end{bmatrix} \end{aligned} \tag{5.7}$$

The resulting noise is given by

$$\begin{aligned} \bar{\boldsymbol{\eta}}_{\mathcal{F}}(i) &= \left[\boldsymbol{\eta}_{\mathcal{F}}^T(2i),\ \boldsymbol{\eta}_{\mathcal{F}}^T(2i+1)\right]^T \\ &= \mathcal{D}_U^H \left[\mathbf{n}_{\mathcal{F}}^T(2i),\ \mathbf{n}_{\mathcal{F}}^H(2i+1)\right]^T, \end{aligned} \tag{5.8}$$

and it is easy to verify that $\bar{\boldsymbol{\eta}}_{\mathcal{F}}(i)$ is still white since its autocorrelation matrix is diagonal. This decoupling process, in fact, performs the role of STBC decoder, as illustrated in Figure 5.1. We can simplify Equation (5.7) in subblock form:

$$\mathbf{y}_{\mathcal{F}}(i) = \mathbf{D}_{12}\mathbf{F}_J\mathbf{s}(i) + \boldsymbol{\eta}_{\mathcal{F}}(i). \tag{5.9}$$

Then the problem of developing FDE schemes for such STBC block transmissions is reduced to designing equalization schemes for the above subblock $\mathbf{y}_{\mathcal{F}}(i)$.

We also need to note here that, in the remaining of this thesis, the ZP-only scheme, as described in Chapter 4, is adopted as the transmission format for information-bearing data signals; that is, we have

$$\mathbf{s}(i) = \Theta\, \mathbf{d}(i) = \left[\mathbf{d}^T(i) \quad \mathbf{0}_{v\times 1}^T\right]^T, \tag{5.10}$$

where the precoder Θ is defined as $\Theta = [\mathbf{I}_N^T \quad \mathbf{0}_{v\times N}^T]^T$. So recovery of symbol block $\mathbf{d}(i)$ is equivalent to the recovery of $\mathbf{s}(i)$. $\hat{\mathbf{d}}(i)$ can be obtained by a simple implementation of ZP removal on $\hat{\mathbf{s}}(i)$. Now let us proceed to the equalization schemes based on Equation (5.9). This section covers block equalizers based on the ZF criterion, where both linear equalizer and decision-feedback equalizer are investigated.

5.1.1 Linear ZF equalization

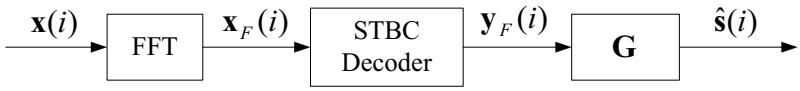

Figure 5.1: The linear filterbank equalizer

The $J \times J$ matrix $\mathbf{D}_{12}$, as defined in (5.4), is a full-rank matrix with nonnegative diagonal entries, and $\mathbf{F}_J$ is also full rank, then we can easily verify that $\mathbf{D}_{12}\mathbf{F}_J$ is also full rank and invertible. Based on Equation (5.9), there exists a ZF solution $\mathbf{G}_{ZF}$ that can offer almost perfect recovery of $\mathbf{s}(i)$ in noise free or high SNR environments; that is

$$\mathbf{s}(i) = \hat{\mathbf{s}}(i) = \mathbf{G}_{ZF}\left[\mathbf{D}_{12}\mathbf{F}_J\mathbf{s}(i)\right]. \tag{5.11}$$

where $\mathbf{G}_{ZF}$ is a $J \times J$ matrix, denoting a FIR linear filterbank. Recovery of $\mathbf{s}(i)$ from the decoupled subblock $\mathbf{y}_{\mathcal{F}}(i)$ can also be regarded as a least-squares problem with the cost function given by

$$\mathbf{J}(\hat{\mathbf{s}}(i)) = \| \mathbf{y}_{\mathcal{F}}(i) - \mathbf{D}_{12}\mathbf{F}_J\hat{\mathbf{s}}(i)\|^2 \tag{5.12}$$

where $\|\cdot\|^2$ denotes the squared Euclidean norm, viz., $\|\mathbf{a}\|^2 = \mathbf{a}^H\mathbf{a} = \sum_{k=1}^{K} |\mathbf{a}(k)|^2$., and $\mathbf{a}(k)$ stands for the k-th entry of the $K \times 1$ vector $\mathbf{a}$.

According to [52], when $\mathbf{D}_{12}\mathbf{F}_J$ has full rank, there is a unique solution $\hat{\mathbf{s}}(i)$ minimizing the cost function $\mathbf{J}(\hat{\mathbf{s}}(i))$ that can be expressed as

$$\hat{\mathbf{s}}(i) = \mathbf{G}_{ZF}\mathbf{y}_{\mathcal{F}}(i) = \mathbf{G}_{ZF}\mathbf{D}_{12}\mathbf{F}_J\mathbf{s}(i) + \mathbf{G}_{ZF}\boldsymbol{\eta}_{\mathcal{F}}(i).$$

where $\hat{\mathbf{s}}(i)$ is the equalized block, and $\mathbf{G}_{ZF}$ is the equalizer which can be formulated as

$$\begin{aligned} \mathbf{G}_{ZF} &= (\mathbf{D}_{12}\mathbf{F}_J)^+ \\ &= (\mathbf{F}_J^H\mathbf{D}_{12}^H\mathbf{D}_{12}\mathbf{F}_J)^{-1}\mathbf{F}_J^H\mathbf{D}_{12}^H = \mathbf{F}_J^{-1}\mathbf{D}_{12}^{-1} \end{aligned} \tag{5.13}$$

The above expression for $\mathbf{G}_{ZF}$ indicates that operation of $\mathbf{G}_{ZF}$ actually consists of two steps: firstly, multiplying the equalizer input $\mathbf{y}_{\mathcal{F}}(i)$ by $\mathbf{D}_{12}^{-1}$; secondly, transforming the equalized output that is in frequency domain form, back to time domain by means of IFFT operations. Figure 5.1 depicts the structure of this linear filterbank equalizer, where $\mathbf{G}$ is replaced by $\mathbf{G}_{ZF}$ under the ZF criterion.

5.1.2 ZF-DFE

Previously in Chapter 3, we have pointed out that, the linear ZF equalizers can excessively enhance noise at frequencies where the folded channel spectrum has high attenuations, because they don't take into account the noise at the receiver. That is the same situation for the linear ZF equalizer $\mathbf{G}_{ZF}$ that we have just introduced. The BER performance, in fact, can be further improved. One possible way is to

employ some other optimization criterions instead of the ZF one, for example, the MMSE criteria where the channel noise is considered and performance improvement can be expected (especially at low SNR). We will explain this MMSE criterion in detail in the next section, together with the linear and nonlinear equalizers that are developed based on it. Another possible way is to design nonlinear

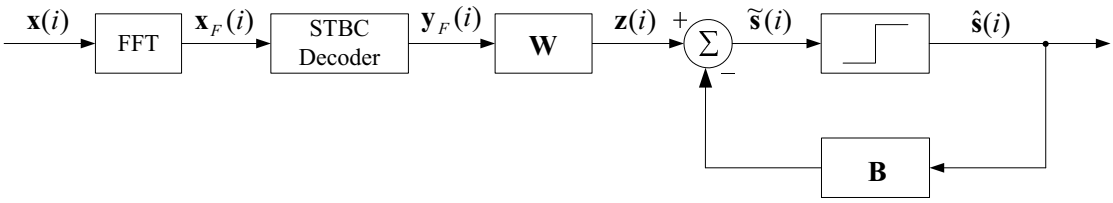

Figure 5.2: The decision feedback filterbank equalizer

equalizers rather than linear ones, for example, the decision-feedback equalizer. In the following, we develop the decision-feedback equalization scheme that remains based on the ZF criterion, namely, ZF-DFE.

Figure. 5.2 illustrates the structure of the decision-feedback equalizer, which consists of three parts:

1. The feedforward filterbank denoted by the $J \times J$ matrix $\mathbf{W}$, which is expected to eliminate ISI from *future* symbols within the current block.

2. The decision making device, which may take the form of a slicer or quantizer.

3. The feedback filter denoted by the $J \times J$ matrix $\mathbf{B}$, which is expected to eliminate ISI from *past* symbols within the current block.

Let us define the feedforward filterbank output as $\mathbf{z}(i)$, and the difference between

feedforward filterbank output and feedback filterbank output as $\tilde{\mathbf{s}}(i)$. Both $\mathbf{z}(i)$ and $\tilde{\mathbf{s}}(i)$ are $J \times 1$ vectors, as specified respectively by

$$\begin{aligned} \mathbf{z}(i) &= [z(iJ),\ z(iJ+1),\ \ldots,\ z(iJ+J-1)]^T \\ \tilde{\mathbf{s}}(i) &= [\tilde{s}(iJ),\ \tilde{s}(iJ+1),\ \ldots,\ \tilde{s}(iJ+J-1)]^T \end{aligned} \tag{5.14}$$

From Figure 5.2, we may conclude the following input-output relationships:

$$\mathbf{z}(i) = \mathbf{W}\mathbf{y}_{\mathcal{F}}(i) = \mathbf{W}\mathbf{D}_{12}\mathbf{F}_J\mathbf{s}(i) + \mathbf{W}\boldsymbol{\eta}_{\mathcal{F}}(i) \tag{5.15}$$

$$\tilde{\mathbf{s}}(i) = \mathbf{z}(i) - \mathbf{B}\hat{\mathbf{s}}(i) \tag{5.16}$$

$$\hat{\mathbf{s}}(i) = \mathcal{Q}(\tilde{\mathbf{s}}(i)) \tag{5.17}$$

where $\mathcal{Q}$ represents the slicer or quantizer used by the decision device. Our problem now, is reduced to find solutions for the feedforward matrix $\mathbf{W}$ and the feedback matrix $\mathbf{B}$, given the input blocks $\mathbf{y}_{\mathcal{F}}(i)$. Before tackling this problem, let us consider several special requirements imposed by such ZF block decision-feedback equalizer.

Firstly, we consider requirement of the ZF optimization criterion. By such criterion, we mean that when there is no noise, and the past decisions are assumed to be ideally correct, the decision statistic should be equal to the transmitted data, i.e.,

$$\tilde{\mathbf{s}}(i) = \hat{\mathbf{s}}(i) = \mathbf{s}(i). \tag{5.18}$$

From Equation (5.18), we can relate Equations (5.15) and (5.16) by

$$\begin{aligned} \mathbf{s}(i) &= \mathbf{W}\mathbf{D}_{12}\mathbf{F}_J\mathbf{s}(i) - \mathbf{B}\hat{\mathbf{s}}(i) \\ \Longrightarrow \quad \mathbf{W}\mathbf{D}_{12}\mathbf{F}_J &= \mathbf{B} + \mathbf{I}_J. \end{aligned} \tag{5.19}$$

Secondly, we consider the noise at the input of the decision device, which can be expressed as $\mathbf{v}(i) = \mathbf{W}\boldsymbol{\eta}_{\mathcal{F}}(i)$ under the assumption of correct past decisions. Then the covariance matrix of $\mathbf{v}(i)$ is given by:

$$\mathbf{R}_{vv} = E\left\{[\mathbf{W}\boldsymbol{\eta}_{\mathcal{F}}(i)][\mathbf{W}\boldsymbol{\eta}_{\mathcal{F}}(i)]^H\right\} = \mathbf{W}\mathbf{R}_{\eta\eta}\mathbf{W}^H$$

where $\mathbf{R}_{\eta\eta} = E\{\boldsymbol{\eta}_{\mathcal{F}}(i)\boldsymbol{\eta}_{\mathcal{F}}^H(i)\}$. In general, the noise at the input of the decision device $\mathbf{v}(i)$ is not white. Whitening the noise is one approach to improve the BER performance [53], which can be accomplished by properly selecting $\mathbf{W}$ such that

$$\mathbf{W}\mathbf{R}_{\eta\eta}\mathbf{W}^H = \boldsymbol{\mathcal{V}}_J \tag{5.20}$$

here $\boldsymbol{\mathcal{V}}_J$ is a $J \times J$ diagonal matrix.

Thirdly, we explore successive cancellation at the feedback filterbank $\mathbf{B}$. By successive cancellation we mean that for each block indexed by i, the J-th entry or the last symbol $s(iJ + J - 1)$ is recovered first. Its estimate, $\hat{s}(iJ + J - 1)$, is used as the input to a one-tap filter; output of the filter is removed from the $z(iJ + J - 2)$ so that the $(J-1)$ th entry or the second last symbol $s(iJ + J - 2)$ is recovered. After that, both estimates $\hat{s}(iJ + J - 1)$ and $\hat{s}(iJ + J - 2)$ are rendered to a two-tap filter; output of the filter is removed from the corresponding entry in $\mathbf{z}(i)$ so that the relevant symbol is recovered. This procedure is carried out until all the symbols of the same block i have been recovered. Accordingly, the tap number of each feedback filter is increased until it reaches $(J - 1)$. Figure 5.3 shows the simplified diagram of the feedback filterbank structure, where the tap delay between neighboring taps is omitted here. To make possible such successive cancellation, the feedback matrix $\mathbf{B}$ needs to be strictly upper triangular.

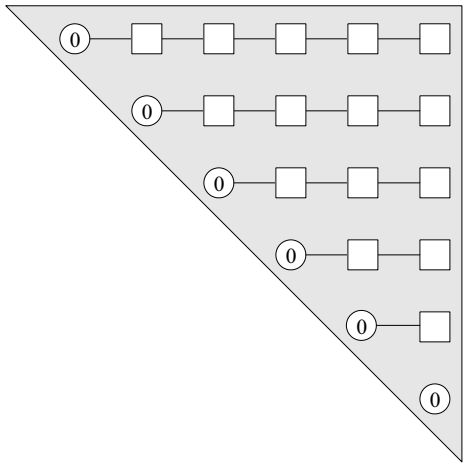

Figure 5.3: The structure of the feedback filterbank with $J = 6$

Therefore, our design of ZF-DFE scheme should satisfy the above three requirements. Let us consider the first requirement as expressed in Equation (5.19). Since $\mathbf{D}_{12}\mathbf{F}_J$ is full rank, using Equation (5.19), the feedforward matrix $\mathbf{W}$ can be solved:

$$\mathbf{W} = (\mathbf{B} + \mathbf{I}_J)(\mathbf{D}_{12}\mathbf{F}_J)^{-1}. \tag{5.21}$$

Substituting the result into Equation (5.20), we have

$$(\mathbf{D}_{12}\mathbf{F}_J)^H \mathbf{R}_{\eta\eta}^{-1}(\mathbf{D}_{12}\mathbf{F}_J) = (\mathbf{B} + \mathbf{I}_J)^H \boldsymbol{\mathcal{V}}_J^{-1}(\mathbf{B} + \mathbf{I}_J) \tag{5.22}$$

Previously we have pointed that after the implementation of decoupling, the resulting noise vector $\boldsymbol{\eta}_{\mathcal{F}}(i)$ remains white. Let us define $\mathbf{R}_{\eta\eta} = \mathbf{I}_J$[1], then Equation (5.22) changes to

$$(\mathbf{D}_{12}\mathbf{F}_J)^H(\mathbf{D}_{12}\mathbf{F}_J) = (\mathbf{B} + \mathbf{I}_J)^H \boldsymbol{\mathcal{V}}_J^{-1}(\mathbf{B} + \mathbf{I}_J), \tag{5.23}$$

[1]Here we don't take into account of the noise power by simply defining it as unity. Actually it can be specified as other values, which may result in slight difference in the following Cholesky factorization.

and the $(\mathbf{D}_{12}\mathbf{F}_J)^H(\mathbf{D}_{12}\mathbf{F}_J)$ can be reformulated as

$$(\mathbf{D}_{12}\mathbf{F}_J)^H(\mathbf{D}_{12}\mathbf{F}_J) = \mathbf{F}_J^H\mathbf{D}_{12}^2\mathbf{F}_J. \tag{5.24}$$

Since $\mathbf{D}_{12}^2$ is a $J \times J$ diagonal matrix with nonnegative diagonal entries, here we can construct a $J \times J$ circulant matrix $\boldsymbol{\mathcal{H}}$ with its first column equal to the J-point IDFT [2] of the diagonal entries of $\mathbf{D}_{12}^2$. According to the eigendecomposition property of circulant matrices [50], we have

$$\mathbf{D}_{12}^2 = \mathbf{F}_J\boldsymbol{\mathcal{H}}\mathbf{F}_J^H \tag{5.25}$$

Substituting Equation (5.25) into Equation (5.24), we get

$$(\mathbf{D}_{12}\mathbf{F}_J)^H(\mathbf{D}_{12}\mathbf{F}_J) = \mathbf{F}_J^H\mathbf{F}_J\boldsymbol{\mathcal{H}}\mathbf{F}_J^H\mathbf{F}_J = \boldsymbol{\mathcal{H}}.$$

Hence Equation (5.23) can be rewritten as

$$\boldsymbol{\mathcal{H}} = (\mathbf{B} + \mathbf{I}_J)^H\boldsymbol{\mathcal{V}}_J^{-1}(\mathbf{B} + \mathbf{I}_J).$$

As stated in the third requirement, the feedback equalization matrix $\mathbf{B}$ should be strictly upper triangular, then matrix $(\mathbf{B} + \mathbf{I}_J)$ is upper triangular with unit diagonal. Now let us consider the Cholesky factorization of the circulant matrix $\boldsymbol{\mathcal{H}}$:

$$\boldsymbol{\mathcal{H}} = \boldsymbol{\mathcal{L}}^H\boldsymbol{\mathcal{V}}\boldsymbol{\mathcal{L}}$$

where $\boldsymbol{\mathcal{L}}$ is an upper triangular matrix with unit diagonal, and $\boldsymbol{\mathcal{V}}$ is a diagonal matrix. Since $\boldsymbol{\mathcal{H}}$ is Toeplitz (because it is circulant), its Cholesky factorization can be obtained by using Schur algorithm [51] to achieve reduction in complexity.

[2] It is noted that the operation here is IDFT, rather than orthonormal IDFT as described by $\mathbf{F}_N^H$.

By setting $\mathbf{B}+\mathbf{I}_J = \boldsymbol{\mathcal{L}}$, and using Equation (5.21), we obtain the solutions for both $\mathbf{B}$ and $\mathbf{W}$:

$$\begin{aligned} \mathbf{B} &= \boldsymbol{\mathcal{L}} - \mathbf{I}_J \\ \mathbf{W} &= \boldsymbol{\mathcal{L}}(\mathbf{D}_{12}\mathbf{F}_J)^{-1}. \end{aligned} \tag{5.26}$$

It is easy to verify that $\mathbf{W}\mathbf{W}^H = \boldsymbol{\mathcal{V}}^{-1}$, which indicates that the noise at the input of the decision device is decorrelated or whitened. With the help of Equation (5.13), the feedforward filterbank $\mathbf{W}$ in Equation (5.26) can be written as

$$\mathbf{W} = (\mathbf{B}+\mathbf{I}_J)\mathbf{G}_{ZF} \;=\; \boldsymbol{\mathcal{L}}\mathbf{G}_{ZF},$$

which implies that the feedforward filter is the linear ZF filter followed by $(\mathbf{B}+\mathbf{I}_J)$ that takes into account the feedback filterbank $\mathbf{B}$.

5.2 Linear and Nonlinear MMSE Equalization

5.2.1 Linear MMSE equalization

In this section we consider the block equalizers based on the MMSE criterion, which minimize the mean square error $E\{\|\hat{\mathbf{s}}(i)-\mathbf{s}(i)\|^2\}$. We consider the linear equalizer first, and its structure is depicted in Figure 5.1. The equalizer $\mathbf{G}$, in fact, belongs to a special category of optimum linear filters known as Wiener filters. The cost function can be written as a function of the equalizer $\mathbf{G}$:

$$\mathbf{J}(\mathbf{G}) = E\{\|\hat{\mathbf{s}}(i) - \mathbf{s}(i)\|^2\}$$

The equalizer output is given by $\hat{\mathbf{s}}(i) = \mathbf{G}\,\mathbf{y}_{\mathcal{F}}(i) = \mathbf{G}\mathbf{D}_{12}\mathbf{F}_J\mathbf{s}(i) + \mathbf{G}\boldsymbol{\eta}_{\mathcal{F}}(i)$. we can rewrite the cost function as

$$\begin{aligned}\mathbf{J}(\mathbf{G}) &= E\{\|(\mathbf{G}\mathbf{D}_{12}\mathbf{F}_J - \mathbf{I}_J)\mathbf{s}(i) + \mathbf{G}\boldsymbol{\eta}_{\mathcal{F}}\|^2\} \\ &= E\left\{\,\mathrm{Tr}\{[(\mathbf{G}\mathbf{D}_{12}\mathbf{F}_J - \mathbf{I}_J)\mathbf{s}(i) + \mathbf{G}\boldsymbol{\eta}_{\mathcal{F}}]\,[(\mathbf{G}\mathbf{D}_{12}\mathbf{F}_J - \mathbf{I}_J)\mathbf{s}(i) + \mathbf{G}\boldsymbol{\eta}_{\mathcal{F}}]^H\}\right\}\end{aligned}$$

By setting gradient of the cost function to zero, i.e.,

$$\nabla_G \mathbf{J}(\mathbf{G}) = 0,$$

and solving for $\mathbf{G}$, we can obtain the MMSE solution

$$\mathbf{G}_{MMSE} = \mathbf{R}_{ss}(\mathbf{D}_{12}\mathbf{F}_J)^H[\mathbf{R}_{\eta\eta} + (\mathbf{D}_{12}\mathbf{F}_J)\mathbf{R}_{ss}(\mathbf{D}_{12}\mathbf{F}_J)^H]^{-1}, \tag{5.27}$$

where $\mathbf{R}_{ss} = E\{\mathbf{s}(i)\,\mathbf{s}^H(i)\}$ and $\mathbf{R}_{\eta\eta} = E\{\boldsymbol{\eta}_{\mathcal{F}}(i)\,\boldsymbol{\eta}_{\mathcal{F}}^H(i)\}$ are correlation matrices for symbol vector $\mathbf{s}(i)$ and noise vector $\boldsymbol{\eta}_{\mathcal{F}}(i)$, respectively. The noise vector $\boldsymbol{\eta}_{\mathcal{F}}(i)$, as we pointed out at the beginning of this chapter, remains white; by defining its variance as σ_η^2, we obtain $\mathbf{R}_{\eta\eta} = \sigma_\eta^2\mathbf{I}_J$. As for the symbol vector $\mathbf{s}(i)$, we assume it to be white with variance σ_s^2, and we have $\mathbf{R}_{ss} = \sigma_s^2\mathbf{I}_J$. Also noting that $\mathbf{D}_{12}$ is a $J \times J$ diagonal matrix with nonnegative diagonal entries, we can simplify Equation (5.27) to

$$\mathbf{G}_{MMSE} = \mathbf{F}_J^{-1}\mathbf{D}_{12}(\mathbf{D}_{12}^2 + \mathbf{I}_J/\mathrm{SNR})^{-1}$$

where SNR is defined as $\mathrm{SNR} = \sigma_s^2/\sigma_\eta^2$. This linear MMSE equalizer $\mathbf{G}_{MMSE}$ can reduce to the linear ZF equalizer $\mathbf{G}_{ZF}$ by simply setting $\sigma_\eta^2 = 0$.

The equalizer $\mathbf{G}_{MMSE}$ can be realized in the form of linear filterbank. Or alternatively, we can divide it into two parts, similar with the ZF equalizer $\mathbf{G}_{ZF}$.

The first part is $\mathbf{D}_{12}(\mathbf{D}_{12}^2 + \mathbf{I}_J/\text{SNR})^{-1}$, which is a $J \times J$ diagonal matrix, and can be readily implemented by a filter. This part actually constitutes the frequency-domain equalization. The second part is related to $\mathbf{F}_J^{-1}$, which is a J-point IFFT transform.

5.2.2 MMSE-DFE

Structure of the MMSE decision-feedback equalizer is also depicted in Figure 5.2, which is the same as the ZF decision-feedback equalizer. And the input-output relationships of Equations (5.15), (5.16), and (5.17) also apply here. Since we take into account the noise here, the input to the decision device, $\tilde{\mathbf{s}}(i)$, will not be simply assumed equal to the transmitted data $\mathbf{s}(i)$. Instead, we define

$$\mathbf{e}(i) = \tilde{\mathbf{s}}(i) - \mathbf{s}(i)$$

as the performance measure of this DF equalizer, where $\mathbf{e}(i)$ is specified by

$$\mathbf{e}(i) = [e(iJ),\ e(iJ+1),\ \ldots,\ e(iJ+J-1)]^T.$$

We still keep the assumption of correct past decisions. Then by using the input-output relationships in Equations (5.15)-(5.17), we have

$$\mathbf{e}(i) = \mathbf{W}\mathbf{y}_{\mathcal{F}}(i) - (\mathbf{B} + \mathbf{I}_J)\mathbf{s}(i). \tag{5.28}$$

Our problem now, is to find solutions for the feedforward matrix $\mathbf{W}$ and the feedback matrix $\mathbf{B}$ that can minimize the mean square error $E\{\|\mathbf{e}(i)\|^2\}$, given the input data blocks $\mathbf{y}_{\mathcal{F}}(i)$, input symbol correlation $\mathbf{R}_{ss}$ and the noise correlation

$\mathbf{R}_{\eta\eta}$. The feedback filter matrix $\mathbf{B}$ should be strictly upper triangular as illustrated in Figure 5.3, so that successive cancellation can be carried out.

Our first step is to obtain the matrix $\mathbf{W}$ that minimizes $E\{\|\mathbf{e}(i)\|^2\}$ by fixing the feedback matrix $\mathbf{B}$. Applying the orthogonality principle to Equation (5.28), we find that $\mathbf{e}(i)$ should be orthogonal to $\mathbf{y}_{\mathcal{F}}(i)$, i.e.,

$$\begin{aligned} E\{\mathbf{e}(i)\mathbf{y}_{\mathcal{F}}^H(i)\} &= \mathbf{0}_{J\times J} \\ \Longrightarrow \mathbf{W}E\{\mathbf{y}_{\mathcal{F}}(i)\mathbf{y}_{\mathcal{F}}^H(i)\} &= (\mathbf{B}+\mathbf{I}_J)E\{\mathbf{s}(i)\mathbf{y}_{\mathcal{F}}^H(i)\} \end{aligned} \tag{5.29}$$

In view of the fact that the noise vector $\boldsymbol{\eta}_{\mathcal{F}}(i)$ is independent of the transmitted data $\mathbf{s}(i)$, by using Equation (5.9), we can obtain

$$\begin{aligned} \mathbf{R}_{sy} &= E\{\mathbf{s}(i)\mathbf{y}_{\mathcal{F}}^H(i)\} \\ &= E\{\mathbf{s}(i)[\mathbf{D}_{12}\mathbf{F}_J\mathbf{s}(i)+\boldsymbol{\eta}_{\mathcal{F}}(i)]^H\} \\ &= \mathbf{R}_{ss}(\mathbf{D}_{12}\mathbf{F}_J)^H = \mathbf{R}_{ys}^H \end{aligned} \tag{5.30}$$

and

$$\begin{aligned} \mathbf{R}_{yy} &= E\{\mathbf{y}_{\mathcal{F}}(i)\mathbf{y}_{\mathcal{F}}^H(i)\} \\ &= (\mathbf{D}_{12}\mathbf{F}_J)\mathbf{R}_{ss}(\mathbf{D}_{12}\mathbf{F}_J)^H + \mathbf{R}_{\eta\eta} \\ &= \mathbf{R}_{\vartheta\vartheta} + \mathbf{R}_{\eta\eta} \end{aligned} \tag{5.31}$$

The $\mathbf{R}_{\vartheta\vartheta}$ in Equation (5.31) is defined as $\mathbf{R}_{\vartheta\vartheta} = (\mathbf{D}_{12}\mathbf{F}_J)\mathbf{R}_{ss}(\mathbf{D}_{12}\mathbf{F}_J)^H$. From Equations (5.29), (5.30) and (5.31), we have

$$\begin{aligned} \mathbf{W} &= (\mathbf{B}+\mathbf{I}_J)\mathbf{R}_{sy}\mathbf{R}_{yy}^{-1} \\ &= (\mathbf{B}+\mathbf{I}_J)\mathbf{R}_{ss}(\mathbf{D}_{12}\mathbf{F}_J)^H[(\mathbf{D}_{12}\mathbf{F}_J)\mathbf{R}_{ss}(\mathbf{D}_{12}\mathbf{F}_J)^H+\mathbf{R}_{\eta\eta}]^{-1} \end{aligned} \tag{5.32}$$

which actually links the feedforward and feedback filterbanks together. Quite similar with the ZF-DFE we have previously developed, the feedforward filterbank $\mathbf{W}$, with the help of $\mathbf{G}_{MMSE}$ in Equation (5.27), can be simplified as

$$\mathbf{W} = (\mathbf{B} + \mathbf{I}_J)\mathbf{G}_{MMSE},$$

which indicates that the feedforward filter is the linear MMSE filter followed by $(\mathbf{B} + \mathbf{I}_J)$ that relates the feedforward and feedback filterbanks.

Our next step is to whiten the noise at the input of the decision device, which is similar with what we have done in the development of ZF-DFE. By substituting the $\mathbf{W}$ of Equation (5.32) into Equation (5.28), $\mathbf{e}(i)$ can be rewritten as

$$\begin{aligned} \mathbf{e}(i) &= (\mathbf{B} + \mathbf{I}_J)\mathbf{R}_{sy}\mathbf{R}_{yy}^{-1}\mathbf{y}_{\mathcal{F}}(i) - (\mathbf{B} + \mathbf{I}_J)\mathbf{s}(i) \\ &= (\mathbf{B} + \mathbf{I}_J)\boldsymbol{\varepsilon}(i) \end{aligned} \tag{5.33}$$

where $\boldsymbol{\varepsilon}(i)$ is defined as

$$\boldsymbol{\varepsilon}(i) = \mathbf{R}_{sy}\mathbf{R}_{yy}^{-1}\mathbf{y}_{\mathcal{F}}(i) - \mathbf{s}(i).$$

Then the covariance of $\mathbf{e}(i)$ can be expressed as

$$\mathbf{R}_{ee} = E\{\mathbf{e}(i)\mathbf{e}^H(i)\} = (\mathbf{B} + \mathbf{I}_J)E\{\boldsymbol{\varepsilon}(i)\boldsymbol{\varepsilon}^H(i)\}(\mathbf{B} + \mathbf{I}_J)^H. \tag{5.34}$$

Thus, to obtain the covariance of $\mathbf{e}(i)$, we have to solve the covariance of $\boldsymbol{\varepsilon}(i)$ in advance.

Let $\mathbf{R}_{\varepsilon\varepsilon} = E\{\boldsymbol{\varepsilon}(i)\boldsymbol{\varepsilon}^H(i)\}$. By applying the results in Equations (5.30) and

(5.31), we may write

$$\begin{aligned}
\mathbf{R}_{\varepsilon\varepsilon} &= E\{[\mathbf{R}_{sy}\mathbf{R}_{yy}^{-1}\mathbf{y}_{\mathcal{F}}(i) - \mathbf{s}(i)][\mathbf{R}_{sy}\mathbf{R}_{yy}^{-1}\mathbf{y}_{\mathcal{F}}(i) - \mathbf{s}(i)]^H\} \\
&= \mathbf{R}_{sy}\mathbf{R}_{yy}^{-1}E\{\mathbf{y}_{\mathcal{F}}(i)\mathbf{y}_{\mathcal{F}}^H(i)\}\mathbf{R}_{yy}^{-H}\mathbf{R}_{sy}^H - \mathbf{R}_{sy}\mathbf{R}_{yy}^{-1}E\{\mathbf{y}_{\mathcal{F}}(i)\mathbf{s}^H(i)\} \\
&\quad -E\{\mathbf{s}(i)\mathbf{y}_{\mathcal{F}}^H(i)\}\mathbf{R}_{yy}^{-H}\mathbf{R}_{sy}^H + E\{\mathbf{s}(i)\mathbf{s}^H(i)\} \\
&= \mathbf{R}_{ss} - \mathbf{R}_{sy}\mathbf{R}_{yy}^{-1}\mathbf{R}_{ys} \\
&= \mathbf{R}_{ss} - \mathbf{R}_{ss}(\mathbf{D}_{12}\mathbf{F}_J)^H[\mathbf{R}_{\eta\eta} + (\mathbf{D}_{12}\mathbf{F}_J)\mathbf{R}_{ss}(\mathbf{D}_{12}\mathbf{F}_J)^H]^{-1} \\
&\quad \cdot(\mathbf{D}_{12}\mathbf{F}_J)\mathbf{R}_{ss} \qquad (5.35)
\end{aligned}$$

Here we can make use of the matrix inversion lemma, which is given by

$$(\mathbb{A} - \mathbb{C}\mathbb{B}^{-1}\mathbb{D})^{-1} = \mathbb{A}^{-1} + \mathbb{A}^{-1}\mathbb{C}(\mathbb{B} - \mathbb{D}\mathbb{A}^{-1}\mathbb{C})^{-1}\mathbb{D}\mathbb{A}^{-1}$$

where $\mathbb{A}$, $\mathbb{B}$, $\mathbb{C}$, and $\mathbb{D}$ are matrices with compatible dimensions and the necessary inverses exist. We first make the following identifications:

$$\mathbb{A} = \mathbf{R}_{ss}^{-1}, \quad \mathbb{B} = \mathbf{R}_{\eta\eta}, \quad \mathbb{C} = (\mathbf{D}_{12}\mathbf{F}_J)^H, \quad \mathbb{D} = -(\mathbf{D}_{12}\mathbf{F}_J),$$

Then, substituting these definitions into the matrix inversion lemma, we get

$$\mathbf{R}_{\varepsilon\varepsilon} = [\mathbf{R}_{ss}^{-1} + (\mathbf{D}_{12}\mathbf{F}_J)^H\mathbf{R}_{\eta\eta}^{-1}(\mathbf{D}_{12}\mathbf{F}_J)]^{-1} \qquad (5.36)$$

Hence the covariance matrix $\mathbf{R}_{ee}$ can be reformulated as:

$$\mathbf{R}_{ee} = (\mathbf{B} + \mathbf{I}_J)[\mathbf{R}_{ss}^{-1} + (\mathbf{D}_{12}\mathbf{F}_J)^H\mathbf{R}_{\eta\eta}^{-1}(\mathbf{D}_{12}\mathbf{F}_J)]^{-1}(\mathbf{B} + \mathbf{I}_J)^H. \qquad (5.37)$$

Since $E\{\|\mathbf{e}(i)\|^2\} = tr\{\mathbf{R}_{ee}\}$, the minimization of mean square error is equivalent to minimizing the trace of $\mathbf{R}_{ee}$, with the constraint that $(\mathbf{B} + \mathbf{I}_J)$ is upper

triangular with unit diagonal. Now we consider the Cholesky factorization of $\mathbf{R}_{\varepsilon\varepsilon}^{-1}$, that is

$$\mathbf{R}_{ss}^{-1} + (\mathbf{D}_{12}\mathbf{F}_J)^H \mathbf{R}_{\eta\eta}^{-1} (\mathbf{D}_{12}\mathbf{F}_J) = \boldsymbol{\mathcal{L}}^H \boldsymbol{\mathcal{V}} \boldsymbol{\mathcal{L}}, \tag{5.38}$$

where $\boldsymbol{\mathcal{L}}$ is a $J \times J$ upper triangular matrix with unit diagonal, and $\boldsymbol{\mathcal{V}}$ is a $J \times J$ diagonal matrix. Let us define $\mathbf{R}_{\eta\eta} = \sigma_\eta^2 \mathbf{I}_J$, $\mathbf{R}_{ss} = \sigma_s^2 \mathbf{I}_J$ and $\text{SNR} = \sigma_s^2/\sigma_\eta^2$. Using the relationship $(\mathbf{D}_{12}\mathbf{F}_J)^H(\mathbf{D}_{12}\mathbf{F}_J) = \boldsymbol{\mathcal{H}}$ that we have developed in ZF-DFE, we can reformulate Equation (5.38) as

$$\frac{1}{\sigma_s^2}\mathbf{I}_J + \frac{1}{\sigma_\eta^2}\boldsymbol{\mathcal{H}} = \boldsymbol{\mathcal{L}}^H \boldsymbol{\mathcal{V}} \boldsymbol{\mathcal{L}},$$

or the scale version

$$\frac{1}{\text{SNR}}\mathbf{I}_J + \boldsymbol{\mathcal{H}} = \boldsymbol{\mathcal{L}}^H \boldsymbol{\mathcal{V}} \boldsymbol{\mathcal{L}},$$

where the factor σ_η^2 has been absorbed in $\boldsymbol{\mathcal{V}}$. As $\boldsymbol{\mathcal{H}}$ is Toeplitz, the Cholesky factorization here can be implemented by means of Schur algorithm [51], so that the reduction in computational complexity can be achieved.

By setting

$$\mathbf{B} = \boldsymbol{\mathcal{L}} - \mathbf{I}_J, \tag{5.39}$$

and substituting Equation (5.38) into Equation (5.52), we have

$$\mathbf{R}_{ee} = \boldsymbol{\mathcal{V}}^{-1}. \tag{5.40}$$

As $\boldsymbol{\mathcal{V}}$ is diagonal, the noise at the input of decision device is white, hence the subsequent symbol-by-symbol detection can be implemented in the optimal sense. After solving $\mathbf{B}$ from Equation (5.39), the feedforward matrix $\mathbf{W}$ can be readily obtained by submitting $\mathbf{B}$ into Equation (5.32), or expressed as $\mathbf{W} = \boldsymbol{\mathcal{L}}\mathbf{G}_{MMSE}$.

5.3 Training-Based Frequency-Domain Channel Estimation

In the last two sections, we have discussed linear and nonlinear (DFE) equalization schemes based on both ZF and MMSE criteria to combat ISI for STBC block transmissions over multipath fading channels. These schemes, as noted in our elaboration, are developed under two essential assumptions regarding the channel. One is the quasi-static assumption; that is, the channel is assumed to be constant over the transmission of a STBC burst (consisting of two data blocks). The other one is that the channel state information (CSI) is available beforehand at the receiver. Therefore, some form of channel estimation must be employed to acquire the CSI before implementation of those various equalization schemes.

There are two classes of methods available for the receiver to acquire the CSI [55]: training method which is based on training symbols that are known a priori to the receiver; and blind method that relies only on the received symbols to acquire CSI blindly. In this section we consider only the training-based method, because it decouples symbol detection from channel estimation, and thus can be easily incorporated with our afore-developed equalization schemes. In addition, our proposed channel estimation scheme is of interest because it is implemented in frequency domain rather than in time domain, which is different from some existing channel estimation schemes (see, e.g., [54] - [58]) for STBC or multiple-antenna transmissions. In the following, we formulate this training-based channel estimation problem for the 2-TX 1-RX scenario. Such analysis can also be generalized to

multiple transmit and receive antennas.

Let us define $N_b \times 1$ vectors $\mathbf{s}_1$ and $\mathbf{s}_2$ to be training blocks, as specified by

$$\begin{aligned} \mathbf{s}_1 &= [s_1(0),\ s_1(1),\ \ldots,\ s_1(N_b-1))]^T \\ \mathbf{s}_2 &= [s_2(0),\ s_2(1),\ \ldots,\ s_2(N_b-1))]^T, \end{aligned}$$

where N_b denotes the block length and should be greater than the channel order v, i.e., $N_b \geq v+1$. In our scheme, elements of the training blocks $\mathbf{s}_1$ and $\mathbf{s}_2$, belong to the same alphabet $\boldsymbol{\mathcal{A}}$ of size N_b (as will be examined later); that is, $\mathbf{s}_1$ and $\mathbf{s}_2$ can be exactly the same, or their only difference may be arrangement of these training symbols. $\mathbf{s}_1$ and $\mathbf{s}_2$ are encoded in space and time at the transmitter as those information blocks, but by using the *CP-only* scheme rather than the *ZP-only* scheme, as we have mentioned previously in Section 4.3. Their encoding and transmission formats are illustrated in Figure 5.4. Then the two consecutive

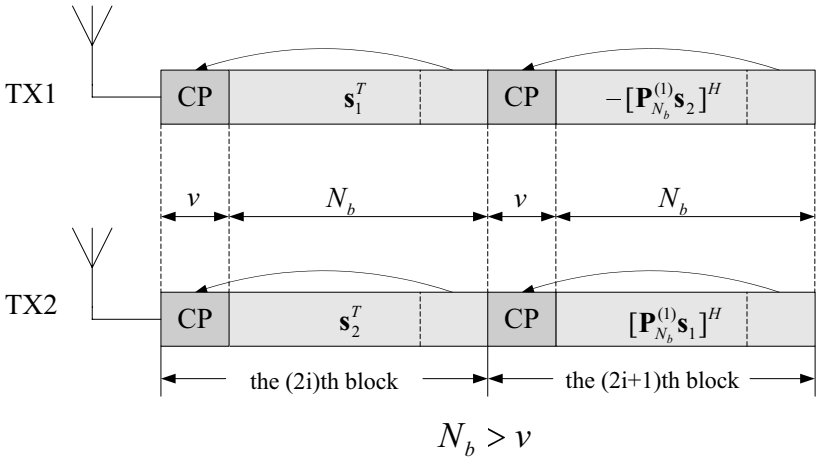

Figure 5.4: Transmission formats for training sequences

received blocks $\mathbf{x}_1$, $\mathbf{x}_2$ are given by

$$\mathbf{x}_1 = \mathbf{H}_1\mathbf{s}_1 + \mathbf{H}_2\mathbf{s}_2 + \mathbf{n}_1 \tag{5.41}$$

$$\mathbf{x}_2 = -\mathbf{H}_1\mathbf{P}_{N_b}^{(1)}\mathbf{s}_2^* + \mathbf{H}_2\mathbf{P}_{N_b}^{(1)}\mathbf{s}_1^* + \mathbf{n}_2. \tag{5.42}$$

where $\mathbf{H}_1$ and $\mathbf{H}_2$ are channel matrices with the size of $N_b \times N_b$; $\mathbf{n}_1$ and $\mathbf{n}_1$ are $N_b \times 1$ noise vectors. According to Equation (4.33), for this CP scheme, Equation (5.42) can be reformulated as

$$\mathbf{x}_2 = -\mathbf{F}_{N_b}^H\mathbf{D}_1\left[\mathbf{F}_{N_b}\mathbf{s}_2\right]^* + \mathbf{F}_{N_b}^H\mathbf{D}_2\left[\mathbf{F}_{N_b}\mathbf{s}_1\right]^* + \mathbf{n}_2. \tag{5.43}$$

Here $\mathbf{D}_1$ and $\mathbf{D}_2$ are both $N_b \times N_b$ diagonal matrices with their diagonals given by $\mathbf{h}_{1\mathcal{F}}$ and $\mathbf{h}_{2\mathcal{F}}$, respectively. $\mathbf{h}_{1\mathcal{F}}$ and $\mathbf{h}_{2\mathcal{F}}$ are similar with what we have previously defined in Chapter 4. The only difference is their size: in Chapter 4, they are $J \times 1$ vectors, here they denote $N_b \times 1$ vectors. It is noteworthy that channel orders for both $\mathbf{h}_1$ and $\mathbf{h}_2$ are also equal to v; that is, they have both $v+1$ tap-weights to be estimated.

Applying the orthonormal DFT $\mathbf{F}_{N_b}$ on Equations (5.41) and (5.43), we can obtain

$$\mathbf{x}_{1\mathcal{F}} = \mathbf{D}_1\mathbf{s}_{1\mathcal{F}} + \mathbf{D}_2\mathbf{s}_{2\mathcal{F}} + \mathbf{n}_{1\mathcal{F}} \tag{5.44}$$

$$\mathbf{x}_{2\mathcal{F}} = -\mathbf{D}_1\mathbf{s}_{2\mathcal{F}}^* + \mathbf{D}_2\mathbf{s}_{1\mathcal{F}}^* + \mathbf{n}_{2\mathcal{F}} \tag{5.45}$$

with help of the following definitions:

$$\mathbf{x}_{1\mathcal{F}} = \mathbf{F}_{N_b}\mathbf{x}_1, \quad \mathbf{s}_{1\mathcal{F}} = \mathbf{F}_{N_b}\mathbf{s}_1, \quad \mathbf{n}_{1\mathcal{F}} = \mathbf{F}_{N_b}\mathbf{n}_1$$

$$\mathbf{x}_{2\mathcal{F}} = \mathbf{F}_{N_b}\mathbf{x}_2, \quad \mathbf{s}_{2\mathcal{F}} = \mathbf{F}_{N_b}\mathbf{s}_2, \quad \mathbf{n}_{2\mathcal{F}} = \mathbf{F}_{N_b}\mathbf{n}_1.$$

Using the diagonal property of $\mathbf{D}_1$ and $\mathbf{D}_2$, we can rewrite Equations (5.44) and (5.45) as

$$\mathbf{x}_{1\mathcal{F}} = \mathbf{S}_{1\mathcal{F}}\mathbf{h}_{1\mathcal{F}} + \mathbf{S}_{2\mathcal{F}}\mathbf{h}_{2\mathcal{F}} + \mathbf{n}_{1\mathcal{F}} \tag{5.46}$$

$$\mathbf{x}_{2\mathcal{F}} = -\mathbf{S}^*_{2\mathcal{F}}\mathbf{h}_{1\mathcal{F}} + \mathbf{S}^*_{1\mathcal{F}}\mathbf{h}_{2\mathcal{F}} + \mathbf{n}_{2\mathcal{F}} \tag{5.47}$$

where $\mathbf{S}_{1\mathcal{F}} = \text{diag}\{\mathbf{s}_{1\mathcal{F}}\}$ and $\mathbf{S}_{2\mathcal{F}} = \text{diag}\{\mathbf{s}_{2\mathcal{F}}\}$. Or by defining $\mathbf{x}_{\mathcal{F}} = [\mathbf{x}^T_{1\mathcal{F}} \quad \mathbf{x}^T_{2\mathcal{F}}]^T$, we can write the above frequency domain input-output relationship into a single block matrix-vector form:

$$\mathbf{x}_{\mathcal{F}} = \underbrace{\begin{bmatrix} \mathbf{S}_{1\mathcal{F}} & \mathbf{S}_{2\mathcal{F}} \\ -\mathbf{S}^*_{2\mathcal{F}} & \mathbf{S}^*_{1\mathcal{F}} \end{bmatrix}}_{\mathbf{S}_{\mathcal{F}}} \underbrace{\begin{bmatrix} \mathbf{h}_{1\mathcal{F}} \\ \mathbf{h}_{2\mathcal{F}} \end{bmatrix}}_{\mathbf{h}_{\mathcal{F}}} + \underbrace{\begin{bmatrix} \mathbf{n}_{1\mathcal{F}} \\ \mathbf{n}_{2\mathcal{F}} \end{bmatrix}}_{\mathbf{n}_{\mathcal{F}}} \tag{5.48}$$

We further define $\mathbf{S}_{\mathcal{F}}$, $\mathbf{h}_{\mathcal{F}}$ and $\mathbf{n}_{\mathcal{F}}$ as shown above, then Equation (5.48) reduces to

$$\mathbf{x}_{\mathcal{F}} = \mathbf{S}_{\mathcal{F}}\mathbf{h}_{\mathcal{F}} + \mathbf{n}_{\mathcal{F}}. \tag{5.49}$$

Hence, our problem of estimating $\mathbf{h}_1$ and $\mathbf{h}_2$ changes to estimating their frequency-domain counterparts from $\mathbf{x}_{\mathcal{F}}$. This problem, similar with our afore-introduced linear ZF equalization, can be solved by using the least-squares method. Or in other words, we need to find the least-squares solution which minimize the cost function defined by

$$\mathbf{J}(\hat{\mathbf{h}}_{\mathcal{F}}) = \| \mathbf{x}_{\mathcal{F}} - \mathbf{S}_{\mathcal{F}}\hat{\mathbf{h}}_{\mathcal{F}}\|^2.$$

Assuming that $\mathbf{S}_{\mathcal{F}}$ is full rank[3], the unique least-squares solution, $\hat{\mathbf{h}}_{\mathcal{F}}$, can be

[3]This is a valid assumption as we can select appropriate training sequences to make sure there are no zeros appearing on their FFT grids.

expressed as

$$\hat{\mathbf{h}}_{\mathcal{F}} = \begin{bmatrix} \hat{\mathbf{h}}_{1\mathcal{F}} \\ \hat{\mathbf{h}}_{2\mathcal{F}} \end{bmatrix} = (\mathbf{S}_{\mathcal{F}}^H \mathbf{S}_{\mathcal{F}})^{-1} \mathbf{S}_{\mathcal{F}}^H \mathbf{x}_{\mathcal{F}}. \tag{5.50}$$

It is easy to verify that $\mathbf{S}_{\mathcal{F}}$ is orthogonal, and $\mathbf{S}_{\mathcal{F}}^H \mathbf{S}_{\mathcal{F}}$ is diagonal and satisfies

$$\mathbf{S}_{\mathcal{F}}^H \mathbf{S}_{\mathcal{F}} = \mathbf{I}_2 \otimes [\mathbf{S}_{1\mathcal{F}}^H \mathbf{S}_{1\mathcal{F}} + \mathbf{S}_{2\mathcal{F}}^H \mathbf{S}_{2\mathcal{F}}]. \tag{5.51}$$

Then the operations in Equation (5.50) consist of only some linear processing, thus can be executed with relatively low computational complexity. Upon solving the estimates $\hat{\mathbf{h}}_{1\mathcal{F}}$ and $\hat{\mathbf{h}}_{2\mathcal{F}}$ from Equation (5.50), we can easily obtain their time-domain counterparts by simply implementing a N_b-point IDFT operation on them.

As for the training sequence in $\mathbf{s}_1$ or $\mathbf{s}_2$, ideally, it should have equal or nearly equal magnitude for all FFT grids, and should have impulse-like autocorrelation as well as zero cross correlation, so that each frequency component of the channel is ensured to be probed uniformly to provide the frequency-domain channel estimate. In fact, our adoption of the CP-only scheme also conforms to this requirement, because if the ZP-only scheme is used instead, those padding zeroes will be involved in the FFT transformation together with the training symbols, and some low values are expected to appear on the FFT grids, hence making the channel estimation inadequate. The Chu sequences [59] are suitable for the above requirements, which belong to the alphabet $\boldsymbol{\mathcal{A}} = \{a_k | k = 0, 1, \cdots, N_b - 1\}$. And a_k is expressed as

$$a_k = \begin{cases} \exp\left\{ i \dfrac{M\pi k^2}{N_b} \right\}, & \text{when } \mathrm{N_b} \text{ is even} \\ \exp\left\{ i \dfrac{M\pi k(k+1)}{N_b} \right\}, & \text{when } \mathrm{N_b} \text{ is odd} \end{cases}$$

where M is relatively prime to N_b.

Now let us examine some performance measures of the channel estimation. One of them is the estimation error; here we define it in the frequency domain, as given by $\mathbf{e}_{\mathcal{F}} = \mathbf{h}_{\mathcal{F}} - \hat{\mathbf{h}}_{\mathcal{F}}$. Then the covariance of $\mathbf{e}_{\mathcal{F}}$ can be expressed as

$$\mathbf{R}_{e_{\mathcal{F}}} = E\{\mathbf{e}_{\mathcal{F}}\mathbf{e}_{\mathcal{F}}^H\} = (\mathbf{S}_{\mathcal{F}}^H\mathbf{S}_{\mathcal{F}})^{-1}\mathbf{S}_{\mathcal{F}}^H\mathbf{R}_{n_{\mathcal{F}}}\mathbf{S}_{\mathcal{F}}(\mathbf{S}_{\mathcal{F}}^H\mathbf{S}_{\mathcal{F}})^{-1} \tag{5.52}$$

where $\mathbf{R}_{n_{\mathcal{F}}} = E\{\mathbf{n}_{\mathcal{F}}\mathbf{n}_{\mathcal{F}}^H\}$. As the orthonormal IDFT operations on the received blocks do not color the additive noise [31], we may let $\mathbf{R}_{n_{\mathcal{F}}} = \sigma_n^2\mathbf{I}_{2N_b}$, and Equation (5.52) changes to

$$\mathbf{R}_{e_{\mathcal{F}}} = \sigma_n^2(\mathbf{S}_{\mathcal{F}}^H\mathbf{S}_{\mathcal{F}})^{-1} \tag{5.53}$$

Making use of the result in Equation (5.51), we can write the frequency-domain channel estimation mean square error (MSE) $\varepsilon_{\mathcal{F}}^2$ as

$$\begin{aligned}
\varepsilon_{\mathcal{F}}^2 &= \mathrm{E}\{\|\mathbf{e}_{\mathcal{F}}\|^2\} = Tr\{\mathbf{R}_{e_{\mathcal{F}}}\} \\
&= 2\sigma_n^2 \cdot Tr\big\{(\mathbf{S}_{1\mathcal{F}}^H\mathbf{S}_{1\mathcal{F}} + \mathbf{S}_{2\mathcal{F}}^H\mathbf{S}_{2\mathcal{F}})^{-1}\big\} \\
&= \sum_{i=1}^{N_b} \frac{2\sigma_n^2}{|s_{1\mathcal{F}}(i)|^2 + |s_{2\mathcal{F}}(i)|^2}
\end{aligned} \tag{5.54}$$

where $s_{1\mathcal{F}}(i)$ and $s_{2\mathcal{F}}(i)$ are elements of $\mathbf{s}_{1\mathcal{F}}$ and $\mathbf{s}_{1\mathcal{F}}$, respectively.

5.4 Simulation Results and Discussion

In this section, we investigate the performance of above-introduced FDE and channel estimation schemes with application to one typical system - EDGE. EDGE (enhanced data rates for GSM evolution) is a digital mobile phone technology that achieves a significant increase in bit rate over its second-generation predecessors GSM and TDMA/136 by applying the modulation format 8-ary phase shift keying

(8-PSK) instead of binary Gaussian minimum shift keying (GMSK) which is used in GSM [34]. The EDGE system is currently being deployed to provide an evolutionary path for delivering third-generation services in existing spectrum band, therefore, there is great interest in evaluating its performance under various practical techniques, such as the work in [30] and [61]; that is the reason why here we take it as a case study.

Our simulations focus on the special case of 2-TX 1-RX, as it conveys the essential concepts of STBCs, and is sufficient for examining the effectiveness of these FDE schemes. We assume that the total transmitted power from the two antennas is the same as the transmit power from the single transmit antenna. In our simulations, we normalize the average energy of the symbols transmitted from each antenna to one, and meanwhile double the noise variance (compared with the 1TX scenario), so that the SNR for both 2TX and 1TX cases are comparable.

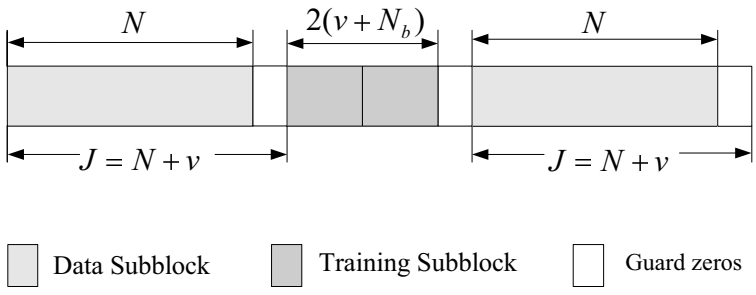

Figure 5.5: Modified burst format for EDGE

We consider 8-PSK modulations without channel coding deployed at the transmitter. The GSM 05.05 EQ wireless channel model [60], which is frequency-selective with channel memory v equal to 3, is adopted in our simulations for the equaliza-

tion test. We deploy the ZP-only scheme as data transmission format, which may result in slight changes to the original EDGE burst structure. The modified burst structure is depicted in Figure 5.5, and the transmission format for training subblock can be found in Figure 5.4. Here we still assume block fading: the channel fading gains are constant over one burst (including both data and training subblocks), and are independent from burst to burst. The data subbock length, N, is set to 61, hence we have the FFT size J as $J = N + v = 64$. In all simulation results, the BER curves are plotted as a function of E_b/N_0.

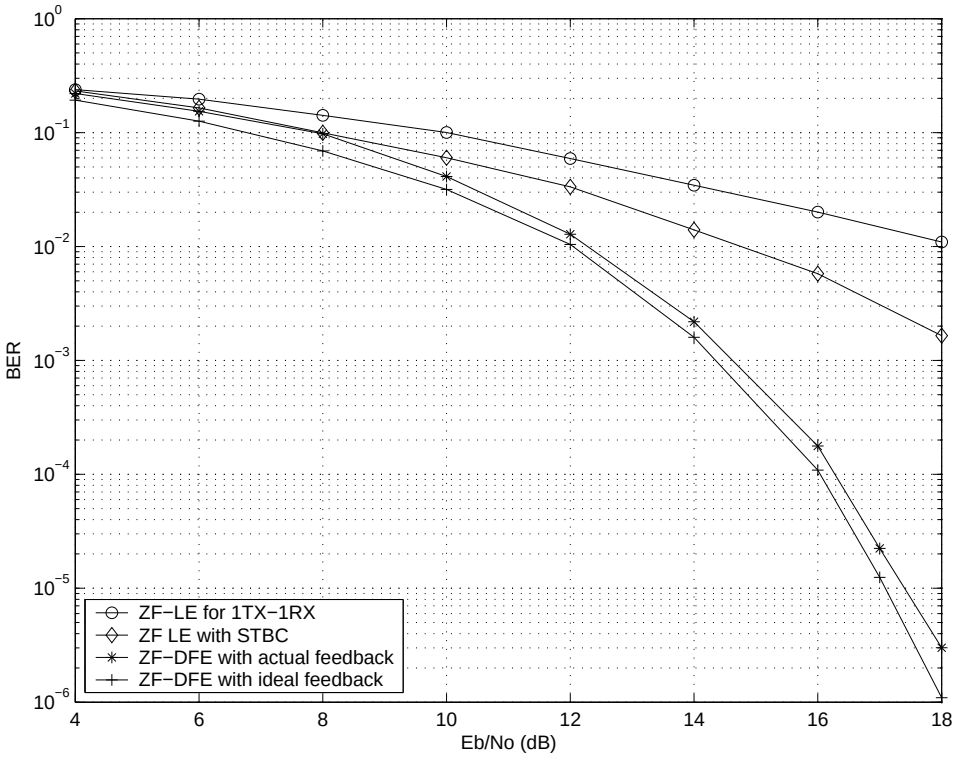

Figure 5.6: BER performance of ZF FDE schemes for STBC transmissions over EDGE EQ channel. Perfect CSI is assumed at the receiver.

Figure 5.6 and Figure 5.7 depict the BER performance corresponding to the

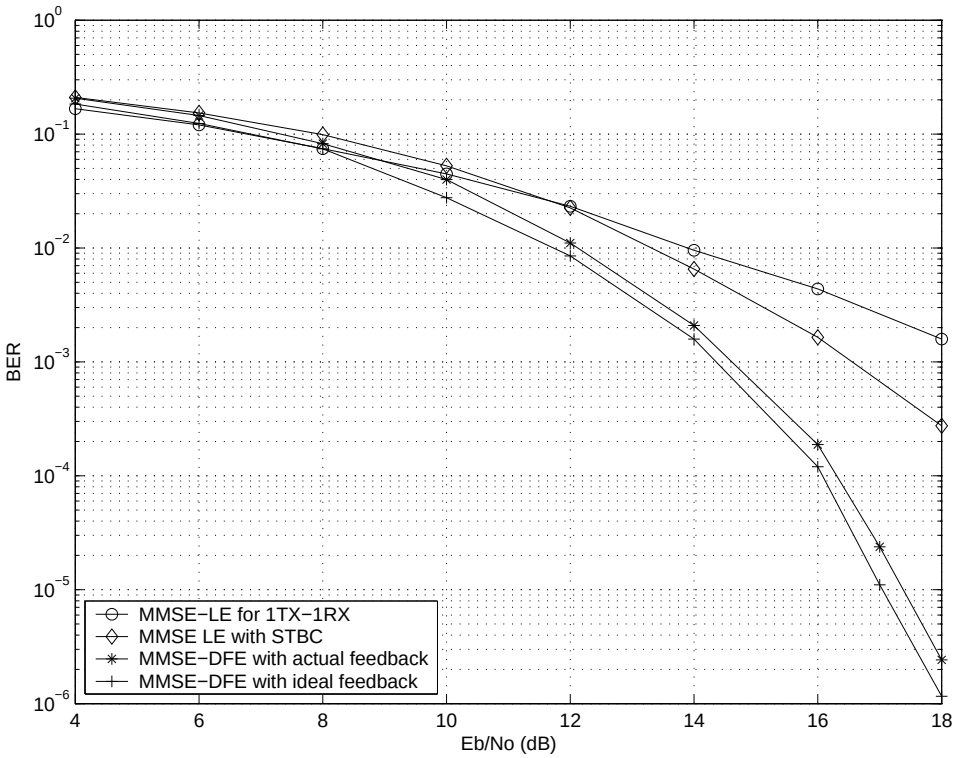

Figure 5.7: BER performance of MMSE FDE schemes for STBC transmissions over EDGE EQ channel. Perfect CSI is assumed at the receiver.

FDE schemes (including linear equalization (LE) and DFE) based on ZF criterion and MMSE criterion, respectively. The CSI is assumed to be perfectly known at the receiver. For the DFE, we depict its performance with both ideal feedback (assuming correct past decisions) and practical feedback (using actual past decisions). Additionally, for the purpose of performance comparison, we also depict the BER performance of frequency-domain ZF-LE (MMSE-LE)[4] for single transmitter case in Figure 5.6 (Figure 5.7). From these two figures, we have some common observations; we list some of them in the following, together with our explanation.

[4]Expression of frequency-domain linear equalizer for such single transmitter case can refer to Equation (3.31) in Chapter 3.

- Performance of LE with STBC, either based on ZF criterion or MMSE criterion, is superior to that of the corresponding LE for single transmitter case. The diversity gain introduced by STBCs may account for such performance improvement.

- The DFE achieves a substantial improvement in BER performance over its linear counterpart, even without the assumption of ideal decision feedback. That is due to the existence of the feedback equalization matrix $\mathbf{B}$, which eliminates the residual ISI from past decisions.

- Performance of the DFE with ideal decision feedback is close to its counterpart with actual decision feedback. That is because:

    1. Implementation of successive cancellation at the feedback filterbank is confined to one data subblock, so that decision errors do not carry on from block to block, and catastrophic error propagation can be minimized.

    2. As we adopt ZP-only scheme as data transmission format, the padding zeros at the end of each data block are actually known to the receiver, and can be regarded as pilot symbols (assuming perfect synchronization), therefore, the successive cancellation in each data subblock can always begin with correct decision feedback.

For the convenience of investigating the effect of criterion choice on the equalization performance, we plot the BER performance curves of those FDE schemes

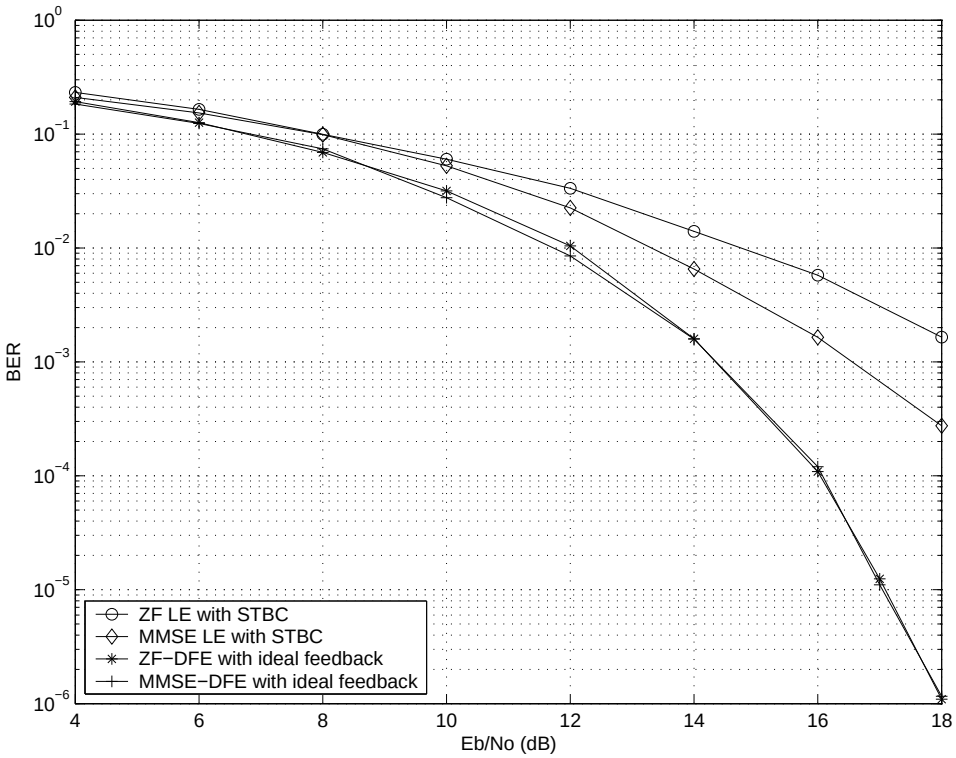

Figure 5.8: Performance comparison of FDE schemes based different optimization criteria: ZF and MMSE

based on both ZF and MMSE criteria in one figure, i.e., Figure 5.8. As for the LE scheme, we observe that performance of MMSE-LE is superior over that of the ZF-LE, which verifies our early assertion that performance improvement can be expected by using MMSE criterion instead of ZF criterion to design the linear equalizer. But for the DFE scheme, as shown in Figure 5.8, we cannot tell the difference between them for the application mentioned, since the performance curves of the ZF-DFE and MMSE-DFE nearly overlap each other.

We also investigate the performance of our proposed training-based frequency-domain channel estimation scheme. In our simulations, we choose the Chu se-

quences [59] as the training sequence. The length of training sequence N_b, in our simulations, is set to $v + 1 = 4$, which is the minimum length to estimate this EDGE EQ channel. The training blocks between two consecutive data subblocks, as shown in Figure 5.5. Such placement retains the relative positions for data symbols and training symbols in the original EDGE burst structure. Figure 5.9 depicts

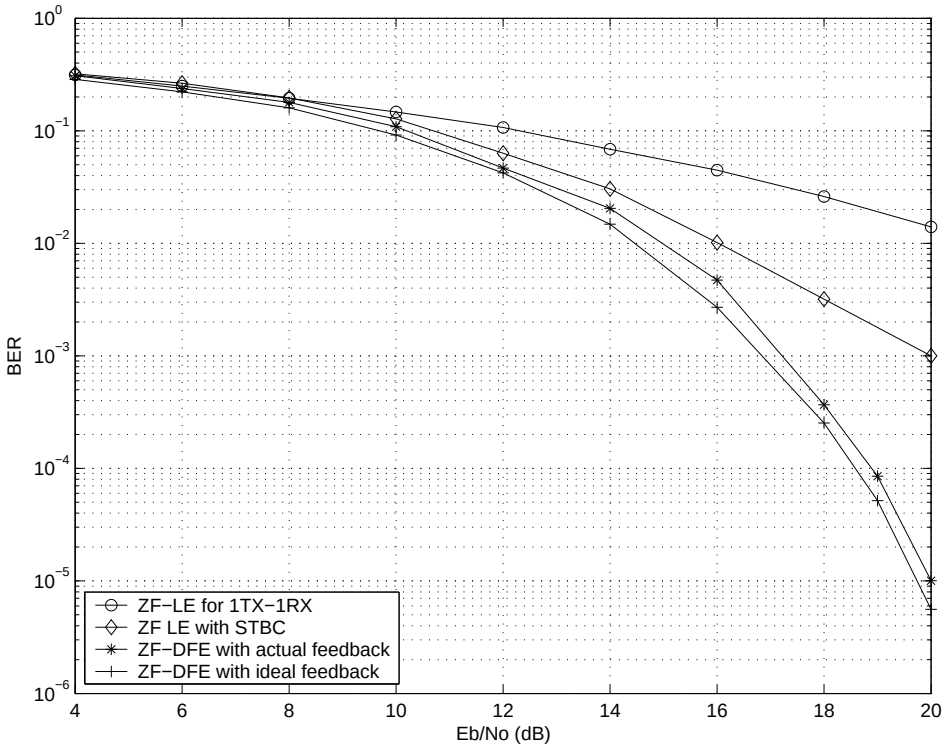

Figure 5.9: BER performance of ZF FDE schemes for STBC transmissions over EDGE EQ channel. Training based channel estimation is adopted.

performance corresponding to the ZF DFE schemes based on the estimated channel; Figure 5.10 depicts the MMSE version with channel estimation. Comparing Figure 5.9 and Figure 5.10 with Figure 5.6 and Figure 5.7, respectively, we observe that our estimation scheme, at its worst, incurs about 3dB penalty for inaccurate channel estimation.

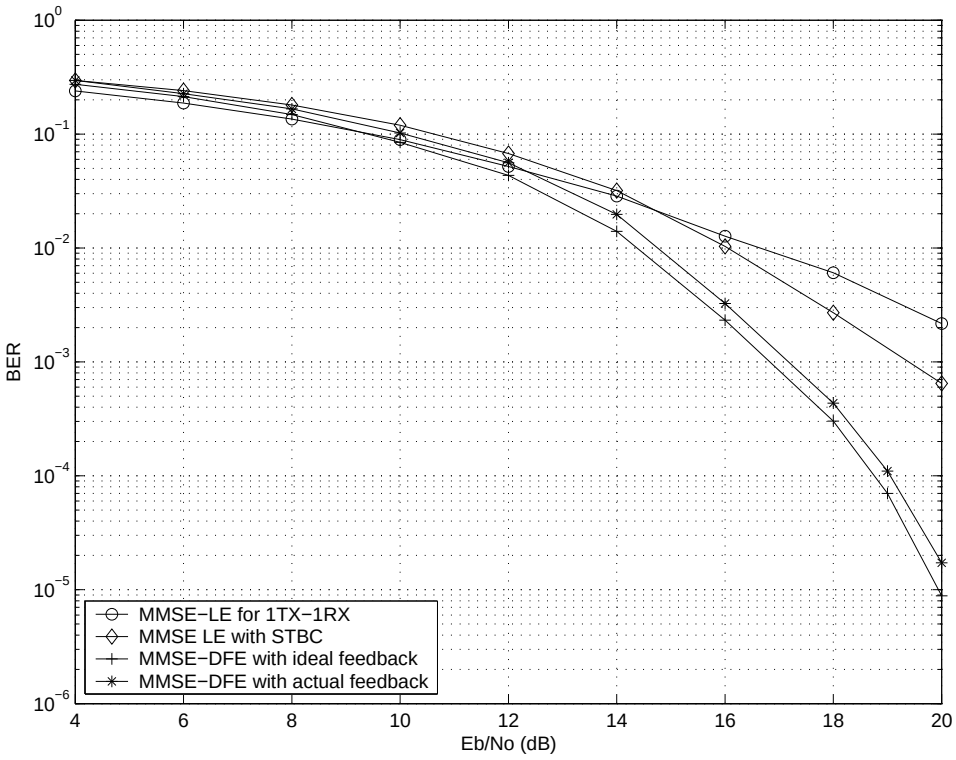

Figure 5.10: BER performance of MMSE FDE schemes for STBC transmissions over EDGE EQ channel. Training based channel estimation is adopted.

Our schemes, including equalization schemes and channel estimation scheme, can also be applied to some broadband wireless systems with comparable computational complexity, e.g., the BWA (broadband wireless access) systems that are under intense research and standardization for application in local and metropolitan area networks [62]. Such BWA systems can offer bit rates of tens of megabits per second or more, but operate on NLOS conditions in which severe multipath is encountered and the resulting ISI may span up 100 or more symbols.

However, wee need to point out that, the DFE schemes, either under ZF or MMSE criterion, although achieve substantial performance improvement over LE

schemes, they are more suitable for applications with relatively small size blocks. That is because in the FDE scheme, to obtain the feedback matrix $\mathbf{B}$, we need implement the matrix Cholesky factorization, which requires relatively high computations, especially when the data size is very large.

Our simulations, in fact, do not reflect the effect of channel variations on the BER performance, as we assume block fading and the fading changes independently from one burst to another. However, in practice, the channel frequency dispersion, or Doppler spread does affect the design of data block size, as well as the selection of equalization schemes.

5.5 Summary

In this chapter, we focused on the channel estimation based FDE for STBC transmissions over multipath fading channels. We developed linear and nonlinear (DFE) FDE schemes based on ZF and MMSE criteria. Closed form expressions for computing tap weights of these equalization schemes, especially the ZF-DFE and MMSE-DFE, are derived in this chapter. We also proposed a training based frequency-domain channel estimation method, in which the training blocks are encoded by the same space-time coder as the data blocks. We evaluated our equalization and estimation schemes by applying them to the EDGE system. Simulation results indicate significant performance improvement as compared to the single transmitter case with FDE, as well as effectiveness of our channel estimation method.

Chapter 6

Adaptive FDE for STBC Transmissions

Those equalization schemes developed in Chapter 5, either linear or nonlinear, unanimously require the CSI available beforehand at the receiver. As a result, some form of channel estimation must be performed before implementation of the channel equalization, such as the the training-based frequency-domain channel estimation which was also proposed for application in Chapter 5. Whereas, as we earlier mentioned in Chapter 1, there exists one alternative equalization method that can obviate the need for channel estimation; that is, the adaptive equalization. In Chapter 3, we have introduced the basic concept of adaptive equalization as well as some commonly used algorithms that update the equalizer coefficients. In this chapter, we will pursue adaptive FDE for the STBC transmissions over multipath fading channels, which realizes joint channel estimation and equalization. Additionally a diversity combining scheme is proposed in this chapter as well.

6.1 Adaptive Linear Equalization

By defining $\mathbf{s}_{\mathcal{F}}(2i) = \mathbf{F}_J\mathbf{s}(2i)$ and $\mathbf{s}_{\mathcal{F}}(2i+1) = \mathbf{F}_J\mathbf{s}(2i+1)$, we can rewrite Equation (4.32) in Chapter 4 as

$$\bar{\mathbf{x}}_{\mathcal{F}}(i) = \underbrace{\begin{bmatrix} \mathbf{D}_1 & \mathbf{D}_2 \\ \mathbf{D}_2^* & -\mathbf{D}_1^* \end{bmatrix}}_{\mathbf{D}} \underbrace{\begin{bmatrix} \mathbf{s}_{\mathcal{F}}(2i) \\ \mathbf{s}_{\mathcal{F}}(2i+1) \end{bmatrix}}_{\bar{\mathbf{s}}_{\mathcal{F}}(i)} + \underbrace{\begin{bmatrix} \mathbf{n}_{\mathcal{F}}(2i) \\ \mathbf{n}_{\mathcal{F}}^*(2i+1) \end{bmatrix}}_{\bar{\mathbf{n}}_{\mathcal{F}}(i)} \tag{6.1}$$

With above definitions of $\mathbf{D}$, $\bar{\mathbf{s}}_{\mathcal{F}}(i)$ and $\bar{\mathbf{n}}_{\mathcal{F}}(i)$, we can further simplify Equation (6.1) to

$$\bar{\mathbf{x}}_{\mathcal{F}}(i) = \mathbf{D}\bar{\mathbf{s}}_{\mathcal{F}}(i) + \bar{\mathbf{n}}_{\mathcal{F}}(i),$$

where it is noteworthy that the noise vector $\bar{\mathbf{n}}_{\mathcal{F}}(i)$ remains white. At this point, the equalization problem can be reformulated as to recovering $\bar{\mathbf{s}}_{\mathcal{F}}(i)$ from $\bar{\mathbf{x}}_{\mathcal{F}}(i)$. Or specifically speaking, we first obtain the frequency estimates of the symbol blocks. Next we can transform these estimates back to the time domain for symbol detection by use of the IDFT operations. That is, the implementation of IDFT is explicitly separated from the equalization and the equalization operates in two-blocks level rather than in one-block (or subblock) level. However, this method, in its nature, is still the same as those linear FDE schemes (inclusive of ZF and MMSE) that we have developed in Chapter 5.

Let $\breve{\mathbf{s}}_{\mathcal{F}}(i) = [\hat{\mathbf{s}}_{\mathcal{F}}^T(2i) \quad \hat{\mathbf{s}}_{\mathcal{F}}^T(2i+1)]^T$ denotes frequency domain estimates of the data blocks, and it can be expressed as

$$\breve{\mathbf{s}}_{\mathcal{F}}(i) = \bar{\mathbf{G}}_{\mathcal{F}}\bar{\mathbf{x}}_{\mathcal{F}}(i) \tag{6.2}$$

where $\bar{\mathbf{G}}_{\mathcal{F}}$ is a $2J \times 2J$ matrix, representing the frequency-domain equalizer. Simply following the procedure that we adopted in Chapter 5 when developing the linear

FDE schemes, we can formulate the equalizer $\bar{\mathbf{G}}_{\mathcal{F}}$ as

$$\bar{\mathbf{G}}_{\mathcal{F}} = (\mathbf{D}^H\mathbf{D} + \mathbf{I}_{2J}/\text{SNR})^{-1}\mathbf{D}^H$$

or the unfolded version

$$\begin{aligned}\bar{\mathbf{G}}_{\mathcal{F}} &= \begin{bmatrix} (\mathbf{D}_{12}^2 + \mathbf{I}_J/\text{SNR})^{-1} & \mathbf{0}_{J\times J} \\ \mathbf{0}_{J\times J} & (\mathbf{D}_{12}^2 + \mathbf{I}_J/\text{SNR})^{-1} \end{bmatrix} \begin{bmatrix} \mathbf{D}_1^* & \mathbf{D}_2 \\ \mathbf{D}_2^* & -\mathbf{D}_1 \end{bmatrix} \\ &= \begin{bmatrix} \mathbf{G}_{1\mathcal{F}} & \mathbf{G}_{2\mathcal{F}} \\ \mathbf{G}_{2\mathcal{F}}^* & -\mathbf{G}_{1\mathcal{F}}^* \end{bmatrix}\end{aligned}$$

where $\mathbf{G}_{1\mathcal{F}}$ and $\mathbf{G}_{2\mathcal{F}}$ are defined by

$$\mathbf{G}_{1\mathcal{F}} = (\mathbf{D}_{12}^2 + \mathbf{I}_J/\text{SNR})^{-1}\mathbf{D}_1^* \quad \text{and} \quad \mathbf{G}_{2\mathcal{F}} = (\mathbf{D}_{12}^2 + \mathbf{I}_J/\text{SNR})^{-1}\mathbf{D}_2.$$

It is easy to verify that both $\mathbf{G}_{1\mathcal{F}}$ and $\mathbf{G}_{2\mathcal{F}}$ are $J \times J$ diagonal matrices. We define their diagonal vectors as $\mathbf{g}_{1\mathcal{F}}$ and $\mathbf{g}_{2\mathcal{F}}$, respectively; that is

$$\mathbf{G}_{1\mathcal{F}} = \text{diag}\{\mathbf{g}_{1\mathcal{F}}\} \quad \text{and} \quad \mathbf{G}_{2\mathcal{F}} = \text{diag}\{\mathbf{g}_{2\mathcal{F}}\} \tag{6.3}$$

We expand Equation (6.2) as below

$$\begin{bmatrix} \hat{\mathbf{s}}_{\mathcal{F}}(2i) \\ \hat{\mathbf{s}}_{\mathcal{F}}(2i+1) \end{bmatrix} = \begin{bmatrix} \mathbf{G}_{1\mathcal{F}} & \mathbf{G}_{2\mathcal{F}} \\ \mathbf{G}_{2\mathcal{F}}^* & -\mathbf{G}_{1\mathcal{F}}^* \end{bmatrix} \begin{bmatrix} \mathbf{x}_{\mathcal{F}}(2i) \\ \mathbf{x}_{\mathcal{F}}^*(2i+1) \end{bmatrix}. \tag{6.4}$$

Let us define

$$\mathbf{X}_{\mathcal{F}}(2i) = \text{diag}\{\mathbf{x}_{\mathcal{F}}(2i)\} \quad \text{and} \quad \mathbf{X}_{\mathcal{F}}(2i+1) = \text{diag}\{\mathbf{x}_{\mathcal{F}}(2i+1)\}. \tag{6.5}$$

By applying Equation (6.3), Equation (6.4) can be reformulated as

$$\underbrace{\begin{bmatrix} \hat{\mathbf{s}}_{\mathcal{F}}(2i) \\ \hat{\mathbf{s}}_{\mathcal{F}}^*(2i+1) \end{bmatrix}}_{\vec{\boldsymbol{s}}_{\mathcal{F}}(i)} = \underbrace{\begin{bmatrix} \mathbf{X}_{\mathcal{F}}(2i) & \mathbf{X}_{\mathcal{F}}^*(2i+1) \\ -\mathbf{X}_{\mathcal{F}}(2i+1) & \mathbf{X}_{\mathcal{F}}^*(2i) \end{bmatrix}}_{\boldsymbol{U}_{\mathcal{F}}(i)} \underbrace{\begin{bmatrix} \mathbf{g}_{1\mathcal{F}} \\ \mathbf{g}_{2\mathcal{F}} \end{bmatrix}}_{\boldsymbol{w}_{\mathcal{F}}(i)}. \tag{6.6}$$

or the simplified version

$$\vec{\boldsymbol{s}}_{\mathcal{F}}(i) = \boldsymbol{U}_{\mathcal{F}}(i)\boldsymbol{w}_{\mathcal{F}}(i) \tag{6.7}$$

where $\vec{\boldsymbol{s}}_{\mathcal{F}}(i)$ is a $2J \times 1$ vector containing estimates of the $(2i)$th data block and conjugate of the $(2i+1)$th block; $\boldsymbol{U}_{\mathcal{F}}(i)$ ia an orthogonal matrix with the size $2J \times 2J$, which is made up of the frequency transform of two consecutive received data blocks; $\boldsymbol{w}_{\mathcal{F}}(i)$ is a $2J \times 1$ vector that contains the elements of $\mathbf{g}_{1\mathcal{F}}$ and $\mathbf{g}_{2\mathcal{F}}$.

Comparing Equation (6.2) and Equation (6.7), we may observe an interesting phenomenon that the $2J \times 2J$ equalization matrix $\bar{\mathbf{G}}_{\mathcal{F}}$ in Equation (6.2) reduces to a $2J \times 1$ equalizer vector $\boldsymbol{w}_{\mathcal{F}}(i)$ in Equation (6.7). This transform largely owes to the orthogonal property of STBCs, and it enables the equalization to be implemented by a single filter. Moreover, Equation (6.7) also suggests that such equalization can be performed adaptively by using some form of block adaptive algorithms to update $\boldsymbol{w}_{\mathcal{F}}(i)$.

In the following, we proceed to the development of adaptive FDE for STBC block transmissions over multipath fading channel, and two specific block recursive algorithms, BLMS and BRLS, will be examined with their application to the equalization. However, we need to point out that, the adaptive FDE that we use here should not be regarded the same as the Type I method of FDE that we formerly described in Chapter 3, even though both of them employ adaptive filter and block recursive algorithms. The frequency-domain characteristic of this adaptive equalization, in fact, attributes to the circulant property of the channel matrix $\mathbf{H}_{\mu}$ together with the specially designed permutation matrix $\mathbf{P}$ as explained in Chapter 4.

6.1.1 BLMS Algorithm

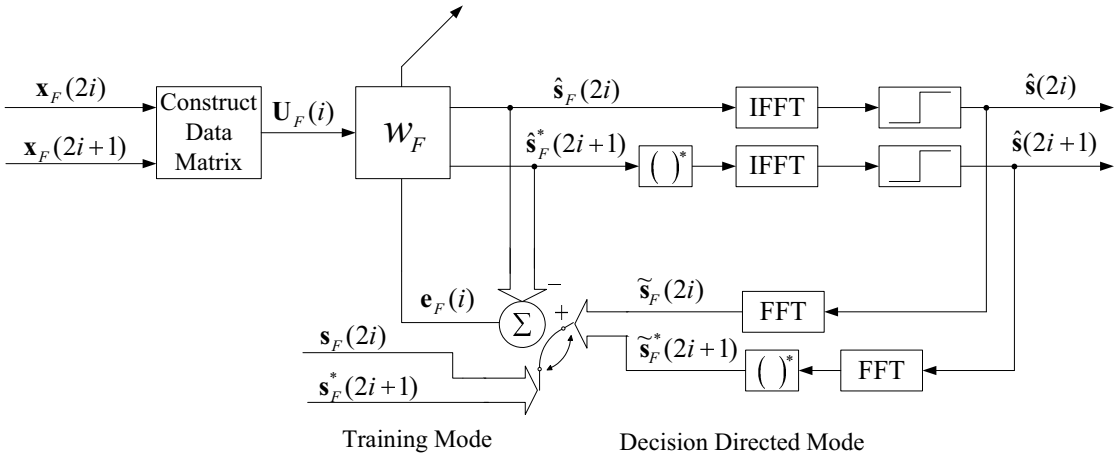

Figure 6.1: Block diagram of the adatpive FDE

Figure 6.1 depicts block diagram of the adaptive FDE[1]. $\boldsymbol{U}_{\mathcal{F}}(i)$ denotes the data matrix, each of its row can be regarded as a single input data block to the filter at a specific time. The equalizer output is the product of the data matrix and the equalizer coefficients, as shown in Equation (6.7). The filter output , $\vec{\boldsymbol{s}}_{\mathcal{F}}(i)$, is transformed back to time domain by means of IFFT operations, and then rendered to a decision-making device for detection.

The error signal, $\boldsymbol{e}_{\mathcal{F}}(i)$, is generated by comparing the equalizer output with the desired response which varies in the definition with respect to the operating modes. Usually there are two modes that an adaptive filter work in: training mode, and decision directed mode. At startup, the equalizer operates in the training mode, where training blocks are sent from the transmitter to make the filter converge. The

[1]Detailed structure of this adaptive equalizer is not shown in Figure 6.1; readers can refer to the linear transversal equalizer in Chapter 3.

desired response, in fact, is already available at the receiver, as defined by

$$\boldsymbol{s}'_{\mathcal{F}}(i) = \begin{bmatrix} \mathbf{s}_{\mathcal{F}}(2i) \\ \mathbf{s}^*_{\mathcal{F}}(2i+1) \end{bmatrix} = \begin{bmatrix} \mathbf{F}_J \mathbf{s}(2i) \\ \mathbf{F}^*_J \mathbf{s}^*(2i+1) \end{bmatrix}$$

After achieving convergence, the equalizer switches to the decision directed mode, where frequency transform of previous decisions are used to update the equalizer coefficients for tracking the channel variation. Under this mode, the desired response is expressed as

$$\vec{\boldsymbol{s}}\,'_{\mathcal{F}}(i) = \begin{bmatrix} \tilde{\mathbf{s}}_{\mathcal{F}}(2i) \\ \tilde{\mathbf{s}}^*_{\mathcal{F}}(2i+1) \end{bmatrix} = \begin{bmatrix} \mathbf{F}_J \hat{\mathbf{s}}_{\mathcal{F}}(2i) \\ \mathbf{F}^*_J \hat{\mathbf{s}}^*_{\mathcal{F}}(2i+1) \end{bmatrix}$$

The equalizer coefficients can be updated according to the BLMS algorithm that we have covered earlier in Chapter 3. Compared with the classical LMS algorithm, BLMS has the advantage of substantially reduced computational complexity, since the tap weights, e.g., in this scenario, is updated every two received blocks, rather than every recited symbol. Details regarding the BLMS algorithm will not be given here; readers can refer to [41] or [42]. We express the coefficients updating formulae as below:

1. Equalizer output:

$$\vec{\boldsymbol{s}}_{\mathcal{F}}(i) = \boldsymbol{U}_{\mathcal{F}}(i)\boldsymbol{w}_{\mathcal{F}}(i) \tag{6.8}$$

2. Error signal:

$$\boldsymbol{e}_{\mathcal{F}}(i) = \begin{cases} \boldsymbol{s}'_{\mathcal{F}}(i) - \vec{\boldsymbol{s}}_{\mathcal{F}}(i), & \text{Training mode} \\ \\ \vec{\boldsymbol{s}}\,'_{\mathcal{F}}(i) - \vec{\boldsymbol{s}}_{\mathcal{F}}(i), & \text{Decision directed mode} \end{cases} \tag{6.9}$$

3. Coefficients adaptation:

$$\boldsymbol{w}_{\mathcal{F}}(i+1) = \boldsymbol{w}_{\mathcal{F}}(i) + \mu \boldsymbol{U}_{\mathcal{F}}^{H}(i)\boldsymbol{e}_{\mathcal{F}}(i) \tag{6.10}$$

where μ denotes the step size.

The BLMS algorithm, similar with its step-by-step counterpart, is slow in the convergence rate, since there is only one single parameter, i.e., μ, to control the rate of adaption, as can be seen from Equation (6.10). To achieve faster convergence, we can resort to another algorithm, namely, BRLS algorithm, which involves additional parameters in adapting the equalizer coefficients, at a block level too.

6.1.2 BRLS Algorithm

The BRLS algorithm, also known as SU-RLS (subsampled-updating RLS) algorithm, is a block-exact version of the classical RLS algorithm. As for details about this algorithm, readers can refer to [63]. With a slight modification, this BRLS algorithm can be applied here to iteratively update the equalizer coefficients, as formulated in the following steps:

1. Compute equalizer output:

$$\vec{\boldsymbol{s}}_{\mathcal{F}}(i+1) = \boldsymbol{U}_{\mathcal{F}}(i+1)\boldsymbol{w}_{\mathcal{F}}(i) \tag{6.11}$$

2. Compute error signal:

$$\boldsymbol{e}_{\mathcal{F}}(i+1) = \begin{cases} \boldsymbol{s}'_{\mathcal{F}}(i+1) - \vec{\boldsymbol{s}}_{\mathcal{F}}(i+1), & \text{Training mode} \\ \vec{\boldsymbol{s}}\,'_{\mathcal{F}}(i+1) - \vec{\boldsymbol{s}}_{\mathcal{F}}(i+1), & \text{Decision directed mode} \end{cases} \tag{6.12}$$

3. Compute Kalman gain matrix:

$$\boldsymbol{\mathcal{C}}(i+1) = \boldsymbol{\mathcal{P}}(i)\boldsymbol{U}_{\mathcal{F}}^{H}(i+1); \tag{6.13}$$

$$\boldsymbol{\mathcal{Z}}(i+1) = \lambda \mathbf{I}_{2J} + \boldsymbol{U}_{\mathcal{F}}(i+1)\boldsymbol{\mathcal{C}}(i+1); \tag{6.14}$$

$$\boldsymbol{\mathcal{K}}(i+1) = \boldsymbol{\mathcal{C}}(i+1)\boldsymbol{\mathcal{Z}}^{-1}(i+1) \tag{6.15}$$

4. Update inverse of the correlation matrix:

$$\boldsymbol{\mathcal{P}}(i+1) = \frac{1}{\lambda}[\boldsymbol{\mathcal{P}}(i) - \boldsymbol{\mathcal{K}}(i+1)\boldsymbol{U}_{\mathcal{F}}(i+1)\boldsymbol{\mathcal{P}}(i)] \tag{6.16}$$

5. Update equalizer coefficients:

$$\boldsymbol{w}_{\mathcal{F}}(i+1) = \boldsymbol{w}_{\mathcal{F}}(i) + \boldsymbol{\mathcal{K}}(i+1)\boldsymbol{e}_{\mathcal{F}}(i+1) \tag{6.17}$$

$$= \boldsymbol{w}_{\mathcal{F}}(i) + \boldsymbol{\mathcal{P}}(i+1)\boldsymbol{U}_{\mathcal{F}}^{H}(i+1)\boldsymbol{e}_{\mathcal{F}}(i+1) \tag{6.18}$$

where $\boldsymbol{e}_{\mathcal{F}}(i+1)$ is the a priori error vector; $\boldsymbol{\mathcal{K}}(i+1)$ denotes the Kalman gain; $\boldsymbol{\mathcal{P}}(i+1)$ represents the inverse correlation matrix; λ is the forgetting factor that is set based on the channel variation. Initial values of the $\boldsymbol{w}_{\mathcal{F}}(0)$ and $\boldsymbol{\mathcal{P}}(0)$ are given by

$$\boldsymbol{w}_{\mathcal{F}}(0) = \mathbf{0}_{2J\times 1}; \quad \boldsymbol{\mathcal{P}}(0) = (1/\delta)\mathbf{I}_{2J}, \tag{6.19}$$

where δ is a small value.

Substituting Equation (6.15) into Equation (6.16), we can reformulate $\boldsymbol{\mathcal{P}}(i+1)$ as

$$\boldsymbol{\mathcal{P}}(i+1) = \frac{1}{\lambda}\left[\boldsymbol{\mathcal{P}}(i) - \frac{\boldsymbol{\mathcal{P}}(i)\boldsymbol{U}_{\mathcal{F}}^{H}(i+1)\boldsymbol{U}_{\mathcal{F}}(i+1)\boldsymbol{\mathcal{P}}(i)}{\lambda\mathbf{I}_{2J} + \boldsymbol{U}_{\mathcal{F}}(i+1)\boldsymbol{\mathcal{P}}(i)\boldsymbol{U}_{\mathcal{F}}^{H}(i+1)}\right]. \tag{6.20}$$

Comparing Equation (6.18) with Equation (6.10), we can observe that the BRLS algorithm adopts a matrix, rather than a single parameter to control the rate

of adaption. Such fact, to a certain extent, explains why the BRLS algorithm can achieve a quick convergence as compared to the BLMS algorithm. However, the quick convergence achieved by the BRLS algorithm, is at the cost of a heavy increase in computational complexity. Due to the existence of matrix inversion, calculation of the inverse correlation matrix $\boldsymbol{\mathcal{P}}(i+1)$, as shown in Equation (6.20), requires quite a number of computations, which accounts for a majority of the computational complexity increase. A fast version of the BRLS algorithm, namely FSU-RLS (fast subsampled-updating RLS) algorithm [63], can be used to achieve some complexity reduction by using FFT in computations. But here, by exploiting the special structure of the STBCs instead, we can achieve a substantial reduction in the complexity; such complexity reduction method is also available in [64]. We explain it in the following.

As we pointed out before, the data matrix $\boldsymbol{U}_{\mathcal{F}}(i)$ that is given by

$$\boldsymbol{U}_{\mathcal{F}}(i) = \begin{bmatrix} \mathbf{X}_{\mathcal{F}}(2i) & \mathbf{X}^*_{\mathcal{F}}(2i+1) \\ -\mathbf{X}_{\mathcal{F}}(2i+1) & \mathbf{X}^*_{\mathcal{F}}(2i) \end{bmatrix} \tag{6.21}$$

is a $2J \times 2J$ orthogonal matrix, we have

$$\boldsymbol{U}^H_{\mathcal{F}}(i)\boldsymbol{U}_{\mathcal{F}}(i) = \mathbf{I}_2 \otimes \boldsymbol{\mathcal{X}}_{\mathcal{F}}(i) \tag{6.22}$$

where $\boldsymbol{\mathcal{X}}_{\mathcal{F}}(i)$ is a $J \times J$ diagonal matrix as defined by

$$\boldsymbol{\mathcal{X}}_{\mathcal{F}}(i) = \mathbf{X}_{\mathcal{F}}(2i)\mathbf{X}^*_{\mathcal{F}}(2i) + \mathbf{X}_{\mathcal{F}}(2i+1)\mathbf{X}^*_{\mathcal{F}}(2i+1).$$

By using Equation (6.22) and following the definition of the inverse correlation matrix, we may induce that $\boldsymbol{\mathcal{P}}(i+1)$ is a $2J \times 2J$ diagonal matrix with the form of

$$\boldsymbol{\mathcal{P}}(i+1) = \mathbf{I}_2 \otimes \boldsymbol{P}(i+1), \tag{6.23}$$

where $\boldsymbol{P}(i+1)$ is also a diagonal matrix with size of $J \times J$. Clearly Equation (6.23) holds true at the initialization, where $\boldsymbol{\mathcal{P}}(0) = (1/\delta)\mathbf{I}_{2J}$ and $\boldsymbol{P}(0) = (1/\delta)\mathbf{I}_J$. Then we have

$$\begin{aligned} & \boldsymbol{U}_{\mathcal{F}}^H(i+1)\boldsymbol{U}_{\mathcal{F}}(i+1)\left[\lambda\,\mathbf{I}_{2J} + \boldsymbol{U}_{\mathcal{F}}(i+1)\boldsymbol{\mathcal{P}}(i)\boldsymbol{U}_{\mathcal{F}}^H(i+1)\right]^{-1} \\ = \;& \mathbf{I}_2 \otimes \left\{\boldsymbol{\mathcal{X}}_{\mathcal{F}}(i)[\lambda\,\mathbf{I}_J + \boldsymbol{P}(i)\boldsymbol{\mathcal{X}}_{\mathcal{F}}(i)]^{-1}\right\}, \\ = \;& \mathbf{I}_2 \otimes [\lambda\,\mathbf{I}_J\boldsymbol{\mathcal{X}}_{\mathcal{F}}^{-1}(i) + \boldsymbol{P}(i)]^{-1} \end{aligned} \tag{6.24}$$

Let us define

$$\boldsymbol{\Omega}(i+1) = [\lambda\,\mathbf{I}_J\boldsymbol{\mathcal{X}}_{\mathcal{F}}^{-1}(i) + \boldsymbol{P}(i)]^{-1}.$$

We can easily verify that $[\lambda\,\mathbf{I}_J\boldsymbol{\mathcal{X}}_{\mathcal{F}}^{-1}(i)+\boldsymbol{P}(i)]$ is a diagonal matrix with size of $J\times J$, and so is $\boldsymbol{\Omega}(i+1)$. Hence, the computation of $\boldsymbol{\Omega}(i+1)$ turns to be quite simple, and a lower computational complexity can be achieved here.

Substituting Equation (6.24) into Equation (6.20), we obtain

$$\begin{aligned} \boldsymbol{\mathcal{P}}(i+1) &= \mathbf{I}_2 \otimes \left\{\lambda^{-1}[\boldsymbol{P}(i) - \boldsymbol{P}(i)\boldsymbol{\Omega}(i+1)\boldsymbol{P}(i)]\right\}, \\ \boldsymbol{P}(i+1) &= \lambda^{-1}[\boldsymbol{P}(i) - \boldsymbol{P}(i)\boldsymbol{\Omega}(i+1)\boldsymbol{P}(i)]. \end{aligned}$$

And the coefficients adaption equation changes to

$$\boldsymbol{w}_{\mathcal{F}}(i+1) = \boldsymbol{w}_{\mathcal{F}}(i) + \begin{bmatrix} \boldsymbol{P}(i+1) & \mathbf{0}_{J\times J} \\ \mathbf{0}_{J\times J} & \boldsymbol{P}(i+1) \end{bmatrix} \boldsymbol{U}_{\mathcal{F}}^H(i+1)\boldsymbol{e}_{\mathcal{F}}(i+1). \tag{6.25}$$

It is clear that computation of the inverse correlation matrix $\boldsymbol{\mathcal{P}}(i+1)$ has been simplified a lot, as the matrix inversion in $\boldsymbol{\mathcal{P}}(i+1)$ requires only simple processing at the receiver. Therefore, the BRLS algorithm, with its application to this scenario, can be implemented at a lower computational complexity that is even comparable to the classical LMS schemes.

6.2 Adaptive FDE With Diversity Combining

The adaptive FDE schemes developed in the last section is effective in combating the multipath fading in wireless environments with small channel variation or high block-to-block fading[2] correlation, as will be shown in our simulation results. But as the frequency dispersion or Doppler spread increases[3], the BER performance will incur distinct degradation, even making the link unusable, as also shown by the simulation results. This is due to the inability of these recursive algorithms in tracking faster channel variations. In [64], Younis et al proposed some possible

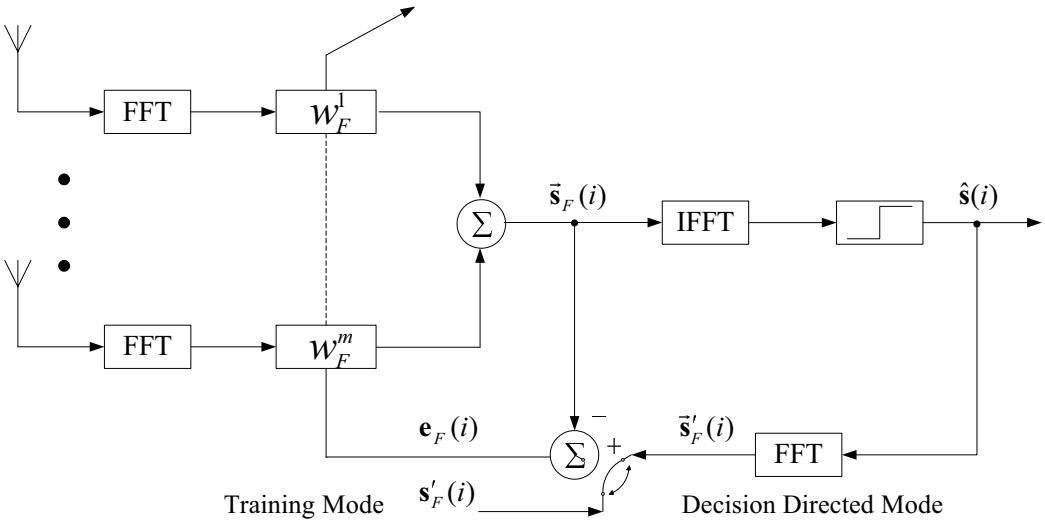

Figure 6.2: The structure of adaptive FDE with diversity combining

solving methods, such as using smaller data block or retraining more. Whereas, these methods, when applied to those channels with large delay spread, may lower the system throughput. Here we propose a method of incorporating the adaptive FDE with diversity combining to mitigate the detrimental effect introduced by

[2]We assume *block fading*; for details, readers can refer to Chapter 4.

[3]We assume channels experience *slow fading*, even under such increase in the Doppler shift.

frequency dispersion of fading channels. The diversity combining employed here is different from those commonly used receive diversity schemes, as the combined branches are in the frequency domain rather in the time domain.

Figure 6.2 depicts the block diagram of adaptive FDE with diversity combining. There are m branches arranged at the receiver. The received data blocks at each branch are transformed to the frequency domain by using FFT. The data matrix is formed according to Equation (6.21), and then weighted by respective filter coefficients. Each filter output is combined with outputs of the other branches. The combining output is transformed back to the time domain by means of IFFT, and rendered to a slicer or quantizer for decision-making. The error signal, is generated by comparing the equalizer output with the desired response, and transformed to frequency domain to adapt the coefficients of each equalizers according to some specific recursive algorithms.

This diversity arrangement can assist the equalization and improve the BER performance, because it is unlikely that all the m branches will experience a deep fade at the same FFT grid. This concept, actually we have introduced earlier in Chapter 4. Each branch at the receiver needs to be separated from each other sufficiently so that the signals they receive are independent or highly uncorrelated. As both transmit diversity and receive diversity are employed here, this system actually comes out to be a MIMO (multi-input-multi-output) system. And the wireless environment is MIMO frequency-selective fading channels.

6.3 Simulation Results and Discussion

In this section, we provide simulation results for the adaptive FDE scheme. Here we still focus on the STBC scheme with two transmit antennas and one receive antenna (unless we specified it purposely). The overall transmitter power is the same as for a single transmit antenna (normalized to one), i.e, the the transmission power at each transmit antenna is normalized and multiplied by a factor 1/2. This is slightly different from what we have used in the last chapter, but both approaches are equivalent in the sense of SNR, and consequently the results are comparable.

For all results we consider 8-PSK modulations without channel coding. And the GSM 05.05 EQ wireless channel model [60] with channel order $v = 3$ is still employed in our simulations for equalization test. We deploy the ZP-only scheme as data transmission format. The burst structure follows the frame format as shown in Figure 4.5, which is different from the one that we have used in Chapter 5 (as illustrated in Figure 5.5). This is because the adaptive equalization eliminates the need for additional channel estimation by implementing the channel estimation and equalization jointly.

Block fading is still assumed in our simulations; but the channel fadings are no longer independent from burst to burst, instead, they are correlated in the time domain. That is, the Doppler spread is introduced in the simulations, which may affect performance of the adaptive FDE, as will be shown later. To generate the correlated Rayleigh fading, the simulator as depicted in Figure 6.3 is adopted in our simulations, where f_d denotes the maximum Doppler frequency shift. Detailed

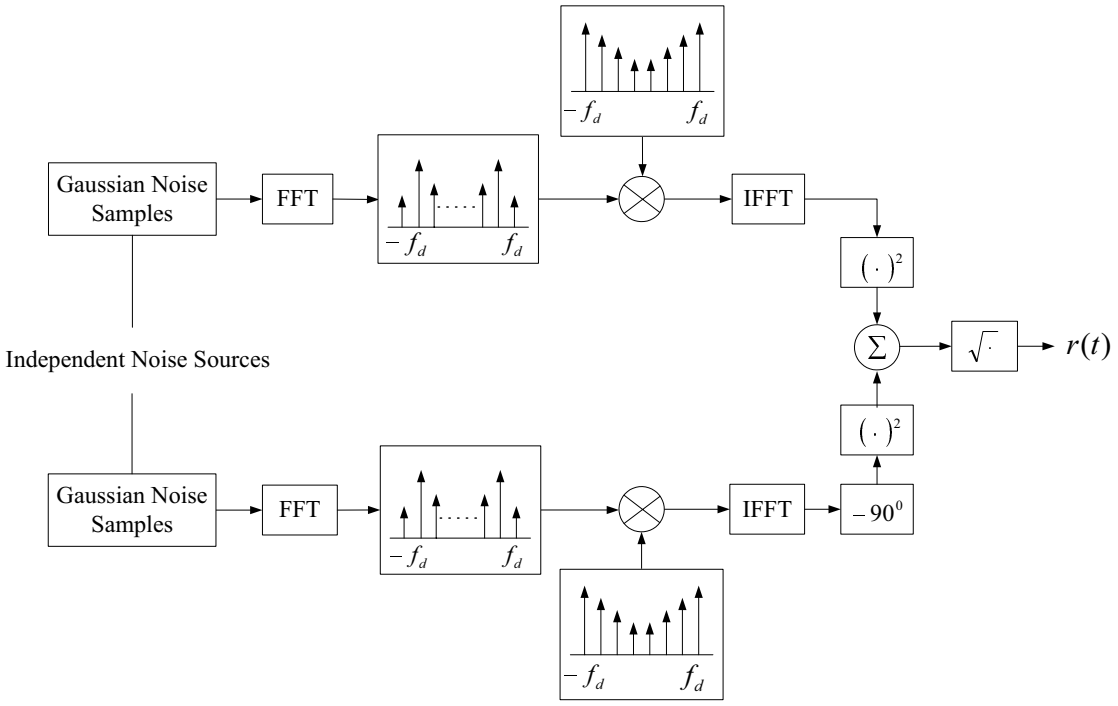

Figure 6.3: Frequency-domain implementation of a correlated Rayleigh fading simulator at baseband

steps regarding implementing the simulator can be found in [2]. As in this thesis, only slow fading is considered, and block fading is assumed, therefore, the rate of fading in the Monte Carlo simulations can be determined by $f_dT = f_d/f_b$, where T and f_b denotes the burst period and burst rate, respectively. A larger value of f_dT implies faster fading and vice versa. In our simulations, the data subbock length, N, is set to 61, therefore the burst length $2J$ or $2(N + v)$ is equal to 128.

We first present a comparison of the ensemble-average error performance of the BLMS algorithm to the BRLS algorithm with $f_dT = 0.0001$ and $E_b/N_0 = 15\,\text{dB}$, as shown in Figure 6.4. We used $\mu = 0.12$ and $\lambda = 0.95$ for the BLMS and BRLS algorithms, respectively. The BRLS algorithm reaches a MSE of less than 16dB

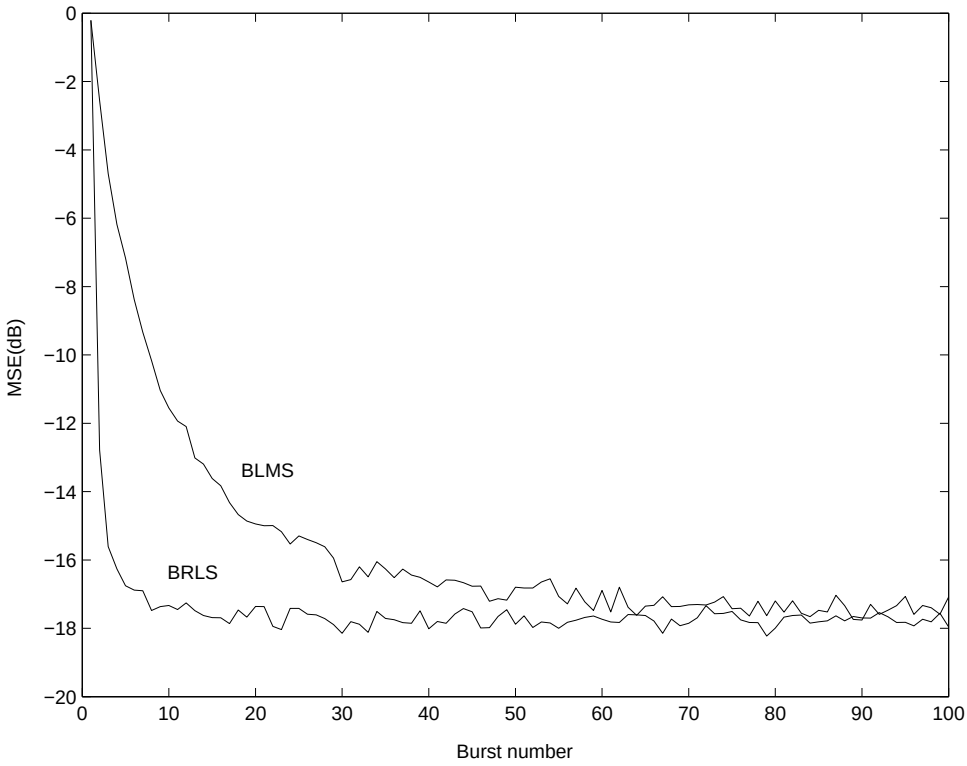

Figure 6.4: Comparison of the learning curves of the BLMS and BRLS algorithms. 2TX, 1RX; $J = 64,\ v = 3,\ N = 61$**;** $f_dT = 0.0001$**;** $E_b/N_0 = 15\,\text{dB};\ \mu = 0.12;\ \lambda = 0.95$**.**

within a few bursts (less than 5), while the BLMS takes a number of (more than 30) bursts to reach the same performance. The BRLS algorithm outperforms the BLMS algorithm in both the rate of convergence and excess MSE with comparable complexity, hence is more appropriate for practical applications. Hereafter in our simulations, we adopt only the BRLS algorithm, and use 5 bursts for equalizer training, and 45 bursts for data transmission.

Figure 6.5 shows the BER performance of the adaptive FDE with regard to different Doppler spread. For the convenience of comparing, we also plot the BER

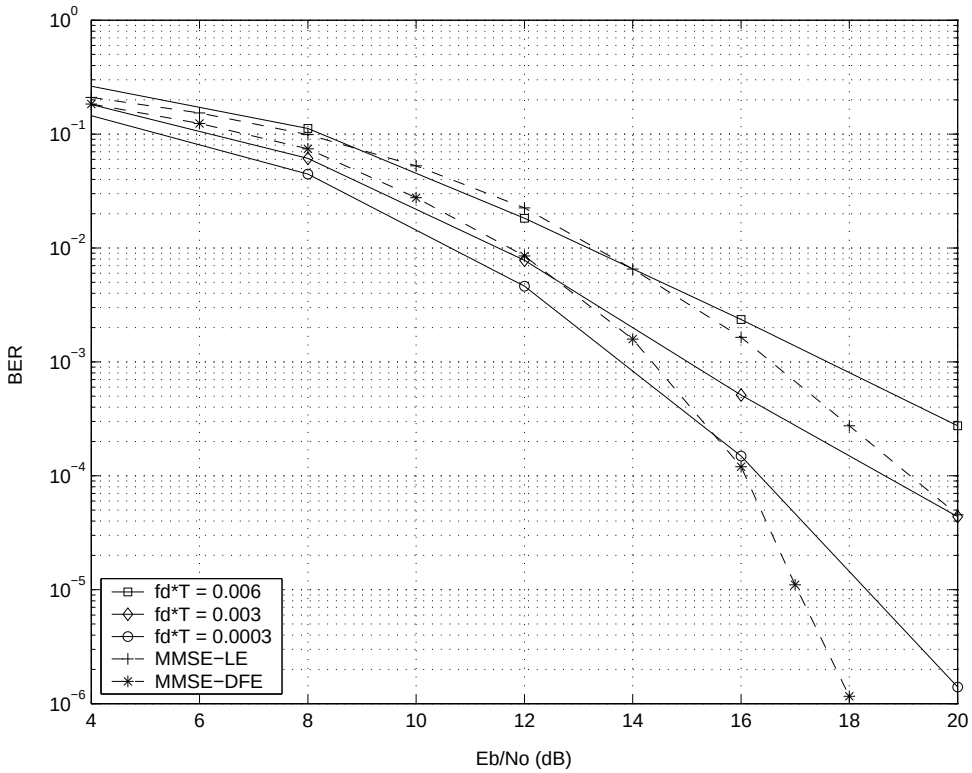

Figure 6.5: BER performance of the adaptive FDE with three different doppler spread. 2TX 1RX; $J = 64,\ v = 3,\ N = 61$**;** $\lambda = 0.8, 0.7,$ **and** 0.5 **for** $f_dT = 0.0003,\ 0.003,$ and 0.006**, respectively.**

performance of MMSE-DFE and MMSE-LE (assuming ideal knowledge of CSI) in the same figure. It is clear that when the channel correlation is high, the BER performance is quite good, or even comparable with performance of the MSE-DFE. But as the Doppler spread increases, the BER performance degrades rather observably, which is even inferior to that of the MMSE-LE. We can further predict that, if the Doppler spread continues to increase, the link, even with the presence of adaptive FDE, may become unusable.

We also investigate the performance of our proposed frequency domain diver-

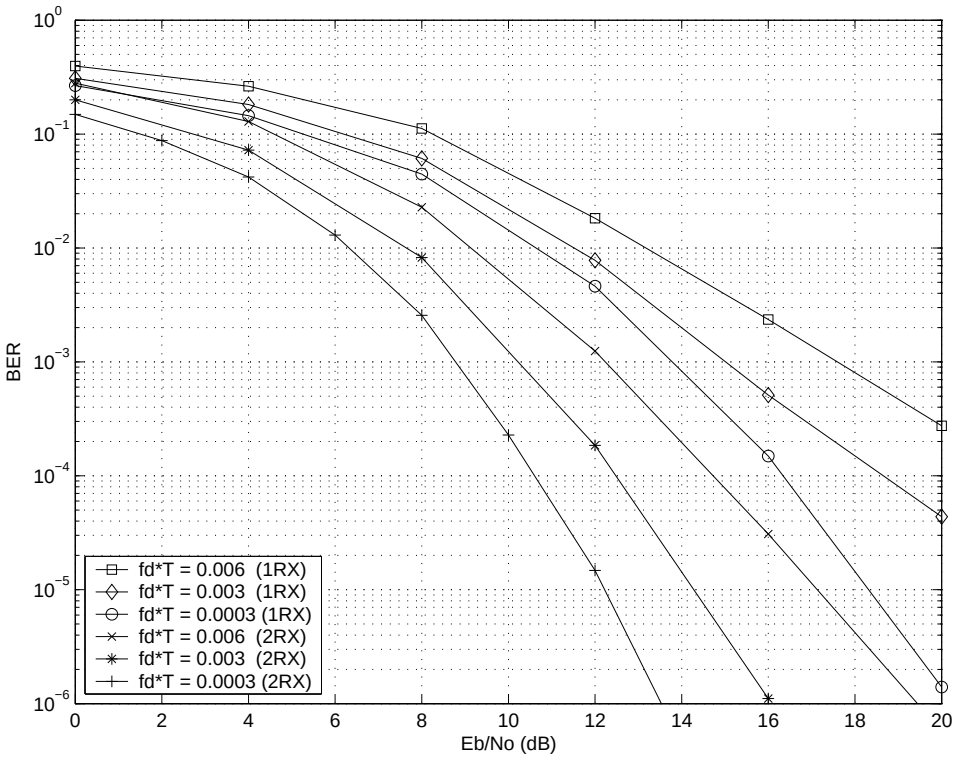

Figure 6.6: BER performance comparison of adaptive FDE with and without diversity combining, with regard to three different doppler spread. $J = 64,\ v = 3,\ N = 61$**;** $\lambda = 0.8,\ 0.7,$ **and** 0.5 **for** $f_dT = 0.0003,\ 0.003,$ **and** 0.006**, respectively.**

sity combining scheme in junction with the adaptive FDE to combat the effect induced by channel variations. The simulation results are presented in Figure 6.6, where 2 receiver antennas are used with compared to the case of single receive antenna. It is clear that the performance improvement due to diversity combining is significant. We take the case of $f_dT = 0.006$ as an example; by fixing the BER at 10^{-3}, we observe that the diversity combining (2RX) outperforms the non-combining (1RX) by about 6dB. Additionally, Figure 6.7 presents the comparison of learning curves for the diversity combining scheme (2RX) and non-combining

scheme (1RX). It is obvious that by using diversity combining at the receiver, the learning curves become smoother, and the excess MSE is also reduced. The adaptive FDE as well as the diversity combining scheme, can also apply to the broadband wireless systems, such as the BWA [62]. We present the simulation results in Figure 6.8, where $J = 512$, $N = 449$, $v = 63$, and a uniform power delay profile is adopted. The performance improvement due to diversity combining is also substantial.

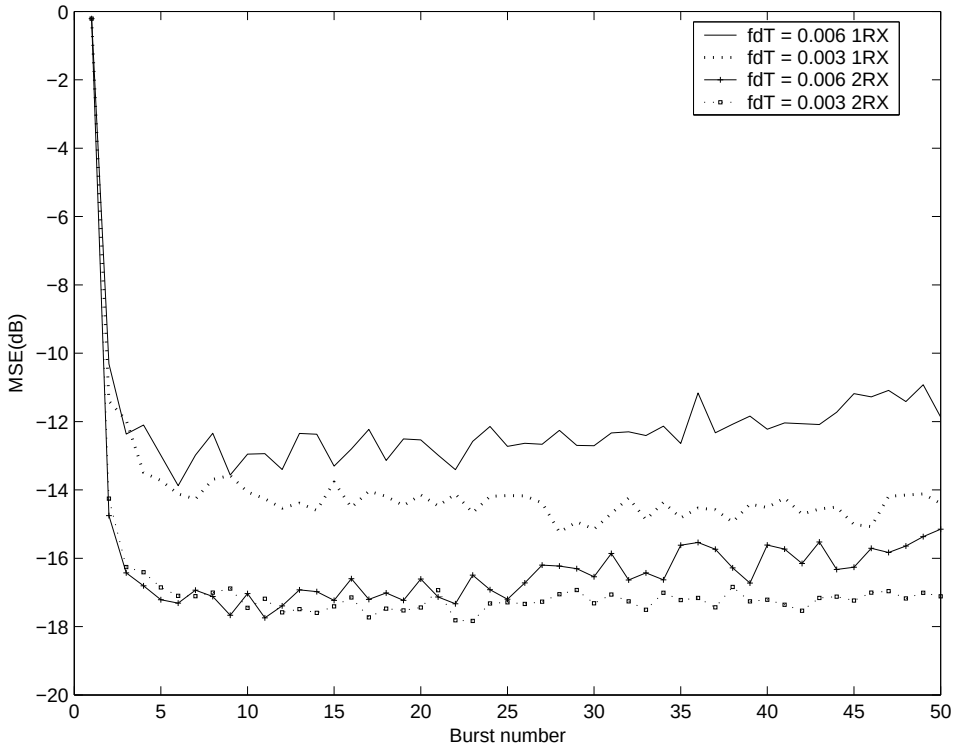

Figure 6.7: Comparison of the learning curves of the adaptive FDE with and without diversity combining, with regard to three different doppler spread. $J = 64,\ v = 3,\ N = 61$**;** $\mathrm{E_b/N_0} = 12\,\mathrm{dB}$**;** $\lambda = 0.7$ **and** 0.4 **for** $f_dT = 0.003$ **and** 0.006**, respectively.**

In our Monte-Carlo simulations, we have not specified the actual Doppler

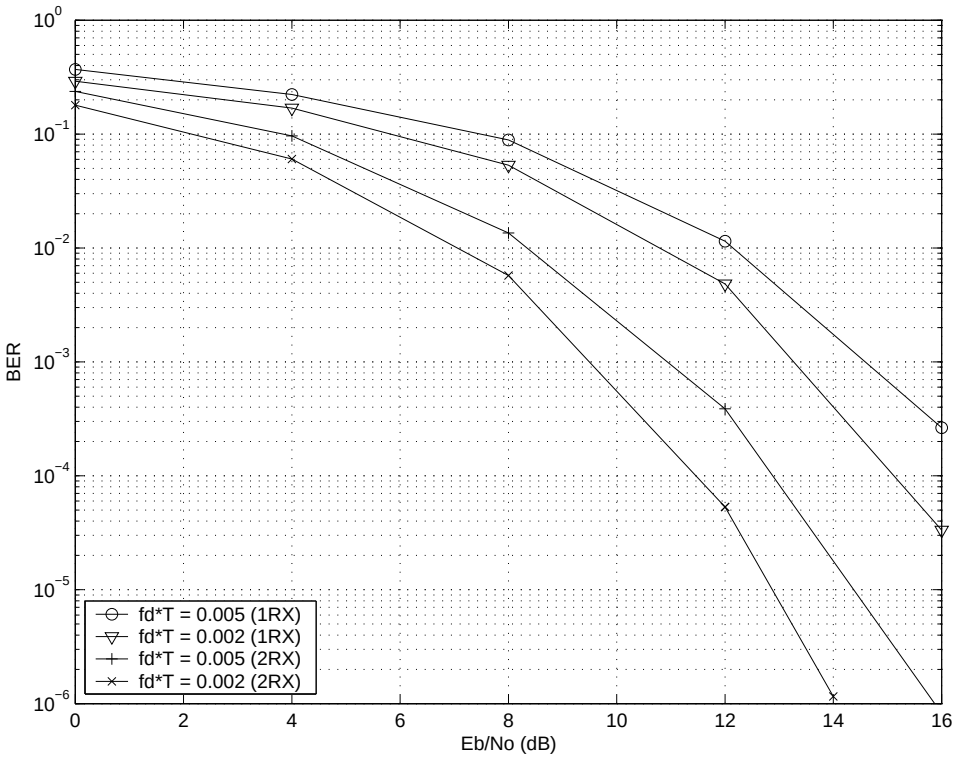

Figure 6.8: BER performance comparison of adaptive FDE with and without diversity combining, with regard to two different doppler spread. $J = 512,\ v = 63,\ N = 449$**;** $\lambda = 0.7,$ **and** 0.5 **for** $f_dT = 0.002,$ **and** 0.005**, respectively.**

frequency or the mobile speed; instead, we only used the f_dT to denote the Doppler spread. Now let us consider some typical systems. Here we still take the EDGE system as a case study, whose symbol rate is 271 kb/s. As we have 128 symbols in one burst, the burst rate is about 2117 bursts/s. Then $f_dT = 0.006$ corresponds to the mobile speed of 15 km/h. Such speed, in reality, may appear rather slow. If the speed increases, the Doppler spread will increase accordingly, finally making the adaptive equalizer unable to track the changes of the channel impulse response. Therefore, the adaptive FDE, although enjoys the advantage of low complexity,

may not appear suitable to those systems that operate in the environments with relatively high Doppler spread, such as the EDGE system. For the EDGE system, it is more appropriate to employ the FDE schemes (especially the DFE) that we developed in the last chapter for two main reasons:

1. Only slight changes need to be carried out to the original burst structure, and the relative positions of data blocks with regard to training blocks are still retained.

2. The use of FD DFE (either ZF or MMSE) can achieve significant improvement in performance over linear equalizers at a cost of comparable complexity increase, because the data subblock size is not so large.

On the other hand, the adaptive FDE schemes, together with the frequency-domain diversity combining, is suitable to those systems with large delay spread but relatively small Doppler spread, for example, the BWA systems [62]. Using the adaptive FDE scheme can achieve a satisfactory BER performance with relatively low computational complexity as compared to those training-based FDE schemes, because only linear processing is involved in the computations.

6.4 Summary

In this chapter, we presented the adaptive FDE scheme that is based on the BLMS or BRLS recursive algorithms. This adaptive scheme obviates the need for distinct channel estimation, and realizes joint channel estimation and equalization. Simulations results indicated the adaptive FDE scheme (based on BRLS) to be effective

in combating the ISI caused by multipath fading with relatively lower complexity. We also proposed a diversity combining method which is implemented in the frequency domain to mitigate the detrimental effect induced by channel variations. It was shown by simulations that this diversity combining scheme can efficiently ameliorate the BER performance when the Doppler spread increases. Finally, we presented our recommendations about applications of both training based FDE schemes and the adaptive FDE schemes to practical communication systems.

Chapter 7

Conclusion

7.1 Thesis Summary

This thesis develops FDE schemes for STBC transmissions over frequency-selective fading channels. Our objective is to exploit benefits of the two techniques: FDE and STBC, by combining them together with application to typical communication systems.

To have a better understanding of these two techniques of FDE and STBC, we presented detailed descriptions about them in Chapter 3 and Chapter 4, respectively. In Chapter 3, based on our thorough literature survey, we categorized the FDE techniques that ever appear in the literature into two types: FDE based on block adaptive filter and FDE based on circulant matrices. We further pointed out the similarities and differences between these two types. The first type is actually a fast implementation of the block adaptive filter; while the second type is to use the eigen-decomposition property of circulant matrices, and usually necessitates some

form of transmitter design to construct such circulant matrices. In this thesis, we considered only the second type of FDE.

The STBC technique was discussed in Chapter 4. We focused on the block STBC scheme that was proposed recently in the literature for frequency-selective fading channels. This block scheme is of interest as it can provide diversity gains as the Alamouti's original scheme does, and may facilitate the implementation of FDE, hence was adopted in our work for transmitter design. Additionally, we also introduced two specific block STBC schemes: CP-only and ZP-only, which were chosen in our work for data transmission and channel estimation, respectively.

In this thesis, we have investigated two FDE schemes for STBC transmissions over multipath fading channels: the channel estimation based non-adaptive version and the adaptive version. In Chapter 5, we focused on the nonadaptive version, where we developed both linear and nonlinear (DFE) STBC-FDE schemes according to the ZF and MMSE optimizing criteria. Closed form expressions for tap coefficients of these equalization schemes, especially the ZF-DFE and MMSE-DFE, were derived. We also indicated that our work in FDE can be readily extended to perform channel estimation, and hereby we proposed a training based frequency-domain channel estimation method, in which training blocks can be encoded by the same space-time coder as the data blocks. Performance of the channel equalization and estimation schemes was examined by applying them to the EDGE communication system. Simulation results indicated significant performance improvement archived by these STBC-FDE schemes as compared to the case of single transmitter with FDE. Simulation results also demonstrated effectiveness of the frequency-

domain channel estimation scheme, which, at its worst, incurs about 3 dB SNR performance penalty for inaccurate channel estimation.

Chapter 6 presented the adaptive FDE scheme that is based on the BLMS or BRLS recursive algorithm. This adaptive scheme eliminates the need for distinct channel estimation by performing channel estimation and equalization jointly. Simulations results showed that the adaptive FDE scheme (based on BRLS algorithm) is effective in combating the ISI caused by multipath fading with relatively lower complexity. We also proposed a diversity combining method which is implemented in the frequency domain to mitigate the detrimental effect induced by frequency dispersion of the channel impulse response. It was indicated by simulations that this diversity combining scheme, in conjunction with the adaptive FDE, can efficiently ameliorate the BER performance as the Doppler spread increases.

Our recommendations were put forward in the end for the applications of both training based FDE and adaptive FDE schemes to practical communication systems. That is, the training based FDE schemes are more appropriate for those systems with small delay spread (small block size) and relatively high Doppler spread, such as the EDGE system; the adaptive FDE scheme, on the other hand, is suitable to those systems with large delay spread (large block size) and relatively low Doppler spread, such as the BWA systems.

7.2 Future Work

Based upon our work presented in this thesis, there are a few possible research topics lying ahead of us, as listed in the following:

- Throughout this thesis, the block fading is assumed, so that the orthogonality of STBC can be ensured. However, this assumption may not be justified in the case of rapidly varying multipath fading channel. Under such circumstance, how to design the equalization schemes to combat both the multipath fading as well as the loss in orthogonality of STBC comes to be a possible future research topic.

- In Chapter 6, we considered only the adaptive linear equalizer. In fact, it is possible to use an adaptive DFE instead to combat the multipath fading. But how to design the feedforward and feedback filters as well as the recursive algorithms to adapt them, is a challenging topic because a tradeoff should be reached between the performance improvement and complexity increase.

- As FDE and STBC can also be jointly applied to CDMA system (e.g., [65]), these various DFE schemes presented in this thesis, including the channel estimation based schemes and adaptive scheme, can be readily extended to CDMA system, which is an interesting research topic worthwhile being looked into.

Bibliography

[1] J. E. Padgett, C. G. Günther and T. Hattori, "Overview of wireless personal communications", *IEEE Communications Magazine*, vol. 33, pp. 28-41, January 1995.

[2] T. S. Rappaport, *Wireless Communications: Principles and Practice*, Prentice-Hall, Upper Saddle River, NJ, 2th Edition, 2002.

[3] J. D. Parsons, *The Mobile Radio Propagation Channel*, John Wiley & Sons, Singapore, 2th Edition, 2000.

[4] J. G. Proakis, *Digital Communications*, McGraw-Hill, Singapore, 4th Edition, 2001.

[5] J. G. Proakis, "Adaptive equalization for TDMA digital mobile radio", *IEEE Transactions on Vehicular Technology*, vol. 40, pp. 333-341, May 1991.

[6] J. G. Proakis and D. G. Manolakis, *Digital Signal Processing : Principles, Algorithms, and Applications*, Prentice-Hall, Upper Saddle River, NJ, 3th Edition, 1996.

[7] S. U. H. Qureshi, "Adaptive equalization", *Proceedings of the IEEE*, vol. 73, pp. 1340-1387, September 1985.

[8] E. R. Ferrara, Jr., "Frequency-domain adaptive filtering", in *Adaptive Filters*, C. F. N. Cowen and P. M. Grant, Eds., Prentice-Hall, Englewood Cliffs, NJ, ch. 6, pp. 145-179, 1985.

[9] J. Shynk, "Frequency-domain and multirate adaptive filtering", *IEEE Signal Processing Magazine*, vol. 9, pp. 14-37, January 1992.

[10] T. Walzman and M. Schwartz, "Automatic equalization using the discrete frequency domain", *IEEE Transactions on Information Theory*, vol. IT-19, pp. 59-68, January 1973.

[11] H. Sari, G. Karam and I. Jeanclaude, "Frequency-domain equalization of mobile radio and terrestrial broadcast channels", in *Proceedings of GLOBECOM*, San Francisco, CA, pp. 1-5, 1994.

[12] H. Sari, G. Karam and I. Jeanclaude, "Transmission techniques for digital terrestrial TV broadcasting", *IEEE Communications Magazine*, vol. 33, pp. 100-109, February 1995.

[13] A. Czylwik, "Comparison between adaptive OFDM and single carrier modulation with frequency domain equalization", in *Proceedings of VTC*, Phoenix, AZ, pp. 865-869, May 1997.

[14] N. Benvenuto and S. Tomasin, "On the comparison between OFDM and single carrier modulation with a DFE using a frequency-domain feedforward filter", *IEEE Transactions on Communications*, vol. 50, pp. 947-955, June 2002.

[15] A. Gusmão, R. Dinis and N. Esteves, "On frequency-domain equalization and diversity combining for broadband wireless communications", *IEEE Transactions on Communications*, vol. 51, pp. 1029-1033, July 2003.

[16] G. Kadel, "Diversity and equalization in frequency domain–a robust and flexible receiver technology for broadband mobile communication systems", in *Proceedings of VTC*, Phoenix, AZ, pp. 894-898, May 1997.

[17] M. V. Clark, "Adaptive frequency-domain equalization and diversity combining for broadband wireless communications", *IEEE Journal on Selected Areas in Communications*, vol. 16, pp. 1385-1395, October 1998.

[18] D. Falconer, S. L. Ariyavisitakul, A. Benyamin-Seeyar and B. Eidson, "Frequency-domain equalization for single-carrier broadband wireless systems", *IEEE Communications Magazine*, vol. 40, pp. 58-66, April 2002.

[19] D. Falconer and S. L. Ariyavisitakul, "Broadband wireless using single carrier and frequency domain equalization", in *Proceedings of the 5th International Symposium on Wireless Personal Multimedia Communications*, Honolulu, pp. 27- 36, October 2002.

[20] S. Alamouti, "A simple transmit diversity technique for wireless communications", *IEEE Journal on Selected Areas in Communications*, vol. 16, pp. 1451-1458, October 1998.

[21] V. Tarokh, H. Jafarkhani and A. R. Calderbank, "Space-time block codes from orthogonal designs", *IEEE Transactions on Information Theory*, vol. 45, pp. 1456-1467, July 1999.

[22] V. Tarokh, N. Seshadri and A. R. Calderbank, "Space-time codes for high data rate wireless communication: performance criterion and code construction", *IEEE Transactions on Information Theory*, vol. 44, pp. 744-765, March 1998.

[23] TIA 45.5 Subcommittee, "The CDMA 2000 Candidate Submission. Draft", June 1998.

[24] Texas Instruments, "Additional results on space time block coded transmit antenna diversity for WCDMA", Tdoc 25/99, ETSI SMG2 UMTS-L1, Espoo, Finland, January 1999.

[25] L. J. Cimini Jr., J. C-I Chuang and N. R. Sollenberger, "Advanced cellular internet service (ACIS)", *IEEE Communications Magazine*, vol. 36, pp. 150-159, October 1998.

[26] P. W. Wolniansky, G. J. Foschini, G. D. Golden and R. A. Valenzuela, "V-BLAST: An architecture for realizing very high data rates over the rich-scattering wireless channel", in *Proceedings of ISSSE-98*, pp. 295 - 300, September 1998.

[27] E. Lindskog and A. Paulraj, "A transmit diversity scheme for channels with intersymbol interference", in *Proceedings of ICC*, New Orleans, LA, pp. 307-311, June 2000.

[28] F. W. Vook and T. A. Thomas, "Transmit diversity schemes for broadband mobile communication systems", in *Proceedings of VTC*, vol. 6, Boston, MA, pp. 2523-2529, Fall 2000.

[29] N. Al-Dhahir, "Single-carrier frequency-domain equalization for space-time block-coded transmissions over frequency-selective fading channels", *IEEE Communications Letters*, vol. 5, pp. 304-306, July 2001.

[30] N. Al-Dhahir, "Overview and comparison of equalization schemes for space-time-coded signals with applications to EDGE", *IEEE Transactions on Signal Processing*, vol. 50, pp. 2477-2488, October 2002.

[31] S. Zhou and G. B. Giannakis, "Single-carrier space-time block-coded transmissions over frequency-selective fading channels", *IEEE Transactions on Information Theory*, vol. 49, pp. 164-179, January 2003.

[32] J. K. Tugnait, L. Tong and Z. Ding, "Single-user channel estimation and equalization", *IEEE Signal Processing Magazine*, vol. 17, pp. 17-28, May 2000.

[33] A. F. Molisch, Ed., *Wideband Wireless Digital Communications*, Prentice-Hall, Upper Saddle River, NJ, 2001.

[34] A. Furuskär, S. Mazur, F. Müller and H. Olofsson, "EDGE: Enhanced data rates for GSM and TDMA/136 evolution", *IEEE Personal Communications*, vol. 6, pp. 56-66, June 1999.

[35] A. Papoulis and S. U. Pillai, *Probability, Random Variables, and Stochastic Processes*, McGraw-Hill, Singapore, 4th Edition, 2002.

[36] B. Sklar, "Rayleigh fading channels in mobile digital communication systems Part I: Characterization", *IEEE Communications Magazine*, vol. 35, pp. 136-146, September 1997.

[37] B. Sklar, "Rayleigh fading channels in mobile digital communication systems Part II: Mitigation", *IEEE Communications Magazine*, vol. 35, pp. 148-155, September 1997.

[38] B. Widrow, "Adaptive filter, I: Fundamentals", Stanford Electronics Laboratory, Stanford University, Stanford, CA, Tech. Rep. 6764-6, December 1966.

[39] K. Berberidis and J. Palicot, "A frequency-domain decision feedback equalizer for multipath echo cancellation", in *Proceedings of GLOBECOM*, Singapore, pp. 98-102, November 1995.

[40] P. A. Dmochowski and P. J. McLane, "Frequency domain equalization for high data rate multipath channels", in *Proceedings of the IEEE Pacific Rim Conference on Communications, Computers and signal Processing*, pp. 534-537, 2001.

[41] B. Farhang-Boroujeny, *Adaptive Filters : Theory and Applications*, John Wiley & Sons, Singapore, 1998.

[42] S. Haykin, *Adaptive Filter Theory*, Prentice-Hall, Upper Saddle River, NJ, 4th Edition, 2002.

[43] R. M. Gray, *Toeplitz and Circulant Matrices : A Review*, available online at http://www-ee.stanford.edu/ gray/toeplitz.pdf, 2002.

[44] A. V. Oppenheim, R. W. Schafer and J. R. Buck, *Discrete-time Signal Processing*, Prentice-Hall, Upper Saddle River, NJ, 1999.

[45] Z. Wang and G. B. Giannakis, "Wireless multicarrier communications: Where Fourier meets Shannon", *IEEE Signal Processing Magazine*, vol. 20, pp. 29-48, May 2000.

[46] Z. Liu, G. B. Giannakis, B. Muquet and S. Zhou, "Space-time coding for broadband wireless communications", *Wireless Communications and Mobile Computing*, vol. 1, pp. 33-53, John Wiley & Sons, January-March 2001.

[47] A. J. Paulraj and C. B. Papadias, "Space-time processing for wireless communications", *IEEE Signal Processing Magazine*, vol. 14, pp. 49-83, November 1997.

[48] A. F.Naguib, V. Tarokh, N. Seshadri and A. R. Calderbank, "A space-time coding modem for high-data-rate wireless communications", *IEEE Journal on Selected Areas in Communications*, vol. 16, pp. 1459-1478, October 1998.

[49] A. F. Naguib, N. Seshadri and A. R. Calderbank, "Increasing data rate over wireless channels", *IEEE Signal Processing Magazine*, vol. 17, pp. 76-92, May 2000.

[50] G. H. Golub and C. F. Van Loan, *Matrix Computations*, The Johns Hopkins Univeristy Press, Baltimore, MD, 3rd Edition, 1996.

[51] T. Kailath, "A theorem of I. Schur and its impact on modern signal processing", vol. 18, pp. 9-30 (special issue), in *Operator Theory: Advances and Applications, I. Schur Methods in Operator Theory and Signal Processing*, I. Gohberg and Birkhauser, Eds., 1986.

[52] T. Kailath, A. H. Sayed and B. Hassibi, *Linear Estimation*, Prentice-Hall, Upper-Saddle River, NJ, 2000.

[53] A. Stamoulis, G. B. Giannakis and A. Scaglione, "Block FIR decision-feedback equalizers for filterbank precoded transmissions with blind channel estimation capabilities", *IEEE Transactions on Communications*, vol. 49, pp. 69-83, January 2001.

[54] L. Li, Y. Yao and H. Li, "Channel estimation and equalization for space-time block coded systems in frequency selective fading channels", in *Proceedings of GLOBECOM*, San Antonio, TX , USA, pp. 300-304, November 2001.

[55] X. Ma, G. B. Giannakis and S. Ohno, "Optimal training for block transmissions over doubly-selective wireless fading channels", *IEEE Transactions on Signal Processing*, vol. 51, pp. 1351-1366, May 2003.

[56] X. Ma, L. Yang and G. B .Giannakis, "Optimal training for MIMO frequency-selective fading channels", in *Proceedings of the 36th Asilomar Conference on Signals, Systems, and Computers,* Pacific Grove, CA, pp. 1107-1111, November 2002.

[57] C. Budianu and L. Tong, "Channel estimation for space-time orthogonal block codes", *IEEE Transactions on Signal Processing*, vol. 50, pp. 2515-2528, October 2002.

[58] C. Fragouli, N. Al-Dhahir and W. Turin, "Training-based channel estimation for mulitple-antenna broadband transmissions", *IEEE Transactions on Wireless Communications*, vol. 2, pp. 384-391, March 2003.

[59] D. Chu, "Polyphase codes with good periodic correlation properties", *IEEE Transactions on Information Theory*, vol. IT-18, pp. 531-532, July 1972.

[60] 3GPP TS 05.05 version 8.15.0, *Digital cellular telecommunications system (Phase 2+); Radio transmission and reception*, Release 1999.

[61] J. Mietzner, P. A. Hoeher and M. Sandell, "Compatible improvement of the GSM/EDGE system by means of space-time coding techniques", *IEEE Transactions on Wireless Communications*, vol. 2, pp. 690-702, July 2003.

[62] A. Benyamin-Seeyar et al., "SC-FDE PHY layer system proposal for sub 11GHz BWA (an OFDM compatible solution)", IEEE 802.16.3p-01/31r2, March 12, 2001

[63] D. T. M. Slock and K. Maouche, "The fast subsampled-updating recursive least-squares (FSU RLS) algorithm for adaptive filtering based on displacement structure and the FFT", *Signal Processing*, vol. 40, pp. 5-20, 1994.

[64] W. M. Younis, N. Al-Dhahir and A. H. Sayed, "Adaptive frequency-domain equalization of space-time block-coded transmissions", in *Proceedings of ICASSP*, Orlando, FL, pp. 2353-2356, May 2002.

[65] F. Petré, G. Leus, L. Deneire, M. Engels, M. Moonen and H. De Man, "Space-time block coding for single-carrier block transmission DS-CDMA downlink", *IEEE Journal on Selected Areas in Communications*, vol. 21, pp. 350-361, April 2003.

Appendix A

Proof of $\mathbf{P}_J^{(1)}\mathbf{a} = \mathbf{F}_J^H \mathbf{F}_J^H \mathbf{a}$

$\mathbf{F}_J$ denotes an symmetric $J \times J$ orthonormal DFT matrix whose (p, q) th entry is given by $J^{-1/2}\exp(-j2\pi p\, q/J)$, where $0 \leq p,\, q \leq J-1$. $\mathbf{F}_J$ is unitary transformation, that is, $\mathbf{F}_J^{-1} = \mathbf{F}_J^H = \mathbf{F}_J^*$. So when $\sqrt{J}\,\mathbf{F}_J$ operates on a column vector (e.g., $\mathbf{a}$) of length J, the result is a column vector (e.g., $\mathbf{a}_{\mathcal{F}}$) containing the DFT of the original vector, i.e.,

$$\sqrt{J}\mathbf{F}_J\mathbf{a} = \mathbf{a}_{\mathcal{F}}$$

where $\mathbf{a} = [a(0),\ a(1),\ \ldots\ a(J-1)]^T$, is the same as we have introduced in earlier context.

According to the *complex-conjugate property* of DFT [6], when implementing DFT on the conjugate of $\mathbf{a}$, we have

$$\sqrt{J}\mathbf{F}_J\mathbf{a}^* = \mathbf{a}^*_{\mathcal{F}}((-k))_J = \mathbf{a}^*_{\mathcal{F}}(J-k), \qquad 0 \leq k \leq J-1, \tag{A.1}$$

where $\mathbf{a}^*_{\mathcal{F}}((-k))_J$ is the circular reverse of $\mathbf{a}^*_{\mathcal{F}}$. Conjugate of Equation (A.1) is given

by

$$(\sqrt{J}\mathbf{F}_J\mathbf{a}^*)^* = \sqrt{J}\mathbf{F}_J^H\mathbf{a} = \mathbf{a}_{\mathcal{F}}((-k))_J = \mathbf{a}_{\mathcal{F}}(J-k), \qquad 0 \le k \le J-1,$$

Then applying the IDFT operation, i.e., $\frac{1}{\sqrt{J}}\mathbf{F}_J^{-1}$, on $\mathbf{a}_{\mathcal{F}}((-k))_J$, we can get

$$\begin{aligned} \frac{1}{\sqrt{J}}\mathbf{F}_J^{-1}(\mathbf{a}_{\mathcal{F}}(J-k)) &= \mathbf{a}((-k))_J & \text{(A.2)} \\ &= \frac{1}{\sqrt{J}}\mathbf{F}_J^{-1}\sqrt{J}\mathbf{F}_J^H\mathbf{a} \;=\; \mathbf{F}_J^H\mathbf{F}_J^H\mathbf{a} & \text{(A.3)} \end{aligned}$$

In Equation (A.2) we directly apply the *time-reversal property* of DFT as described in [6]. From Equations (A.2) and (A.3), we can summarize that

$$\mathbf{a}((-k))_J = \mathbf{F}_J^H\mathbf{F}_J^H\mathbf{a}. \tag{A.4}$$

Since $\mathbf{a}((-k))_J = [a(0),\ a(J-1),\ a(J-2),\ \ldots,\ a(1)]^T$ and $\mathbf{P}_J^{(1)}\mathbf{a} = [a(0),\ a(J-1),\ a(J-2),\ \ldots,\ a(1)]^T$, we may conclude that

$$\mathbf{P}_J^{(1)}\mathbf{a} = \mathbf{F}_J^H\mathbf{F}_J^H\mathbf{a}. \tag{A.5}$$